Mechanistic studies of Glycine Betaine Catalysed CO_2 Reduction Using Density Functional Theory

Yifan Wu

Thesis submitted to the University of Nottingham for the degree of Doctor of Philosophy

September 2022

Table of Contents

Acknowledgements

I want to thank my supervisors for their patience, guidance, and support. It has been a great pleasure to work with you.

I would like to thank all members in Dr. Tang's group and friends at University of Nottingham Ningbo China.

I am grateful for access to the University of Nottingham High-Performance Computing Facility in Ningbo China. I thank the University of Nottingham Ningbo China for a PhD scholarship.

Finally, I would also like to thank my family and friends, especially my parents and my sister, for their support during this study.

Thank you.

List of publications

1. Qiao, Z., et al., *An AIE and ESIPT active Schiff base as colorimetric probe of Fe3+ and turn-on fluorescent probe of Al3+: Experimental and theoretical studies.* Tetrahedron Letters, 2019. **60**(32): p. 150918.

List of Figures

List of Tables

Abstract

Fossil fuels (coal, oil and natural gas) are the main energy sources and the primary raw material sources for chemical industry. The society is facing challenging problems caused by over consumption of fossil fuels leading to serious environmental problems. For instance, the increasing concentration of CO_2 in the atmosphere has a significant impact on the earth. Hence, converting CO_2 to useful chemicals would be a feasible way to address global warming. Indeed, research efforts have been made to solve this challenging, by developing technology to convert atmospheric CO_2 into useful fuels.

In this thesis, we first reviewed the current progress in homogeneous CO_2 conversion under and catalysis of non-metal catalysts. Methods developed for converting CO_2 to useful fuels include synthesis of cyclic carbonates or polycarbonates; carboxylation reactions and CO_2 reduction reactions. In terms of CO_2 reduction, catalytic hydrosilylation of CO_2, catalytic hydroboration of CO_2, hydrogenation of CO_2 and catalytic amination of CO_2 have all been reported. In the area of catalytic amination of CO_2, one of the current problems is that aminals are difficult to trap and isolate. Other products from the catalytic amination of CO_2 are formamides and methylamines and their production were widely obtained in experiments. The development of the reaction conditions and the design and discovery of new catalysts are important issues for these transformations. This research aims to study the reaction mechanisms of these reactions using DFT calculations, with the aim to help the design of potential new reactions for this transformation.

Computational chemistry aims to study chemical problems by simulating chemical systems. There are two main methodological families in computational chemistry: those based on quantum chemical (QC) methods

and those based on molecular mechanics (MM). In Chapter 2, a brief introduction of computational methodology was given, including Schrödinger equation, Born–Oppenheimer approximation, Hartree-Fock theory and density functional theory. The thermodynamics in computational chemistry was also introduced with conclusion remarks to finish this chapter.

The main research part lies in chapters 4 to 5, where a detailed computational studies for the reaction mechanism of a glycine betaine catalysed CO_2 reduction, using $PhSiH_3$ with the presence of N-methylaniline, was carried out. Recently, glycine betaine has been reported to be an active catalyst to produce formamides, aminals and methylamines sequentially under mild conditions. However, the reaction mechanism is unclear. To understand the reaction mechanism, we first analysed interactions between the reactants (CO_2, $PhSiH_3$ and N-methylaniline) and the catalyst (glycine betaine) in chapter 3. Then we calculated the reaction mechanism to produce the formamide, the aminal and the methylamine using SMD(CH_3CN) ωB97XD/6-311++G(d,p)//ωB97XD/6-31+G(d,p) in chapter 4 and 5. Energy profiles of the reactions in the reaction mechanism are presented. The activation free energy barriers of the rate-determining steps to produce the formamide, the aminal and the methylamine are 32.2 kcal/mol, 37.8 kcal/mol and 37.8 kcal/mol estimated with SMD(CH_3CN)-ωB97XD/6-311++G(d,p)//ωB97XD/6-31+G(d,p). And when calculated in SMD(CH_3CN)-M06-2X/6-311++G(d,p)//ωB97XD/6-31+G(d,p) level of theory, the activation free energy barriers of the rate-determining steps for the formation of formamide, aminal and methylamine are 20.1 kcal/mol, 28.9 kcal/mol and 28.9 kcal/mol resepctively. Since the experiments occur under mild conditions ($\leqslant$100 °C, $\leqslant$0.5 MPa), the activation free energy barriers found from my DFT calculations are reasonable. This research contributes to the understanding of the reaction mechanism of this novel CO_2 conversion reaction.

Chapter 1 Introduction

1.0 Synopsis

This chapter begins with the background introduction to global warming. It also gives an overview of methods to cope with climate warming. The chapter then introduces non-metal catalysed CO_2 reduction. And the main part is a literature review of the computational studies of non-metal catalyzed CO_2 reduction, as well as the experiment work in non-metal catalysed CO_2 reduction. Finally, Chapter 1 ends by discussing the challenges in non-metal catalyzed CO_2 redction followed by providing an outline of the thesis.

1.1 Global warming

The concentration of CO_2 in the atmosphere is increasing due to the burning of fossil fuels. During daytime, the earth receives heat from the sun. CO_2 can trap the heat and prevent the heat from escaping from the earth. Therefore, the temperature of the earth is increasing. This phenomenon is called global warming and is presented in **figure 1.1.1**. Global warming has a significant influence on the environment. For example, the increased temperature causes more ice melting at the North Pole, which reduces habitat for animals such as polar bears. The ice melt also increases the sea level and some low-lying islands have been submerged. Extreme weather like flooding also occurs due to global warming.[1] To prevent more CO_2 appear in the atmosphere, global warming is known by everyone in the world. People plant trees because trees need CO_2 to grow. People drive less cars to use less energy and thus produces less CO_2. People save energies like clean water, electricity everyday because

energies are produced with CO_2 production. Scientists are also working on reducing the concentration of CO_2 in the atmosphere.

1.2 Carbon neutral and CO_2 reduction

Many scientists have been working on reducing the amount of CO_2 in the atmosphere.[2-4] One possible way is CO_2 transformation, which is to convert CO_2 into useful chemicals.[5, 6] CO_2 transformation includes the synthesis of cyclic carbonates or polycarbonates[7, 8], carboxylation reactions[9, 10] and CO_2 reduction to small molecules fuels[11, 12]. The synthesis of cyclic carbonates or polycarbonates is to react carbon dioxide with epoxides and form either cyclic carbonates or polycarbonates. Cyclic carbonates are widely used as raw materials for polycarbonates, fuel additives, electrolytes in lithium-ion secondary batteries, and aprotic polar solvents. Polycarbonates are CO_2-based polymers with high CO_2 content and are expected to find wide applications in a green and sustainable society. In terms of the catalytic carboxylation reactions, it usually involves the formation of C–C bonds.[13] These reactions can produce useful compounds such as ureas and carbamates.[14] CO_2 reduction is another method of CO_2 transformation.[13] There are two areas in CO_2 reduction: catalytic CO_2 reduction[11, 12] and electrochemical or photochemical reduction of CO_2[15-17]. The catalytic CO_2 reduction can produce various chemicals, for example, carbon monoxide[11], formate[12], methanol[18], methane[19], formamides[20] and methylamines[21]. In the catalytic CO_2 reduction, reductants can be either hydrosilanes[20-22] or H_2[23, 24] and catalysts are organocatalysts[18, 20] or metal catalysts[21, 22]. The electrochemical or photochemical reduction of CO_2 is to activate the chemically inert CO_2 molecule and promotes its conversion under external energy stimuli. During the reaction, the C=O bond will be broken and products can be carbon monoxide (CO), formic acid (HCOOH), methane (CH_4), ethylene (C_2H_4) depending on the nature of electrocatalysts or photocatalysts and

experimental conditions.[15-17] Our project focuses on catalytic CO_2 reduction using hydrosilane and glycine betaine as the reductant and catalyst.

1.3 Non-metal catalyzed CO_2 reduction

Non-metal involved catalytic CO_2 reduction includes three areas: catalytic hydrosilylation of CO_2, catalytic hydroboration of CO_2, hydrogenation of CO_2 and catalytic amination of CO_2.[25] In the hydrosilylation reaction, CO_2 reacts with hydrosilanes to produce chemicals like methoxysilanes[18], formylsilanes[26], methane[19, 27, 28] and silyl formates[29]. The hydroboration of CO_2 uses B-H bonds as the reducing agent.[25] Typical products can be methoxyboranes[30], formatoborates[31] and methane[32]. The hydrogenation of CO_2 can produce two main products: hydrocarbons[33, 34] and methanol[35]. Both methanol and hydrocarbons are excellent fuels in internal combustion engines and are easily stored and transported. Methanol is also a raw material in chemical industries.[36] The catalytic amination of CO_2 uses secondary or primary amines, reductants and CO_2 under the function of catalysts to produce formamides, aminals and methylamines.[25] The catalysts in the amination of CO_2 can be either metal-based catalysts or organocatalysts.[37] Metal-based catalytic systems include Ru[38-42], Fe[43], Cu[44-47], Zn[21, 48], Ni[49] and Cs[50, 51], while organocatalysts can be TBD (1,5,7-triazabicyclo[4.4.0]dec-5-ene)[52], NHCs (N-heterocyclic carbenes)[53], ILs (ionic liquids)[54], proazaphosphatrane superbases[55], $B(C_6F_5)_3$[56] and TBAF (tetrabutylammonium fluoride)[57]. Hydrosilane is a good choice as the reductant in the catalytic amination of CO_2 compared to H_2. Although hydrogen gas is the cleanest and most atom-economical reductant, N-formylation and methylation reactions using H_2 as the reductant generally occur under high pressures (>5 MPa) and high temperatures (>100 °C).[58, 59] The activity of aromatic amines is poor when H_2 is the reductant. Compared to H_2, Si-H bonds in hydrosilanes are kinetically more reactive due to the polarity and lower bond dissociation energy of

hydrosilanes.[59] In recent years, organosilanes have been employed as efficient reductants in CO_2 amination reactions under milder reaction conditions.[38, 59]

1.4 Computational studies of non-metal catalyzed CO_2 reduction

Currently, several articles have considered the reaction mechanisms of formylation, amination and methylation reactions using density functional theory (DFT) calculations.[60-65] Kim and co-workers investigated the reaction mechanism of the model methylation reaction when no catalyst is present.[60] Their calculation shows how CO_2 reacts with $PhSiH_3$ and N-methylaniline in the absence of any catalyst to produce the methylamine (MA). They used M05-2X(THF, SMD)/6-311++G**//M05-2X/6-31G* for calculations. As shown in **figure 1.4.1**, they analysed the methylation reaction in three pathways: pathway 1, pathway 2 and pathway 3. In pathway 1, CO_2 is first reduced by $PhSiH_3$ to produce the formoxysilane (FOS) species. The FOS species can be further reduced by $PhSiH_3$ to form the bis(silyl)-acetal (BSA) species. The hydrosilylation of the BSA species with $PhSiH_3$ delivers both the silylmethoxide (SMO) species and disiloxane (DSO). Finally, the SMO species reacts with the amine to form dimethylaniline (MA) and phenyl silanol ($PhSiH_2OH$). In terms of pathway 2, CO_2 first reacts with the amine and the product is the CA species. The CA species then goes through a hydrosilylation reaction to produce the FA species and $PhSiH_2OH$. Since both $PhSiH_2OH$ and $PhSiH_3$ are hydrosilylation reagents, the FA species then goes through two hydrosilylation reactions and the final products are dimethylaniline (MA) and 1,3-diphenyldisiloxan-1-ol ($PhSiH_2OSiHOHPh$). For pathway 3, the first step reaction is the same as that in pathway 1, which is the hydrosilylation of CO_2. Then the reaction can go through two routes. One is the reaction between FOS and the amine, while the other is FOS reacts with $PhSiH_3$. The reaction between FOS and the amine produces both FA and $PhSiH_2OH$. The reaction after FA in pathway 3 is the same as that in pathway 2. The other route after FOS in pathway 3 is the

hydrosilylation of FOS with $PhSiH_3$ and this reaction is the same as the second reaction in pathway 1. After BSA is formed in pathway 3, the reaction between BSA and the amine will produce a chemical that also appears in pathway 2. By following the final step reaction in pathway 2, MA can be produced. Based on the activation free energy barriers of transition states, the reaction to produce dimethylaniline (MA) happens in the way highlighted in red and the rate-determining step is the initial generation of FOS via the hydrosilylation of CO_2 with $PhSiH_3$ with an energy barrier of 41.7 kcal/mol.[60]

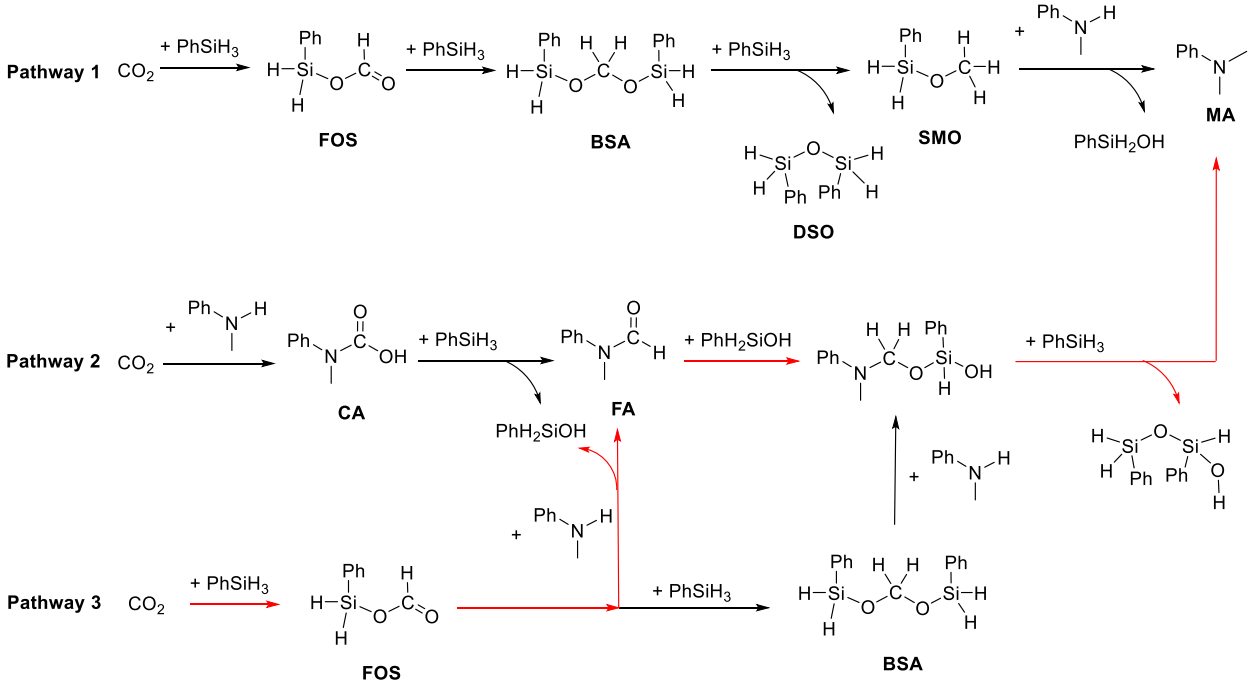

Figure 1.4.1. *The reaction mechanism analysed by Kim and co-workers[60]*

Kinjo and co-workers performed an experiment to show that 1,3,2-diazaphospholene ([NHP]H) can catalyse the formylation and methylation of amines with CO_2 and the hydrosilane (Ph_2SiH_2).[66] Based on the experimental results, Wang and co-workers performed DFT calculations to understand the reaction mechanisms of the formylation of methylaniline and the methylation of 2,2,4,4-tetramethylpiperidine.[62] The calculations used M06-2X(CH_3CN, SMD)/6-311++G(d,p)//M06-2X(CH_3CN, SMD)/6-31G(d,p) and the reaction mechanisms are shown in **figure 1.4.2**. As shown in **figure 1.4.2**, the

catalyst [NHP]H first reacts with CO_2 to form the product [NHP]OCHO. This product can dissociate to $[NHP]^+$ and $HCOO^-$ ions which are useful in the further formylation and methylation reactions. [NHP]OCHO can also be reduced by Ph_2SiH_2 to form both [NHP]H and **10**. The reaction between **10** and [NHP]OCHO produces **11** and regenerate the catalyst [NHP]H. **11** is an important intermediate in both of the formylation and methylation reactions. In terms of the formylation reaction, **11** can go through two routes to reach the final product that is the formamide. One is using both $HCOO^-$ and H_2O as the catalysts, while the other uses only H_2O as the catalyst. For the formylation route where uses both $HCOO^-$ and H_2O as the catalysts, the reaction between **11** and the amine under the catalysis of $HCOO^-$ produces **12** and the formamide. For the other formylation route using H_2O as the catalyst, **11** first reacts with the amine and the catalyst H_2O to form **13**. **13** under the catalysis of H_2O can convert to the formamide and **12**. **12** reacts with the amine under the catalysis of H_2O can form **14**. The reaction between **14** and the catalyst H_2O produces **15** and the formamide. In terms of the methylation reaction after **11**, **11** initially reacts with Ph_2SiH_2 and $HCOO^-$ to form **10** and **16**. The reaction between **16** and $[NHP]^+$ produces **17** and formaldehyde. Formaldehyde next reacts with the amine to produce **18**. The $[NHP]^+$ ion then takes the hydroxy group in **18** and the products are [NHP]OH and **19**. **19** takes the proton from [NHP]H to form both $[NHP]^+$ and the methylamine. Based on the reaction mechanisms of the formylation and methylation reactions, Wang and co-workers think that methylation is unlikely to pass through the formamide as an intermediate. In other words, formamides cannot be further reduced to produce methlyamines.[62]

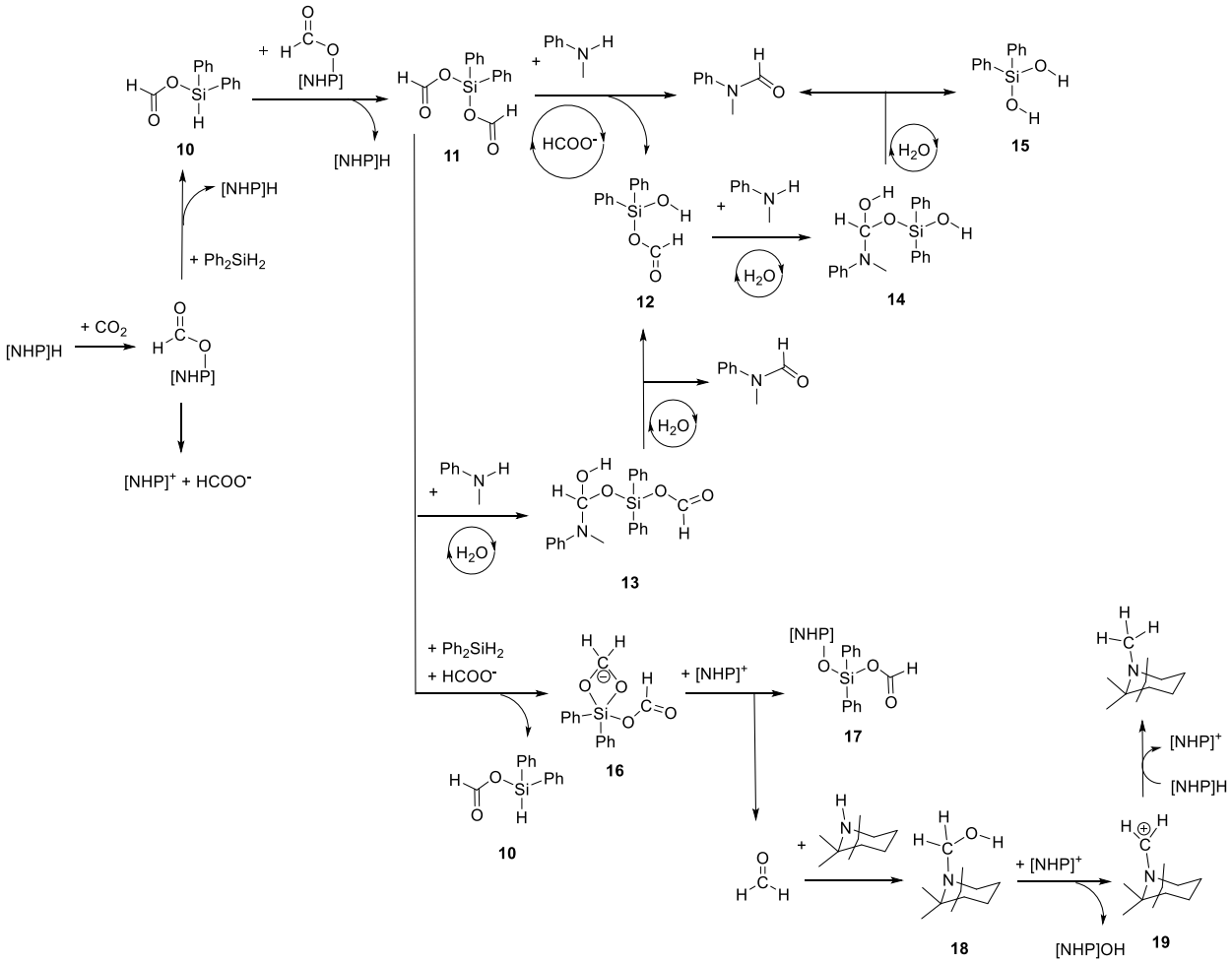

Figure 1.4.2. *The reaction mechanism studied by Wang and co-workers*[62]

In 2011, Cantat and co-workers synthesized formamides using amines, CO_2 and silanes under the catalysis of N-heterocyclic carbenes (NHCs). The reactions happened at room temperature with high yields of formamides.[53] Based on the experimental results, two research groups have studied the reaction mechanisms of the NHC catalysed formylation reactions.[63, 65] Cao and co-workers suggested that NHC activates the reaction using either the covalent binding mechanism or the general base mechanism.[63] However, Li and co-workers proposed that NHC can react with CO_2 and the amine to form an ionic liquid and the ionic liquid can further help formylation.[65] Cao and co-workers used B97-D(THF, SMD)/6-311+G(d,p) // B97-D/6-31G(d) for calculations. They analysed the reaction mechanism in two pathways that are

shown in **figure 1.4.3**. One pathway is through the intermediate of the carbamic acid (CA), while the other pathway is through the intermediate of formoxysilane (FOS). In terms of the first pathway, CO_2 initially reacts with the amine under the catalysis of NHC to produce the carbamic acid (CA). CA is next reduced by $PhSiH_3$ under the catalysis of NHC to form (dimethylamino)(silyloxy)methanol (DSM). Regarding the other pathway, the reaction between CO_2 and $PhSiH_3$ under the catalysis of NHC produces formoxysilane (FOS). Then the NHC-catalysed coupling of FOS and the amine forms DSM. The C–O bond cleavage accompanied by deprotonation of the hydroxyl group in DSM yields the final products that are the formamide and $PhSiH_2OH$. Based on their DFT calculations, the formylation reaction goes via the intermediate of FOS, which is highlighted in red in **figure 1.4.3**. The rate-determining step is the FOS formation with an energy barrier of 20.7 kcal/mol. Cao and co-workers proposed that NHC can catalyse the reaction in two methods: the covalent binding mechanism and the general base mechanism. Transition states using the two activation mechanisms in their calculations are presented in **figure 1.4.4**. In terms of the covalent binding mechanism, bonds are formed between NHC and the chemicals (i.e., the C atom in CO_2, the Si atom in $PhSiH_3$, the Si atom in FOS and the Si atom in DSM). For the general base mechanism applied in **26** and **27**, NHC acts as a base to abstract a proton from the amine of the nucleophile, and facilitates C–N bond formation with the carbonyl compounds. Regarding the general base mechanism applied in **28**, NHC acts as a base to abstract a proton from the hydroxyl group in DSM, and may help C-O cleavage. For the general base mechanism applied in **29**, NHC acts as a base to abstract a proton from the hydroxyl group in CA, and may help the further hydrosilylation of CA by $PhSiH_3$.[63]

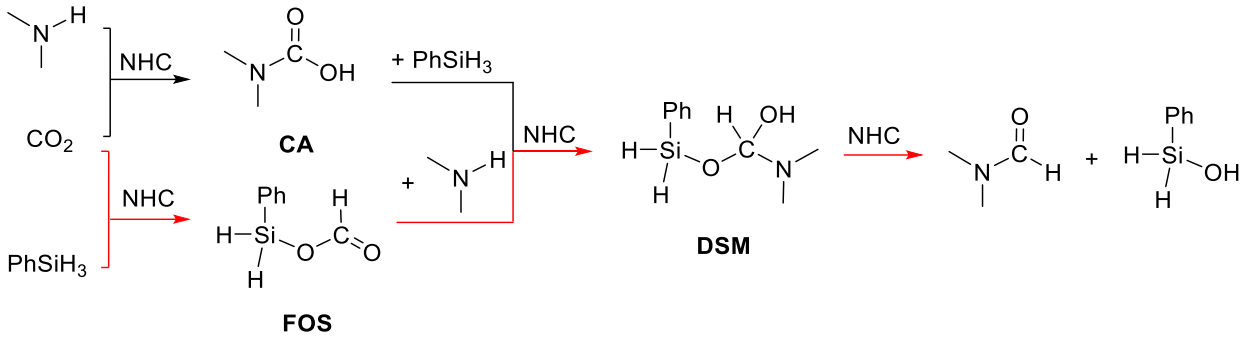

Figure 1.4.3. *The reaction mechanism studied by Cao and co-workers*[63]

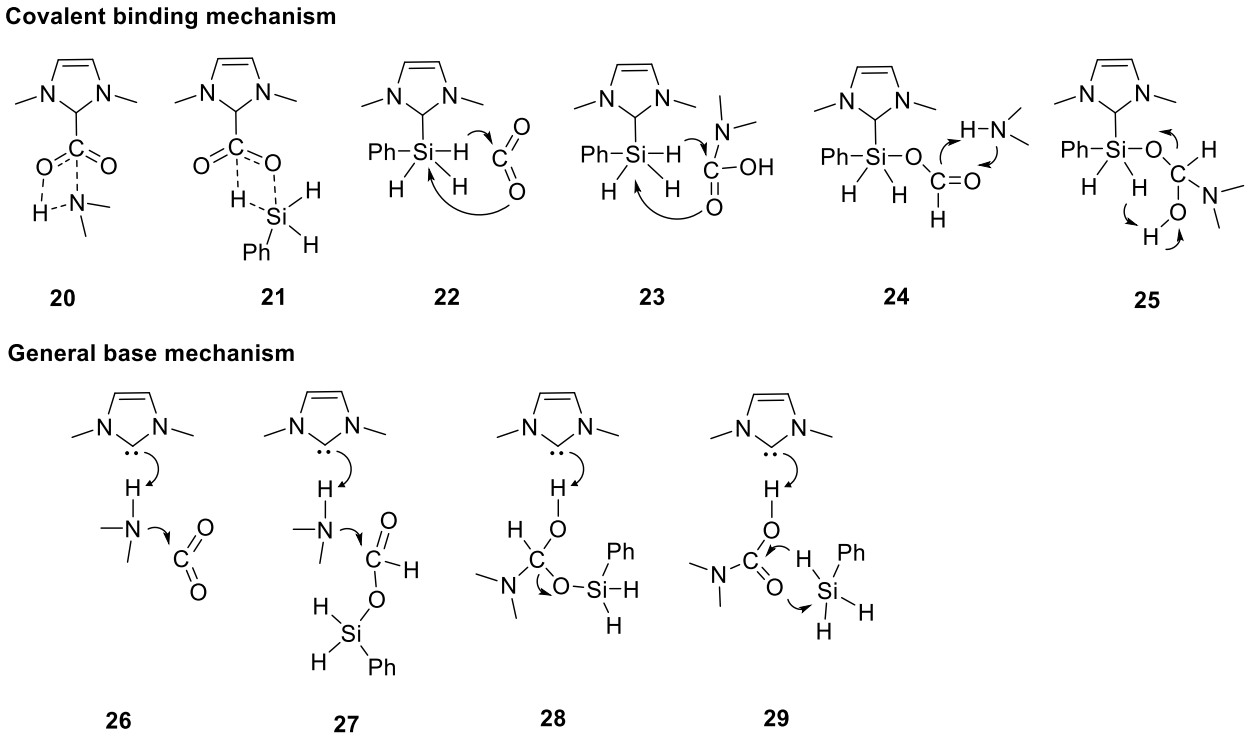

Figure 1.4.4. *Two activation mechanisms of NHC*[63]

Regarding how HNC catalyses the formylation reaction, Li and co-workers hold a different view. They think NHC acts as neither a CO_2 nor a silane activator, but it reacts with CO_2 and the amine to form the ionic liquid $[NHCH]^+[Carbamate]^-$.[65] Reactants in their calculations are Me_2NH, CO_2, $PhSiH_3$ and IPr. M06(THF, SMD)/6-31G* was used to calculate the 2,6-diisopropylphenyl substituent group of IPr, while M06(THF, SMD)/6-311++G** was used for the rest.[65] **Figure 1.4.5** shows all the activation modes analysed by Li and co-workers, ranging from mode **30** to mode **36**.

Mode **30**,[18, 63, 67] mode **31**,[18, 63, 67] mode **32**[68] and mode **33**[20, 63] have been proposed by other studies using different functional and basis sets. To make the activation free energy barriers comparable, Li and co-workers recalculated these modes using the functional and basis set mentioned above. Mode **32'**, mode **30'**, mode **34**, mode **35** and mode **36** were proposed and calculated by Li and co-workers. As shown in **figure 1.4.5**, the activation free energy barrier of the reference point is 0 and the activation free energy barriers of the different activation modes are labelled. In terms of mode **30**, NHC and $PhSiH_3$ form a C−Si bond and the newly formed bond activates a Si−H bond by pushing more electron density to the H atom. The activated Si-H bond promotes the hydride transfer to the electrophilic carbon centre of CO_2.[63, 67] In mode **31**, the CO_2 moiety of the IPr-CO_2 adduct is directly reduced. In the IPr-CO_2 adduct, the O atom of the CO_2 moiety becomes more ready to attack the positive Si centre, while the C atom of the CO_2 moiety becomes reluctant to accept a hydride.[65] In mode **32**, the hydride transfers to the carbon atom in NHC *via* a five-membered ring transition state under the attack of the CO_2 moiety, and the subsequent 1,2-H shift yields the formoxysilane.[65, 68] In mode **33**, the CO_2 moiety in carbamate salt intermediate is directly reduced by silane.[20, 63] Mode **32'** is similar to mode **32**. Mode **32'** is proposed because the carbamate anion in $[IPrH]^+[Carbamate]^-$ is more reactive to activate the Si-H bond than the CO_2 moiety in mode **32**. The difference between mode **30** and mode **30'** is the activation mode of $PhSiH_3$. Mode **30** and mode **30'** use the classical S_N2@Si activation mode and the 'S_N2@Si-Acceptor' activation mode respectively. The difference between the two activation modes is drawn in **figure 1.4.6**. The classical activation mode of $PhSiH_3$ involves two steps. Firstly, NHC reacts with $PhSiH_3$ to form the NHC-Si bond and the product is a penta-coordinated Si intermediate. Secondly, the Si−H bond breaks and the hydride attacks CO_2. However, the 'S_N2@Si-Acceptor' mechanism is an one-step process without intermediate formation. The IPr−Si bond formation, the

Si−H bond break, and the H−C bond formation take place at the same time. Mode **34**, mode **35** and mode **36** use the 'S_N2@Si-Acceptor' activation mechanism. In terms of activation mode **34**, the negatively charged O atom of the IPr-CO_2 adduct activates the Si−H bond in $PhSiH_3$, and the hydride from the activated Si-H bond then attacks a free CO_2 molecule. For mode **35**, the negatively charged O atom of the carbamate anion in $[IPrH]^+[Carbamate]^-$ activates the Si−H bond, and the free CO_2 acts as a hydride acceptor. In mode **36**, the N atom of the amine activates the Si-H bond under the promotion of IPr. Based on the activation free energy barriers of the different activation modes in **figure 1.4.5**, mode **35** is the most favourable activation mode. By comparing the activation free energy barriers of mode **30** and mode **30'**, the 'S_N2@Si-Acceptor' activation mode is more preferred than the classical S_N2@Si activation mode. The reaction mechanism of the formylation reaction is shown in **figure 1.4.7**. The reaction of IPr, the amine and CO_2 forms **37** that is the $[IPrH]^+[Carbamate]^-$ salt complex. **38** is produced from the reaction between CO_2 and $PhSiH_3$ under the catalysis of **37** and activation mode 35 is applied in the reaction. **37** can convert to both CO_2 and **39**. **39** reacts with **38** to produce **40** and the formamide (**42**). The reaction between **40**, CO_2 and Me_2NH forms both **41** and the formamide (**42**).[65]

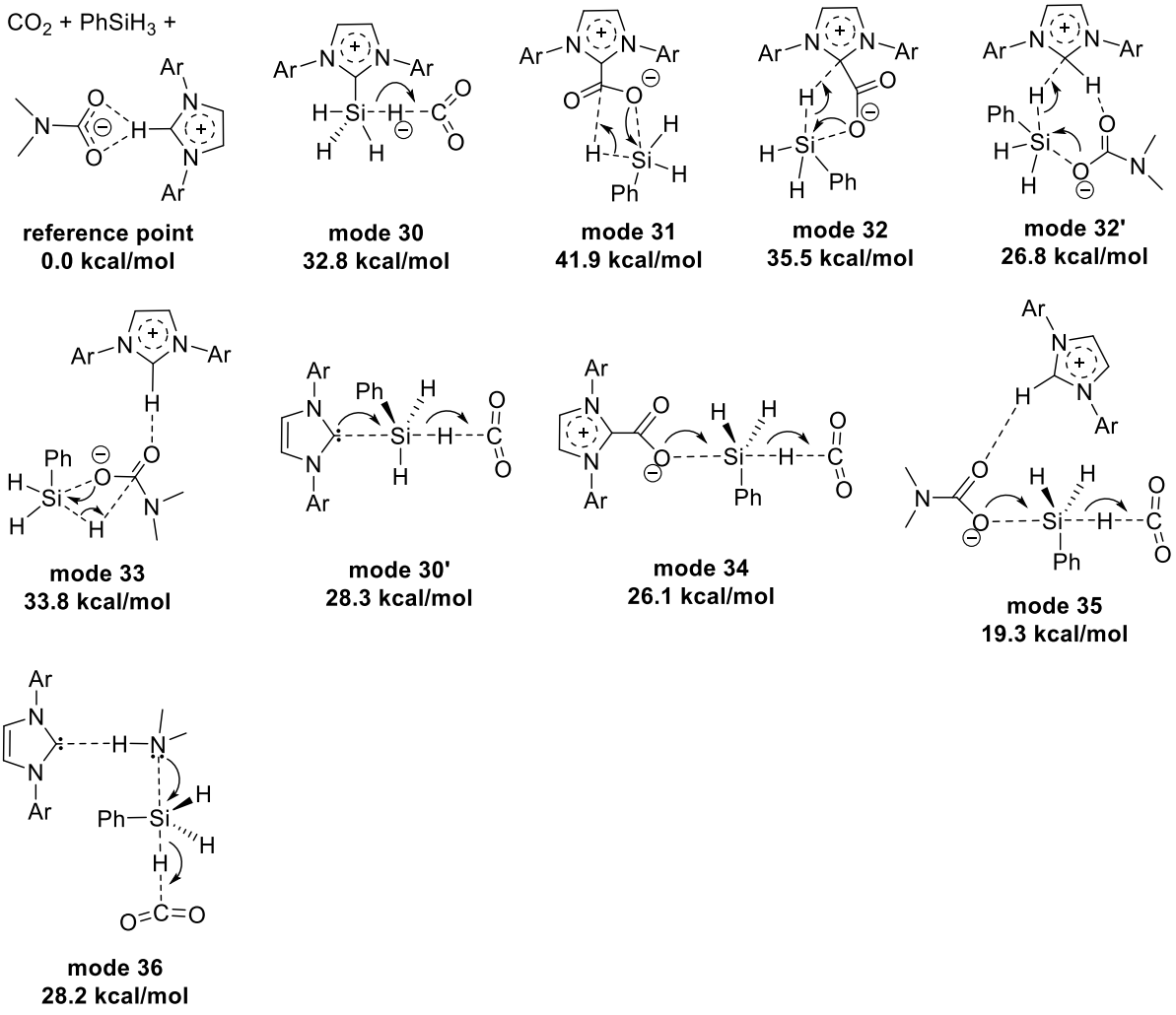

Figure 1.4.5. *Different activation modes studied by Li and co-workers[65]*

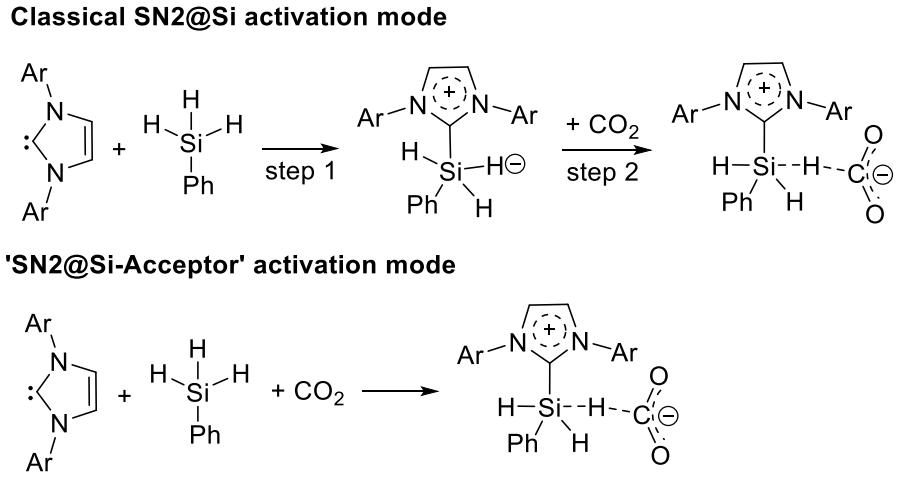

Figure 1.4.6. *The difference between the classical S_N2@Si activation mode and the 'SN2@Si-Acceptor' activation mode[65]*

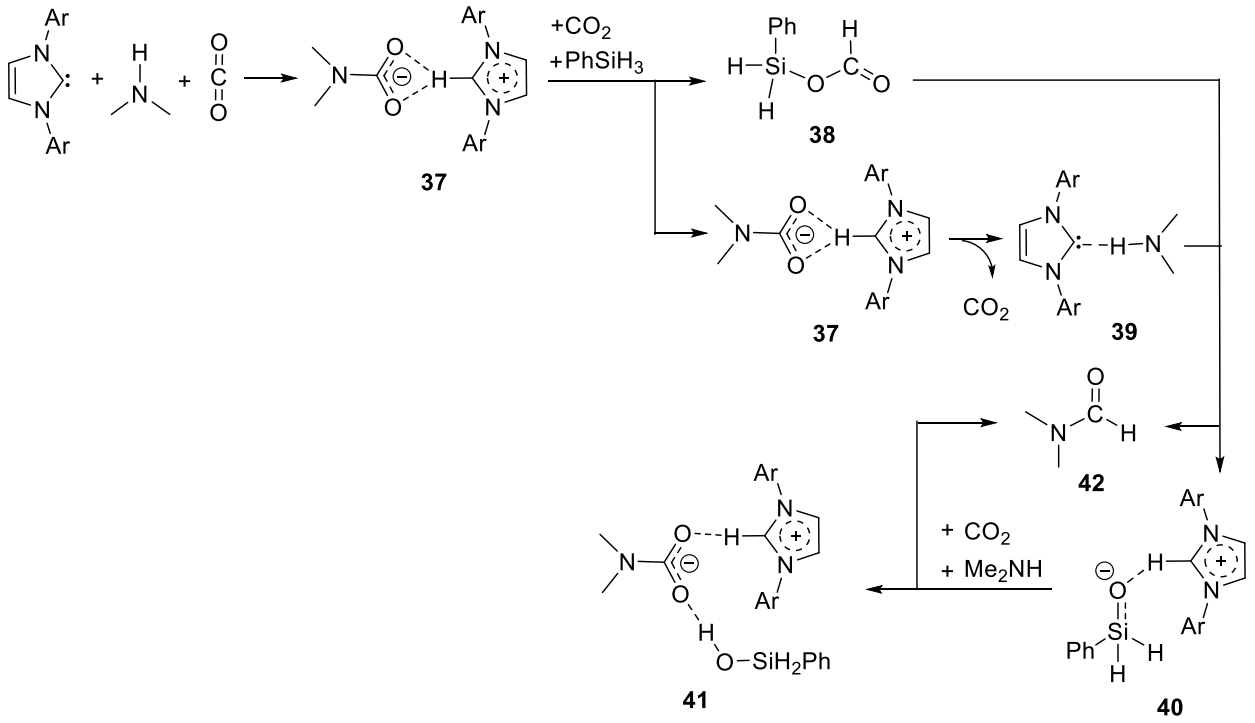

Figure 1.4.7. *The reaction mechanism studied by Li and co-workers*[65]

He and co-workers found that aminals are produced from the reactions between CO_2, amines and silanes under the catalysis of some acetate-based ionic liquids (ILs).[61] Among all the acetate-based ionic liquids analysed, [^{n}Bu$_4$N]OAc shows to be the most efficient catalyst. Based on their experimental results, they did DFT calculations to understand the reaction mechanism. He and co-workers used M06-2X(CH_3CN, SMD)/6-311++G(d,p)//B3LYP/6-31+G(d) for the calculations. The analysed reaction mechanism is detailed in **figure 1.4.8**. CO_2 first reacts with $PhSiH_3$ to produce **43** when CH_3COO^- is the catalyst in the reaction. **43** is further reduced by $PhSiH_3$ under the catalysis of CH_3COO^- to produce **46**. **46** dissociates into **47** and formaldehyde (**48**) under the catalysis of the acetate ion. The addition between formaldehyde and the amine produces **49**. Before **49** has any further reaction, there is an important equilibrium between **43** and CH_3COO^-. The equilibrium is marked in the box in **figure 1.4.8**. In the equilibrium, a complex of both **43** and CH_3COO^-, a complex of both **45** and $HCOO^-$, and **44** can

convert to each other. The reaction between **49** and **45** forms three products: **50**, acetate ion and $PhSiH_2OH$. **50** is positively charged and its reaction with $HCOO^-$ produces **51**. **51** can be converted into either the aminal (**54**) or the methylamine (**53**). When the reactants are **51** and the amine, the products are the aminal (**54**) and HCOOH. When the reactants are **51** and $PhSiH_2OH$, the products are the formamide (**53**) and **52**. In the reaction mechanism shown in **figure 1.4.8**, the rate-determining step is the reaction between **43** and $PhSiH_3$ under the catalysis of acetate ion. This step is highlighted in red in **figure 1.4.8** and its activation free energy barrier is 27.6 kcal/mol.[61]

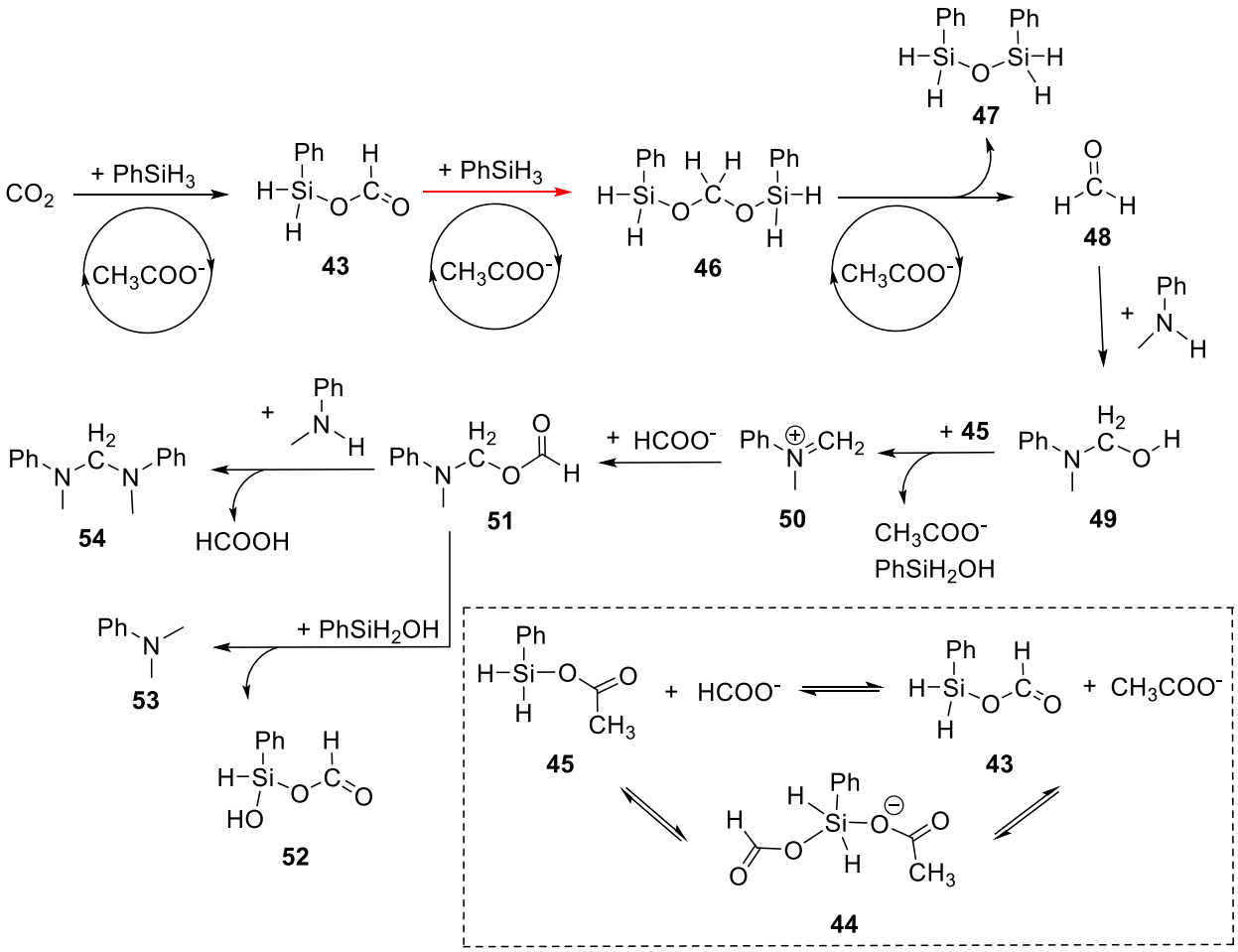

Figure 1.4.8. *Reaction mechanism studied by He and co-workers*[61]

In 2012, Cantat and co-workers did experiments to show that amines can react with CO_2 and $PhSiH_3$ to produce formamides under the catalysis of 1,5,7-triazabicyclo[4.4.0]dec-5-ene (TBD). When the reaction systems have no

solvent, yields of formamides are more than those using THF as the solvent.[20] In 2015, Cantat and co-workers found that TBD efficiently catalyses reactions between amines, CO_2 and $PhSiH_3$ to form aminals when CD_3CN is the solvent.[69] However, how TBD catalyses the formylation and amination reactions is unclear. To understand the reaction mechanisms, Wang and co-workers used M05-2X(SMD)/6-311++G(d,p)//M05-2X/6-31G(d,p) for DFT calculations.[64] **Figure 1.4.9** shows the reaction mechanisms to produce either formamides or aminals. In **figure 1.4.9**, both the neutral mechanism and the anionic mechanism produce the formamide (**60**), while the ionic mechanism forms either the aminal (**73**) or the methylamine (**74**). In terms of the neutral mechanism, the amine reacts with CO_2 and TBD to produce **55**. How **55** converts to **56** is still unknow. **56** is a catalyst in the neutral mechanism and can react with the silane to form **57**. In **57**, a Si-H bond is activated by **56** and the activated Si-H bond enables a free CO_2 molecule to extract the activated hydride. In other words, $PhSiH_3$ reacts with CO_2 under the catalysis of **56** to form **58**. The reaction between **58** and the amine under the catalysis of water produces **59**. Then under the catalysis of H_2O, **59** becomes $PhSiH_2OH$ and the formamide (**60**). No ions appear in the neutral mechanism. However, the ions working in the anionic mechanism are only anions. Regarding the anionic mechanism, **56** converts to both a positively charged ion $[TBD]H^+$ and a negatively charged ion **61**. **61** is a catalyst in the anionic mechanism and its reaction with $PhSiH_3$ forms **62**. In **62**, a Si-H bond is activated by $[N_1]CO_2^-$ and thus helps the hydride from the activated Si-H bond transfer to a free CO_2 molecule. **62** explains how **61** catalyses the reaction between $PhSiH_3$ and CO_2 to form **58**. **58** then reacts with **61** and the amine to produce **63** which further converts to be **64**. Finally, the dissociation of **64** produces $PhSiH_2OH$, **61** and the formamide (**60**). In terms of the ionic mechanism, both a cation and an anion work in reactions. **65** initially becomes a cation **66** and an anion $[TBD]H^+$. Similar to **61** in the anionic mechanism, **66** is able to activate a Si-

H bond in $PhSiH_3$. Therefore, **58** in the ionic mechanism is formed using similar reactions in the anionic mechanism. The reaction between **58**, $PhSiH_3$ and **66** produces both **68** and **69**. The products from the addition of **69** and $[TBD]H^+$ are $PhSiH_2OH$, TBD and formaldehyde (**70**). Formaldehyde reacts with the amine under the catalysis of TBD forms **71**. The reaction between **71** and **68** produces $PhSiH_2OH$, **66** and a positively charged species **72**. When **72** reacts with **66** and $PhSiH_2OH$, products are **75** and the methylamine (**74**). However, the reaction between **72**, **66** and the amine forms $[N_2]COOH$ and the aminal (**73**). In **figure 1.4.9**, the neutral mechanism is calculated in THF solvent, while the anionic mechanism and the ionic mechanism are calculated in CH_3CN solvent. Wang and co-workers hold the view that reactions prefer the neutral mechanism in a weakly polar solvent (e.g. THF), and the reactions in a strongly polar solvent (e.g. CH_3CN) favour either the anionic mechanism or the ionic mechanism. Their explanation was that a strongly polar solvent can promote the dissociation of the zwitterionic carbamate. Wang and co-workers also suggested that aliphatic amines have strong nucleophiles and prefer to undergo formylation, while comparatively weak nucleophiles (e.g. aromatic amines) tend to undergo methylation.[64]

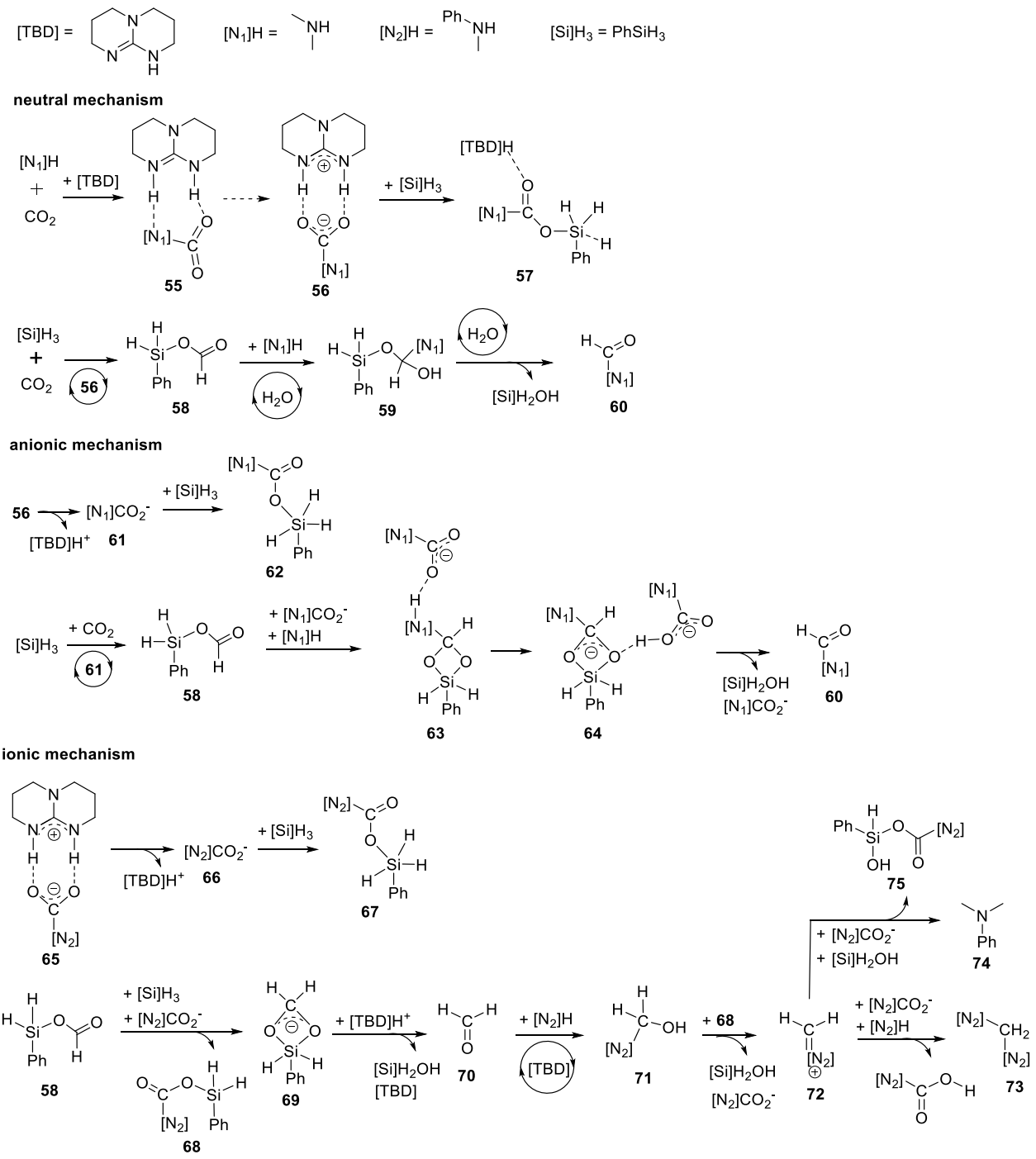

Figure 1.4.9. *Reaction mechanism analysed by Wang and co-workers*[64]

1.5 Experiments analyzing non-metal catalyzed CO_2 reduction

In **chapter 1.4**, reaction mechanisms of formylation, methylation and amination reactions are analysed by DFT calculations. In addition to this

method, this section introduces another way to understand reaction mechanisms that is to examine reaction intermediates in experiments using NMR, GC-MS, exchange NMR spectroscopy (EXSY) and FT-IR.[70, 71] In experiments by Dyson and co-workers, N-methylaniline reacted with phenylsilane in DMSO-d_6 at 25 °C and 20 bar of CO_2 pressure to produce the formamide.[70] Tetrabutylammonium acetate ([TBA][OAc]) was selected as a basic catalyst in their experiments. After using ^{1}H, ^{29}Si and ^{13}C NMR, GC-MS and exchange NMR spectroscopy (EXSY) to find reaction intermediates, they proposed the reaction mechanism in three pathways: pathway 1, pathway 2 and pathway 3. The reaction mechanism is shown in **figure 1.5.1**. In pathway 1, CO_2 is reduced by hydrosilanes to form a mixture of formoxysilanes and the side products are formic acid and various siloxanes.[70] Formoxysilanes then react with amines to form formamides.[72] However, pathway 1 only works for N-methylaniline in the absence of a catalyst.[60] Although [TBA][OAc] can activate the reactions of hydrosilanes with CO_2, N-formylation of amines proceeds along a different pathway in the presence of this catalyst. In terms of pathway 2, the reaction between the amine and CO_2 forms a carbamate salt and this carbamate salt is stabilized by the catalyst. The salt then activates the hydrosilane and the activated hydrosilane reacts with CO_2 to produce the formoxysilane. The reaction between the formoxysilane and the amine forms the formamide. Pathway 2 only works for amines of low basicity. When amines are more basic, N-formylation goes through pathway 3. To understand pathway 3, Dyson changed the amine and the hydrosilane to be benzylamine and triethoxysilane for experiments. Based on their experiments, the amine first reacts with CO_2 to produce benzylcarbamic acid and the acid next reacts with the hydrosilane to form silylcarbamate. Formic acid is also formed in the first two reactions. The reaction between formic acid and silylcarbamate produces formoxysilane and the formoxysilane reacts with the amine to form the final product formamide. When there is excess hydrosilane,

the silylcarbamate is directly reduced to the formamide, which corresponds to pathway 3'.[70]

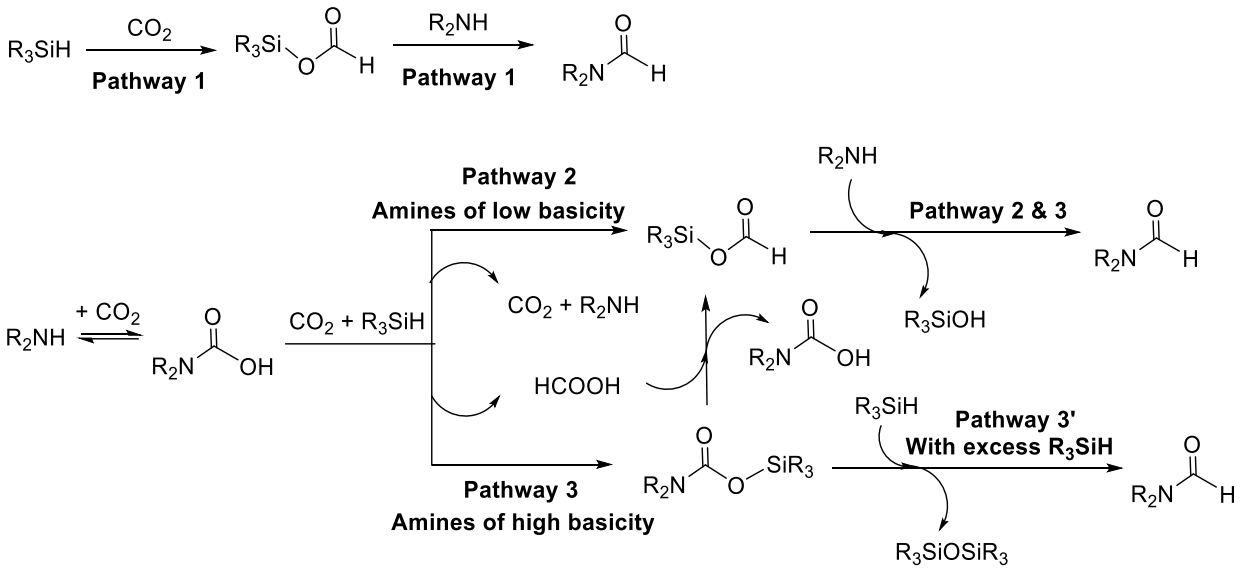

Figure 1.5.1. *The reaction mechanism analysed by Dyson and co-workers[70]*

Nguyen and co-workers did experiments to show that the formamide, the aminal and the methylamine are produced from reactions of the amine, CO_2 and $PhSiH_3$ under the catalysis of N,N,N',N'-tetramethylguanidine (TMG).[71] To investigate their reaction mechanisms, they used NMR, FT-IR, MS and GC to examine reaction intermediates. The reaction mechanisms to produce the formamide, the aminal and the methylamine are proposed in **figure 1.5.2**. In **figure 1.5.2**, reactions happen at two temperatures: 23 °C and 60 °C. At 23 °C, the amine reacts with CO_2 to form Mor-A. Mor-A becomes either Mor-Db or **77**. Mor-Db is converted to either **77** or the formamide (**78**). **77** next produces the formamide (**78**). Since the transformation from Mor-A to **77** is slow, the product (**78**) is most likely produced from Mor-Db through either route **82** or route **83**. At 60 °C, $PhSiH_3$ reacts with CO_2 to produce **77** under the catalysis of TMG. **77** then converts to **79** and the aminal (**80**) sequentially at 60 °C. The subsequent reaction of the aminal in the presence of CO_2 leads to a 1:1 ratio of the methylamine (**81**) and the formamide (**78**) at 23 °C.[71]

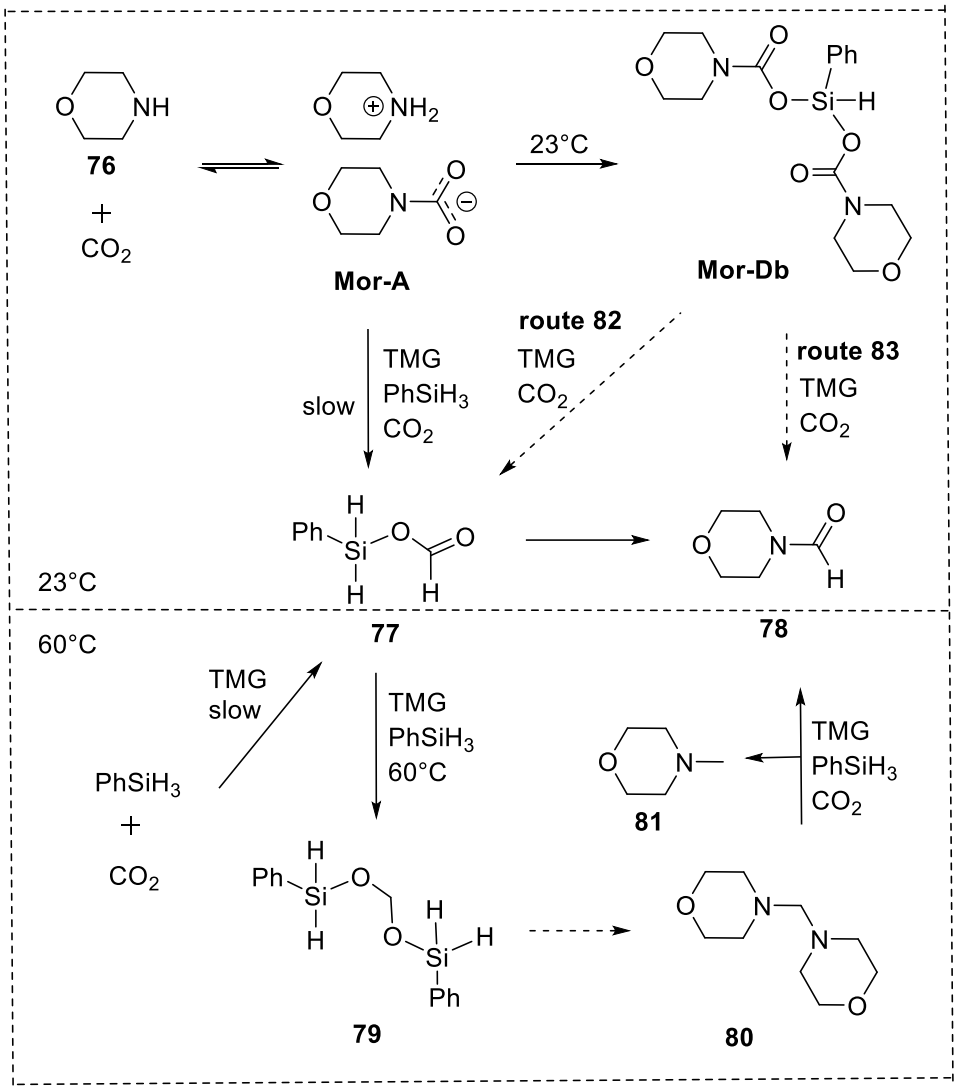

Figure 1.5.2. *Reaction mechanism analysed by Nguyen and co-workers*[71]

1.6 Challenges in non-metal catalyzed CO_2 reduction

One of the promising routes for CO_2 conversion is the synthesis of N-substituted compounds (e.g., formamides, aminals, and methylamines) through the C−N bond formation between CO_2 and amines in the presence of various reductants because these N-substituted compounds are widely used in medicines, agrochemicals, dyes, etc. With H_2 as the reductant, formamides and methylamines can be obtained from the reaction of CO_2 and amines catalysed by metal-based catalysts. However, high temperatures (>100 °C) and/or high pressures (>5 MPa) are generally needed in the reaction. Mild

conversion of CO_2 with amines to form N-substituted compounds is highly attractive in both academia and industry. In recent years, organosilanes have been employed as a class of efficient reductants for converting CO_2 to form N-substituted compounds under milder reaction conditions.[58] Another problem is that the hierarchical reduction of CO_2 with amine and hydrosilane to access formamides, aminals, and methylamines remains unknown.[37] Recently, two research groups reported glycine betaine as an excellent and sustainable organocatalyst for reductive functionalization of CO_2 with various amines and phenylsilane.[37, 58] The two research groups found two-, four-, and six-electron reduction of CO_2 with amines and hydrosilane to give formamides, aminals and methylamines respectively under mild conditions. However, the reaction mechanism of their experiments are unknown.[37, 58]

1.7 Aims and objectives

In this thesis, we utilise computational chemistry methods to study the reaction mechanism of glycine betaine catalysed CO_2 reduction. We investigate the formation of formamides, aminals and methylamines under the catalysis of glycine betaine.

1.8 Thesis outline

This thesis is organised into the following six chapters:

Chapter 1 gives a brief introduction to the field of CO_2 reduction. It identifies the need for the investigation of global warming. It then motivates the need to characterise the role of glycine betaine catalysed CO_2 reduction.

Chapter 2 describes the theoretical background underpinning the work of the thesis. The chapter starts with a description of computational theories.

Chapter 3 starts the investigation into experimental findings of glycine betaine catalysed CO_2 reduction, proposed reaction mechanisms and interactions between reactants and glycine betaine.

Chapter 4 characterises the reaction mechanism to produce formamide, aminal and methylamine under no catalyst.

Chapter 5 investigates the reaction mechanism of glycine betaine catalysed CO_2 reduction.

Chapter 6 summarises research efforts into conclusions and major contributions. The chapter ends by highlighting potential extensions and future research interests.

Chapter 2 Methodology

2.0 Synopsis

This Chapter begins by describing the challenge of modelling chemical systems, which involves using various computational chemistry tools and techniques. It then gives an overview of the core methodologies that allow us to model complex chemical reactions. These include the use of quantum chemical methods to simulate chemical systems, molecular mechanics to characterise chemical systems and thermodynamics to investigate computational chemistry.

2.1 Quantum chemical calculations

Computational chemistry aims to solve chemical problems by simulating chemical systems. There are two main methodological families: those based on quantum chemical (QC) methods and those based on molecular mechanics (MM). Methods based on classical molecular mechanic (MM) are also called force field methods, which ignore the electrons and their motion. The energy of the system is calculated as a function of the nuclear positions only. Because electrons are not explicitly accounted for in the classical MM, very large systems (thousands of atoms) can be simulated to predict conformational flexibility and relative stability. Due to the cheap cost, MM methods are adopted to simulate the dynamics of the nuclear motion within a molecule through molecular dynamic (MD) simulations. In QC methods, electrons are explicitly accounted for, while the presence of electrons in MM is hidden in the force field.

Quantum chemistry (QC) methods are also called electronic structure, first-principles or ab initio methods. QC methods calculate how electrons and nuclei interact by solving the time-independent electronic Schrödinger equation in the Born–Oppenheimer approximation. There are two groups of methods in QC methods: methods based on wave function methods and methods based on the density functional theory (DFT).

2.2 The Schrödinger Equation

Quantum chemical models all ultimately stem from the Schrödinger equation first brought to light in the late 1920's. It treats molecules as collections of nuclei and electrons, without any reference whatsoever to "chemical bonds". The solution to the Schrödinger equation is in terms of the motions of electrons, which in turn leads directly to molecular structure and energy among other observables, as well as to information about bonding. However, the Schrödinger equation cannot actually be solved for any but a one-electron system (the hydrogen atom), and approximations need to be made. Quantum chemical models differ in the nature of these approximations, and span a wide range, both in terms of their capability and reliability and their "cost".

2.3 Born–Oppenheimer approximation

The Born-Oppenheimer approximation is the assumption that the electronic motion and the nuclear motion in molecules can be separated. It leads to a molecular wave function in terms of electron positions and nuclear positions. This involves the following two assumptions. The first assumption is that the electronic wavefunction depends upon the nuclear positions but not upon their velocities, i.e., the nuclear motion is so much slower than electron motion that they can be considered to be fixed. The other assumption is that the nuclear motion (e.g., rotation, vibration) sees a smeared-out potential from the speedy electrons. The Born-Oppenheimer approximation is widely used in quantum chemistry to speed up the computation of molecular wavefunctions

and other properties for large molecules. There are cases where the assumption of separable motion no longer holds, which make the approximation lose validity, but even then the approximation is usually used as a starting point for more refined methods.

2.4 Hartree-Fock theory

Wave function-based methods calculate the explicitly correlated electronic wave functions by solving the electron Schrödinger equation. The simplest wave function-based method is the Hartree–Fock (HF). In the HF, the multielectron wave function is approximated to a single Slater determinant. The approximation neglects the instantaneous electron correlation and leads to a main pitfall of HF. The approximation considers that one electron moves in an averaged field due to the remaining electrons, when in reality the motion of the electrons is correlated (the motion of one electron depends on the instantaneous, mutual interaction with the other electrons). The lack of instantaneous electron correlation introduces an error in the HF wave function. Despite this inaccuracy, the HF solution is systematically improved to produce post-HF methods. One of the post-HF methods uses the many body perturbation theory, which culminates in the Møller–Plesset (MPn) methods. The configuration interaction (CI) methods is another post-HF method. The CI methods express the wave function as a linear combination of Slater determinants. The expression is the HF one plus those representing single, double, triple, etc., excitations. The third post-HF method is the coupled cluster (CC) theory, which also introduces excited state configurations to the wave function. The most popular CC derivation is the CCSD(T) method. Although the post-HF methods have more accurate calculation results, they are computationally expensive and their applicability is hampered by the size of the systems.

2.5 Density Functional Theory

The Density Functional Theory (DFT) was developed by Kohn and Sham in 1965. The central theorem states that the ground state energy of a non-degenerate electronic system can be expressed as a functional E of the total electron density ρ(r), i.e., E[ρ(r)]. In DFT, the ρ(r) for a system of N electrons only depends on 3 spatial coordinates, while the corresponding wave function depends on 3N spatial and N spin variables. Therefore, DFT methods are cheaper than wave function-based methods. In DFT methods, E[ρ(r)] is mathematically demonstrated, but the exact form of E[ρ(r)] is still unknown. Exchange-correlation functional EXC[ρ(r)] searches functionals connecting E and ρ(r), and produces many DFT methods. The simplest approach for EXC[ρ(r)] is the Local Density Approximation (LDA), which implicitly assumes that EXC[ρ(r)] only depends on ρ(r). LDA is improved by the Generalized Gradient Approximation (GGA), in which the EXC[ρ(r)] depends on the density ρ(r) and the gradient of the density ∇ρ(r). Usual GGA methods are PBE, OPBE, PW91 and BLYP. Meta-GGA functionals consider higher order density gradients or the kinetic energy density. The most used meta-GGA functionals are the M06L meta-GGA and the M06. Combination of conventional GGA EXC[ρ(r)] with HF-like electron exchange functional EX(HF) gives the DFT hybrid functionals. Conventional hybrid functionals are B3LYP, BHLYP, PBE0 and wB97X. Because DFT methods do not cope with long-range non-covalent (i.e., dispersion or London) interactions, Grimme proposed a solution to account for dispersion interactions in DFT methods. In Grimme's solution, a posteriori correction term based on an atom–atom additive London-type empirical potential (D) is introduced to supplement the DFT energy. Different correction terms have been proposed (D, D2, D3 and D4).

Although DFT methods are more cost-effective than wave function-based methods, DFT simulations are also limited by the size of the systems up to hundreds or even thousands of atoms. To overcome the size limitations of DFT, semiempirical methods are developed. Semiempirical methods are derived

from the pure QC methods but with different approximations. Due to the simplifications in semiempirical methods, semiempirical methods are faster than their ab initio counterparts, permitting the treatment of large chemical systems.

Basis sets are a linear combination of basic functions that are used to build molecular orbitals. The molecular orbitals constructed in basis sets approximately represent the electronic wave function. Basis sets are used in electronic structure calculations. There are two types of basis sets: Gaussian-type orbitals (GTOs) and plane waves (PWs). GTOs are localized functions centered on the atoms and they are commonly used in molecular calculations. PWs are periodic functions in nature and they are widely used in the simulation of periodic solid-state systems.

2.6 Thermodynamics in computational chemistry

The Gaussian software can provide, through DFT and ab initio calculations, thermodynamic energies (E), enthalpies (H) and Gibbs free energies (G). Calculations for these variables are based on an ideal gas model by assuming non-interacting particles. G is calculated from the summation of the electronic energy (ε_{ele}) and a thermal correction to the Gibbs free energy (G_{corr}). The calculation of G_{corr} consists of two parts: estimation of the entropy (S_{tot}) and a thermal correction to the enthalpy (H_{corr}). H_{corr} is the estimation of how temperature affects enthalpy. H_{corr} is expressed as internal energy (E_{tot}) plus k_BT where k_B is Boltzmann constant. E_{tot} is a sum of the internal energy due to translation (E_t), the internal energy due to electronic motion (E_e), the internal energy due to rotational motion (E_r), and the internal energy due to vibrational motion (E_v). Similarly, S_{tot} is a sum of the entropy due to translation (S_t), the entropy due to electronic motion (S_e), the entropy due to rotational motion (S_r), and the entropy due to vibrational motion (S_v). When Gaussian calculates contributions from electronic motion, the software

assumes that the first electronic excitation energy is much greater than k_BT. Hence, the first and higher excited states are assumed to be inaccessible at any temperature. The energy of the ground state is set to zero when calculating electronic contributions. The contributions from vibrational motions are composed of a product of the contributions from each vibrational mode. Gaussian only considers the real modes, while modes with imaginary frequencies that are flagged with a minus sign in the output file are ignored. The formulae to calculate thermodynamic quantities are shown below.

$$G = \varepsilon_{ele} + G_{corr} \quad \text{(Eqn 2.5.1)}$$

$$G_{corr} = H_{corr} - TS_{tot} \quad \text{(Eqn 2.5.2)}$$

$$H_{corr} = E_{tot} + k_BT \quad \text{(Eqn 2.5.3)}$$

$$S_{tot} = S_t + S_e + S_r + S_v \quad \text{(Eqn 2.5.4)}$$

$$E_{tot} = E_t + E_e + E_r + E_v \quad \text{(Eqn 2.5.5)}$$

2.7 Concluding remarks

In this chapter, we describe quantum chemical methods and thermodynamics in computational chemistry. In the following chapters, we will apply these techniques to compute chemical systems and characterise reaction mechanisms.

Chapter 3 Glycine betaine catalysed CO_2 reduction

3.0 Synopsis

This chapter first introduces experimental findings of glycine betaine catalysed CO_2 reduction for the formation of formamides, aminals, amines. The reaction happens at 100 °C with N-methylaniline, and using hydrosilanes (e.g. $PhSiH_3$) as the hydride source and glycine as the organocatalyst. The proposed reaction mechanism and computational methods used in this research are also presented. Finally, interactions between the reactants and glycine betaine are discussed.

3.1 Experiment findings - glycine betaine catalyzed CO_2 reduction

Recently, Prof. Han's and Prof. He's teams[37, 58] found that glycine betaine is an active organocatalyst which can achieve the hierarchical reduction of CO_2 by changing reaction temperature and the stoichmetric ratio of reactants. In their experiment, CO_2 reacts with amines and hydrosilanes to produce formamides, aminals and methylamines separately in satisfactory yields.[37, 58] **Figure 3.1.1** shows the chemical reaction where the hydrosilane is either $PhSiH_3$ or Ph_2SiH_2. **Table 3.1.1** shows the detailed reaction conditions when forming different products. Han and co-workers mixed 0.5 mmol N-methylaniline, 1 mmol $PhSiH_3$ and 0.5 MPa CO_2 in 1 mL of CH_3CN to make the molar ratio of the amine, $PhSiH_3$ and CO_2 to be 1:2:10. The amount of glycine betaine added into the mixture was 3 mol % and the mixture was kept at room temperature. The experimental results showed that the formamide was

the principal product with small amounts of the methylamine formed, but no aminal was detected. The reaction had over 99% reactant conversion, 95% yield and 95% selectivity. Han and co-workers then changed the molar ratio of the amine, $PhSiH_3$ and CO_2 to be 1:2:2 by mixing 1 mmol N-methylaniline, 2 mmol $PhSiH_3$ and 0.2 MPa CO_2 in 1 mL of CH_3CN. The amount of glycine betaine added was 1.5 mol % and the mixture was then maintained at 100 ° C. After 4 hours reaction, the principal product became the aminal with N,N-dimethylamine and the formamide as side products. The reaction had a conversion of 93 %, a yield of about 84 % and a selectivity of 90 %. The molar ratio of the amine, $PhSiH_3$ and CO_2 was next changed to be 1:4:6 by adding 0.5 mmol N-methylaniline, 2 mmol $PhSiH_3$ and 0.3 MPa CO_2 in 1 mL of CH_3CN. 3 mol % of glycine betaine was also added into the mixture and the temperature of the mixture was at 100 °C. After 6 hours reaction, N,N-dimethylamine was the main product and the side product was only the formamide. The conversion, yield and selectivity of the reaction were 94 %, 80 % and 85 % respectively.[58]

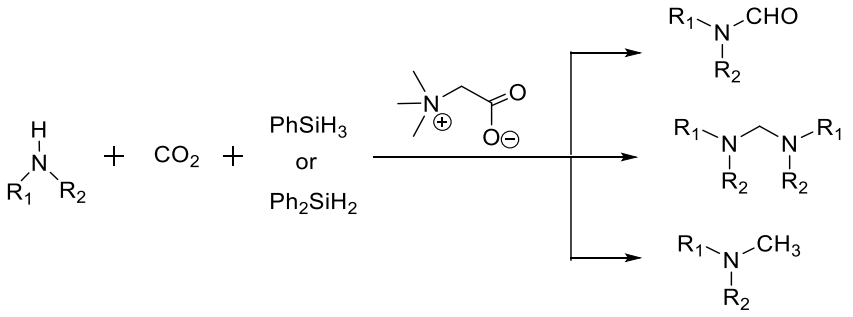

Figure 3.1.1. *Glycine betaine catalysed CO_2 reduction*[58]

Table 3.1.1. *The formation of products under different reaction conditions*[58]

Amines:CO_2: $PhSiH_3$	T (°C)	P (MPa)	Main Product	Time (h)	Yield (%)	Conversion (%)	Selectivity (%)
1:10:2	25	0.5	Formamides	4	95	>99	95
1:2:2	100	0.2	Aminals	4	84	93	90
1:6:4	100	0.3	Methylamines	6	80	94	85

3.2 Reaction mechanism proposal

However, the mechanism of the reaction in **figure 3.1.1** is unclear. This reaction provides a green and efficient method for non-metal catalysed CO_2 reduction. We believe that it is a very promising reaction. Both Prof. Han and Prof. He's teams[37, 58] proposed two reaction mechanisms and the reaction mechanisms are drawn in **figure 3.2.1** and **figure 3.2.2**. The reaction mechanism proposed by Han and co-workers is shown in **figure 3.2.1**. In their proposal, the interaction between glycine betaine and the amine forms intermediate **1**, while the interaction between glycine betaine, the amine and $PhSiH_3$ forms intermediate **2**. In intermediate **2**, the O atom in the carboxylate group in glycine betaine interacts with the H atom in the amine, and the N atom in glycine betaine interacts with the H atom in $PhSiH_3$. Han and co-workers think the interaction between the amine and glycine betaine weakens the intramolecular interaction between the anion and cation groups in glycine betaine, which is beneficial for the interaction between $PhSiH_3$ and glycine betaine. Therefore, Intermediate **2** activates the Si-H bond in $PhSiH_3$ and favours the insertion of CO_2 into the activated Si−H bond. The products from the reaction between CO_2 and Intermediate **2** are various silyl active species which can be silyl formates, bis(silyl)acetal or methoxysilane depending on reaction conditions like the molar ratio of reactants and reaction temperature. In Intermediate **1**, the H atom in the amine interacts with the O atom in the carboxylate group in glycine betaine. By forming Intermediate **1**, the N−H bond in the amine can be activated. The activated nucleophilic N atom in the amine then attacks the carbon atom in the silyl active species to form a new C−N bond. The new generated products are formamides, aminals or methylamines.[58]

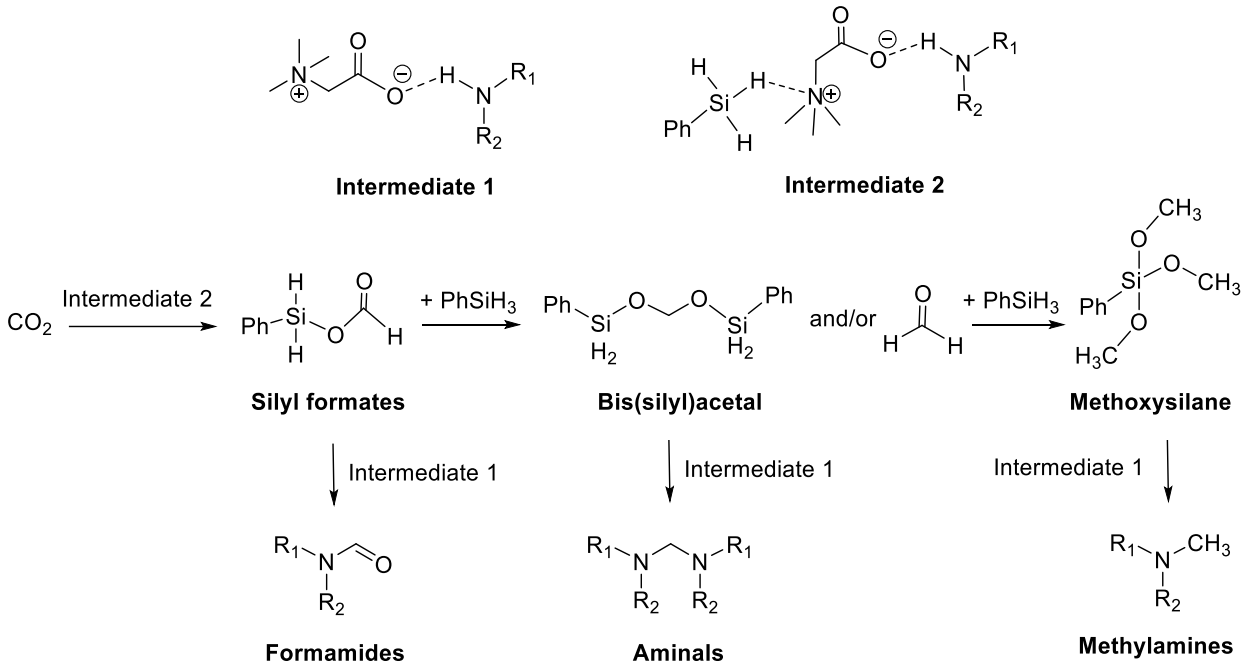

Figure 3.2.1. *The proposed reaction mechanism by Han and co-workers*[58]

The reaction mechanism of the N-methylation reaction proposed by He and co-workers is shown in **figure 3.2.2**. In their experiment, amines, CO_2 and Ph_2SiH_2 under the catalysis of glycine betaine (GB) can produce methylamines and trace amounts of formamides. The formation of formamides may suggest that the formamide might be an intermediate of the methylation reaction. However, He and co-workers found formamides could not be converted into methylamines under the same reaction conditions. Hence, they conclude that formamides should not be the intermediate of the methylation reaction. They also exclude the possibility of ureas and diphenyldimethoxysilane as the intermediates because both ureas and diphenyldimethoxysilane failed to produce methylamines under identical reaction conditions. By using GC-MS, He and co-workers proved the existence of silyl formate, acetal, methoxide, formamides, methylamines and aminals within the reaction time. Aminals were detected with 31 % yield by NMR spectroscopy after 4 hours reaction and they nearly disappeared after 6 hours. He and co-workers consider this phenomenon as an indication of the reaction's intermediate. Further

experiments were carried out to isolate the aminal and react it with Ph_2SiH_2 under identical reaction conditions. The result was that a quantitative yield of the methylamine was produced. Hence, He and co-workers consider the aminal as an intermediate of the N-methylation reaction.[37] According to Cantat and co-workers, the aminal can be obtained from condensation between an amine and C^0 silyl acetal.[69] Based on the experimental evidence from He and co-workers and the paper by Cantat and co-workers, He and co-workers think that N-methylation goes through a C^0 silyl acetal and aminal pathway. To describe the reaction mechanism shown in **figure 3.2.2**, glycine betaine first interacts with Ph_2SiH_2 through the nucleophilic oxygen centre of glycine betaine and silicon centre of Ph_2SiH_2. The interaction forms the hypervalent silicon species **3** bearing an active hydride and the hydride subsequently transfers from **3** to CO_2. The transformation of the hydride delivers the silyl formate **4**, which is further reduced by Ph_2SiH_2 to give the C^0 silyl acetal **5**. Then condensation between **5** and the amine affords the aminal **8**. Finally, **8** is reduced to the methylated product **9** in the presence of glycine betaine and diphenylsilane.[37]

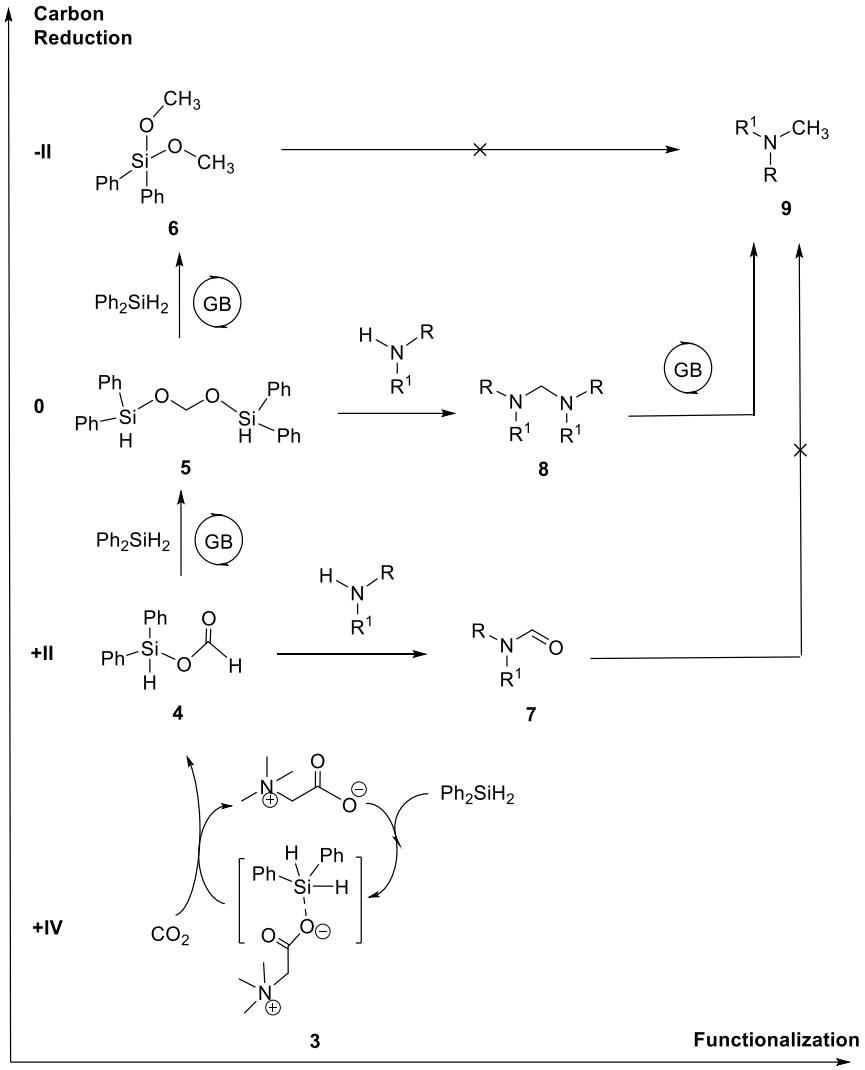

Figure 3.2.2. *The proposed reaction mechanism by He and co-workers*[37]

3.3 Computational methods

As described in **chapter 3.1**, experiments show that amines can react with hydrosilanes and CO_2 under the catalysis of glycine betaine to produce formamides, aminals and methylamines at different reaction conditions.[37, 58] The aim of my project is to understand their reaction mechanisms by DFT calculations. Based on experimental results, when reactants are CO_2, $PhSiH_3$, N-methylaniline and glycine betaine (GB), yields of the formamide, the methylamine and the aminal reach 95%, 80% and 84% respectively.[58] To

understand the reaction mechanisms of the formylation, methylation and amination reactions, interactions between the reactants and the catalyst are first examined to understand how these reactants are activated. These results are discussed from **chapter 3.4.1** to **chapter 3.4.4**. Based on the DFT calculations by Kim and co-workers, energy profiles of the model reactions of CO_2, $PhSiH_3$ and N-methylaniline without the catalyst are presented in **chapter 4**.[60] In **chapter 5**, energy profiles of the formylation, methylation and amination reactions under the catalysis of GB are shown. **Chapter 5.4.2** shows energy profiles of the formylation, methylation and amination reactions under the catalysis of GB when another functional is used for single point calculations. **Chapter 5.4.3** applies an energy correction method to the reaction mechanism of the glycine betaine catalysed formylation, methylation and amination reactions.

Six possible interactions could exist between the catalyst glycine betaine and the three reactants (CO_2, $PhSiH_3$ and N-methylaniline). The six possible interactions are shown in **figure 3.3.1**. Complex **A2** shows the hydrogen bond interaction between glycine betaine and N-methylaniline by the O-H bond. Glycine betaine and $PhSiH_3$ may interact with each other in two possible ways and thus form either complex **B2** or cyclic complex **C**. Complex **B2** indicates the non-bonding interaction of the Si-O bond, while cyclic complex **C** shows the interaction of the N-H bond and the Si-O bond. $PhSiH_3$, glycine betaine and N-methylaniline may also interact in the forms of either complex **D** or cyclic complex **E**. Both complexes show that the three compounds might interact with each other via the N-H bond and the O-H bond. Glycine betaine and CO_2 may interact via a N-O bond and thus form complex **F**. Han and co-workers carried out ^1H NMR studies of the six interactions shown in **figure 3.3.1**.[58] To understand whether the six interactions exist, we carried out DFT calculations using SMD(CH_3CN)[73] ωB97XD[74]/6-31+G(d,p), SMD(CH_3CN)[73] B3LYP[75, 76]/6-31+G(d,p), SMD(CH_3CN)[73] M06-2X[77, 78]/6-31+G(d,p) and

SMD(CH_3CN)[73] B3LYP[75, 76]-D3(BJ)[79]/6-31+G(d,p). Theoretically, ωB97XD, M06-2X and B3LYP-D3 are used when analysing weak interactions, while B3LYP is not suitable to find weak interactions. The diffuse function in 6-31+G(d,p) can help a better indication of non-bonding interactions. The solvation model was added to take into account the reaction environment in the real experiments. Apart from DFT calculations, we calculated NPA charges using NBO 6.0[80], and noncovalent interaction (NCI) using Multiwfn[81] and VMD[82-84]. The calculation results are discussed in **chapter 3.4.1** to **3.4.4**.

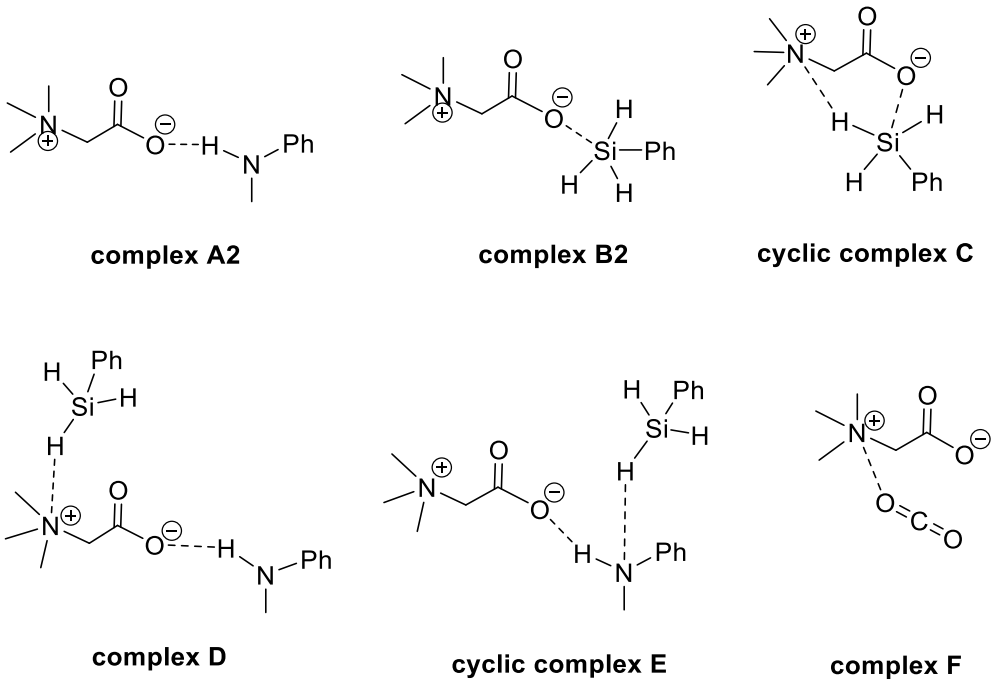

Figure 3.3.1. *Proposed interactions between the reactants and the catalyst*

3.4 Result and discussion

3.4.1 The interaction between N-methylaniline and glycine betaine

In literature, Han and co-workers compared the ^{1}H NMR spectra of N-methylaniline with the ^{1}H NMR spectra of a mixture of N-methylaniline and glycine betaine.[58] Their experiments showed that the ^{1}H signal intensity of N−H in N-methylaniline decreased significantly in the presence of glycine betaine, and the ^{1}H signal of N−CH_3 in N-methylaniline changed from a double

peak (2.77 and 2.76 ppm) to a single peak (2.77 ppm) when glycine betaine was present. Based on the experimental results, they think there is a strong interaction between N-methylaniline and glycine betaine, which can activate the N-H bond in N-methylaniline.[58] **Figure 3.4.1.1** shows the formation of the complex of N-methylaniline and glycine betaine. We used DFT calculations to compute energies (*E*), enthalpies (*H*) and Gibbs free energies (*G*) of N-methylaniline, glycine betaine, and the complex of N-methylaniline and glycine betaine. Energy differences (i.e., Δ*E*, Δ*H* and Δ*G*) of the formation reaction are then calculated. To take Δ*E* as an example, the calculation formula is $\Delta E = E_{\text{complex}} - E_{\text{glycine betaine}} - E_{\text{N-methylaniline}}$. The same methods to calculate Δ*E*, Δ*H* and Δ*G* also apply to **chapter 3.4.2**, **3.4.3** and **3.4.4**. In **table 3.4.1.1**, energy differences in terms of Δ*E*, Δ*H* and Δ*G*, along with the distances between the O atom in glycine betaine and the H atom in N-methylaniline are shown. The values of Δ*E* calculated from the four calculation methods are negative. The O-H bond in H_2O provided from the Gaussian software is 0.96 Å, while the average length of the O-H interaction in complex **A2** is about 1.9 Å. Both of the negative values of Δ*E* and the lengths of the O-H interaction in **table 3.4.1.1** indicate that there is a possible interaction between the O atom in glycine betaine and the H atom in N-methylaniline. A positive or negative Δ*H* shows that the formation of complex **A2** is endothermic or exothermic. A negative sign in Δ*G* is an indication of the bond formation, while a positive Δ*G* means the bond formation cannot happen. **Figure 3.4.1.2** shows the NPA charges calculated by NBO 6.0 using ωB97XD/6-311++G(d,p).[80] The H atom and the O atom in complex **A2** have charges of 0.43 and -0.76 respectively, while the H atom in N-methylaniline and the O atom in glycine betaine have charges of 0.38 and -0.72. The changes in the charges of the H atom and the O atom are about 13% and 5%. The changes in the charge distribution may indicate the O-H interaction in complex **A2**. From **figure 3.4.1.3**, a weak noncovalent interaction is visible

between the hydrogen atom in the amino group of N-methylaniline and the negatively charged oxygen atom in glycine betaine in the noncovalent interaction (NCI) isosurface.[82-84] Based on the judgment from the literature and my calculations, it can be concluded that there is an O-H interaction in the complex of N-methylaniline and glycine betaine.

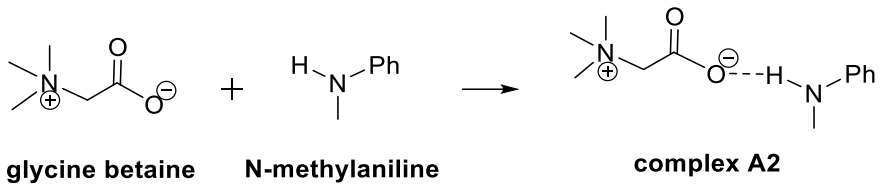

Figure 3.4.1.1. *Formation of the complex of N-methylaniline and glycine betaine*

Table 3.4.1.1. *DFT energetics for the formation of complex* ***A2***

Calculation method	Δ*E* (kcal)	Δ*H* (kcal)	Δ*G* (kcal)	r_{OH} (Å)
SMD(CH_3CN) ωB97XD/6-31+G(d,p)	-7.2	-5.7	5.3	2.0
SMD(CH_3CN) M06-2X/6-31+G(d,p)	-5.5	-3.9	6.3	1.9
SMD(CH_3CN) B3LYP-D3(BJ)/6-31+G(d,p)	-5.8	-4.4	5.3	1.9
SMD(CH_3CN) B3LYP/6-31+G(d,p)	-3.3	-2.0	6.3	1.9

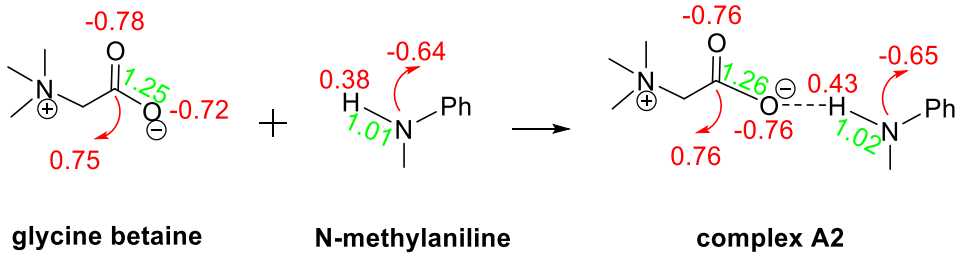

Figure 3.4.1.2. *NPA charges for glycine betaine, N-methylaniline, and their complex. Data were predicted by NBO 6.0 using ωB97XD/6-311++G(d,p) (bond lengths in Å are shown in green; charges are shown in red).*

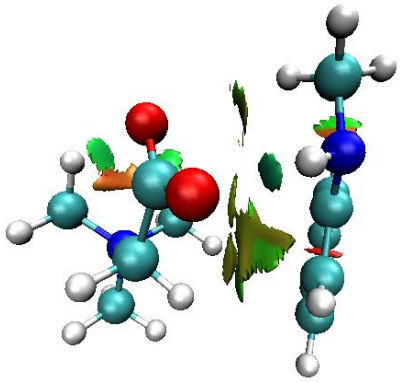

Figure 3.4.1.3. *Glycine betaine and N-methylaniline complex optimised in SMD(CH_3CN) ωB97XD/6-31+G(d,p) level of theory. NCI isosurfaces highlight noncovalent interactions (blue = attractive; green = weakly interacting; red = repulsive). Graphics were produced by CYLview and VMD.*[85, 86]

3.4.2 The interaction between $PhSiH_3$ and glycine betaine

Han and co-workers compared the NMR spectrum of $PhSiH_3$ with the NMR spectrum of the mixture of $PhSiH_3$ and glycine betaine.[58] They found that the ^1H signal of the Si−H proton did not change. Based on this experimental result, Han and co-workers concluded that there was no strong interaction between $PhSiH_3$ and glycine betaine.[58] **Figure 3.4.2.1** shows that two complexes of $PhSiH_3$ and glycine betaine are formed by the Si-O bond, naming as complex **B2** and cyclic complex **C**. In complex **B2**, the ammonium part in glycine betaine seems to interact with the phenyl ring in $PhSiH_3$. However, cyclic complex **C** seems to have the interaction between the hydrogen atom in $PhSiH_3$ and the N atom in glycine betaine. **Table 3.4.2.1** shows the energy differences for forming complex **B2** and cyclic complex **C**, and the lengths of the Si-O interaction in the two complexes. For complex **B2** calculated from the methods ωB97XD and B3LYP-D3(BJ), the values of Δ*E* are quite negative and the distances between the O atom in glycine betaine and the Si atom in $PhSiH_3$ are about 3.5 Å. Since the Gaussian software provides that the bond length of the Si-O bond is 1.83 Å, both of the values of Δ*E* and the lengths of the Si-O interaction show the existence of the Si-O weak interaction. Therefore, the

methods ωB97XD and B3LYP-D3(BJ) indicate that there may be a non-bonding interaction in complex **B2**. In terms of complex **B2** calculated from B3LYP, r_{SiO} is 5.5 Å which is too long for a weak interaction, and the value of Δ*E* is slightly positive. Hence, this method does not find the non-bonding interaction in complex **B2**. For complex **B2** calculated from the M06-2X functional, the length of the Si-O interaction is 2.1 Å which shows the weak interaction. However, Δ*E* is slightly positive. Therefore, it is unclear whether the calculation results from M06-2X are indications of the non-bonding interaction in complex **B2**. In terms of cyclic complex **C** calculated from ωB97XD, M06-2X and B3LYP-D3(BJ), the values of Δ*E* are negative and the average distance of r_{SiO} is around 3.6 Å. Therefore, the three methods can indicate the Si-O non-bonding interaction in cyclic complex **C**. For cyclic complex **C** calculated from B3LYP, Δ*E* is slightly negative. However, the distance between Si and O is 6.2 Å and the distance is too long for a weak interaction. Therefore, this method cannot show the Si-O non-bonding interaction in cyclic complex **C**. It can be concluded from DFT calculations that ωB97XD, M06-2X and B3LYP-D3(BJ) find the Si-O non-bonding interaction in the complex of glycine betaine and $PhSiH_3$, while B3LYP does not indicate the existence of the Si-O interaction. Changes of the NPA charge distribution are shown in **figure 3.4.2.2**. Before the complexes are formed, the O atom in glycine betaine and the Si atom in $PhSiH_3$ have the charges of -0.78 and 0.88 respectively. When the two complexes are formed, the charges of the O atom in glycine betaine and the Si atom in $PhSiH_3$ become -0.79 and 0.90 in both complexes. Charges of the O atom and the Si atom have about 1% and 2% changes. Since the changes in the charge distribution are insignificant, **figure 3.4.2.2** fails to indicate the non-bonding interaction between the Si atom and the O atom in complex **B2** and cyclic complex **C**. In cyclic complex **C**, the H atom in $PhSiH_3$ is initially proposed to interact with the N atom in glycine betaine. However, in **figure 3.4.2.2**, both the H atom and the N atom are negatively charged. Therefore,

the N-H interaction does not exist in cyclic complex **C**. **Figure 3.4.2.3** shows the weak non-bonding interaction between Si and O in both complex **B2** and cyclic complex **C**.[82-84] To sum up, it is very likely that the Si-O non-bonding interaction exists in the complex of glycine betaine and $PhSiH_3$. However, the positive sign in free energy difference suggests that this interaction is not strong enough to overcome the energy loss.

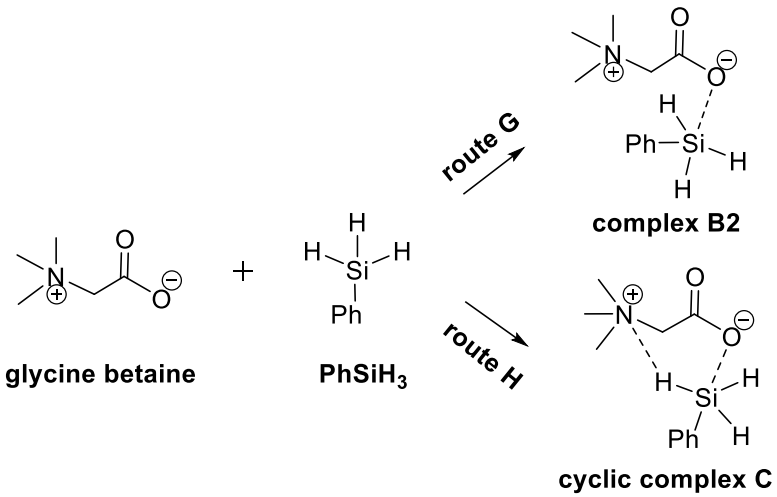

Figure 3.4.2.1. *The formation of the complex of $PhSiH_3$ and glycine betaine*

Table 3.4.2.1. *DFT energetics of the complex **B2** and the cyclic complex **C***

Product	Calculation method	Δ*E* (kcal)	Δ*H* (kcal)	Δ*G* (kcal)	r_{SiO} (Å)
Complex **B2**	SMD(CH_3CN) ωB97XD/6-31+G(d,p)	-4.2	-2.6	8.0	3.3
	SMD(CH_3CN) M06-2X/6-31+G(d,p)	0.0	2.7	14.2	2.1
	SMD(CH_3CN) B3LYP-D3(BJ)/6-31+G(d,p)	-4.3	-3.0	7.2	3.6
	SMD(CH_3CN) B3LYP/6-31+G(d,p)	0.0	1.3	5.9	5.5
Cyclic complex **C**	SMD(CH_3CN) ωB97XD/6-31+G(d,p)	-3.6	-1.9	8.2	3.7
	SMD(CH_3CN) M06-2X/6-31+G(d,p)	-5.5	-3.4	7.4	3.1
	SMD(CH_3CN) B3LYP-D3(BJ)/6-31+G(d,p)	-4.3	-2.9	7.4	3.9
	SMD(CH_3CN) B3LYP/6-31+G(d,p)	-0.2	1.2	8.4	6.2

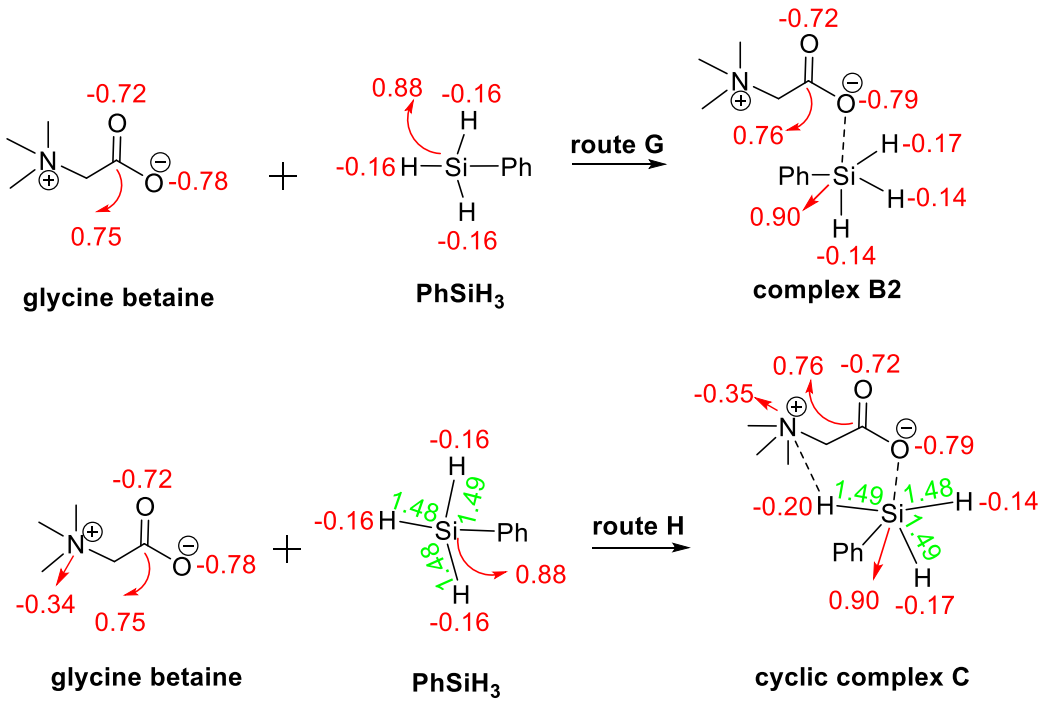

Figure 3.4.2.2. *NPA charges for glycine betaine, $PhSiH_3$, and their complex. Data were predicted by NBO 6.0 using ωB97XD/6-311++G(d,p) (bond lengths in angstroms are shown in green; charges are shown in red).*

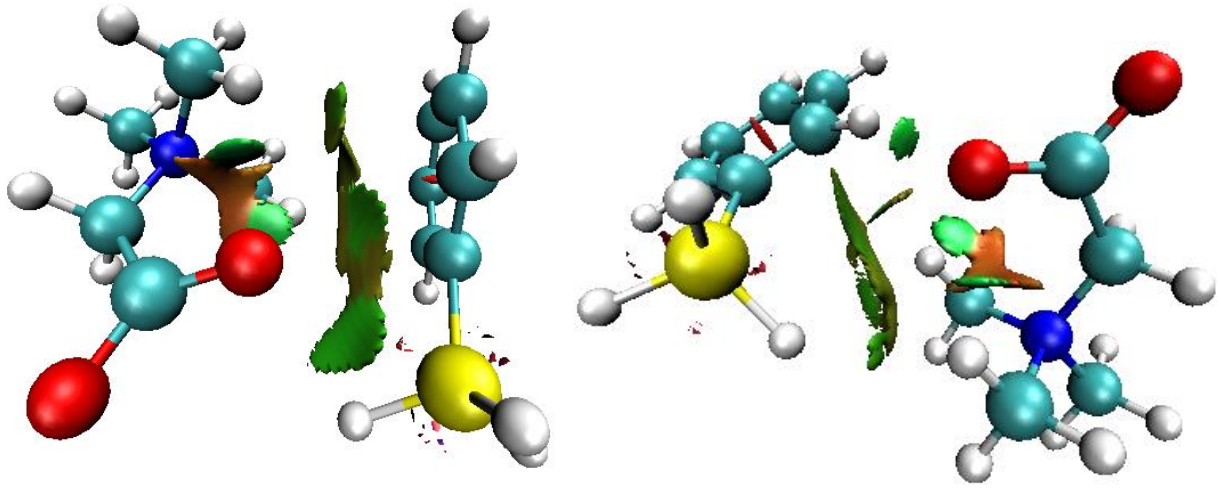

Figure 3.4.2.3. *Glycine betaine and $PhSiH_3$ complexes optimised in SMD(CH_3CN) ωB97XD/6-31+G(d,p) level of theory. NCI isosurfaces highlight noncovalent interactions (blue = attractive; green = weakly interacting; red = repulsive). Graphics were produced by CYLview and VMD.*[85, 86]

3.4.3 The interaction between $PhSiH_3$, N-methylaniline and glycine betaine

Based on the NMR experiments by Han and co-workers, the ^1H signal of the Si−H proton shifted from 4.18 to 4.19 ppm when N-methylaniline was added to the mixture of $PhSiH_3$ and glycine betaine.[58] Therefore, they think there is an interaction between $PhSiH_3$, N-methylaniline and glycine betaine.[58] In **figure 3.4.3.1**, two complexes of $PhSiH_3$, N-methylaniline and glycine betaine are formed which are complex **D** and cyclic complex **E**. Complex **D** was proposed by Han and co-workers and they thought there were N-H and O-H interactions.[58] In cyclic complex **E**, the proposed O-H interaction is the same as the one in complex **D**, while another N-H interaction is proposed. **Table 3.4.3.1** presents the energy differences for forming complex **D** and cyclic complex **E**, and the bond lengths of the N-H interactions in the two complexes. In terms of complex **D** calculated from the four functionals, the values of ΔE are quite negative and the average bond length of the N-H interaction is 4.3 Å. Because the N-H bond provided from the Gaussian software is 1.0 Å, the length of the N-H interaction proposed in complex **D** is too long for the interaction to exist. Since the O-H interaction between glycine betaine and N-methylaniline is already shown in **chapter 3.4.1**, the negative values of ΔE for forming complex **D** may be due to the formation of the O-H interaction. Therefore, the four methods fail to indicate the existence of the N-H interaction in complex **D**. In terms of cyclic complex **E**, calculation results from the four functionals provide negative values of ΔE and an average distance between N and H of 3.4 Å. Since the average distance is too long for the N-H interaction to exist, DFT calculations find that the N-H interaction does not exist in cyclic complex **E**. Therefore, DFT calculations in **table 3.4.3.1** fail to show two N-H interactions in complex **D** and cyclic complex **E**. **Figure 3.4.3.2** presents the charge distribution in isolated structures and their complexes. In complex **D**, the N atom in glycine betaine and the H atom in $PhSiH_3$ are

negatively charged and their NPA charges stay the same before and after forming the complex. In cyclic complex **E**, the N atom in N-methylaniline and the H atom in $PhSiH_3$ have negative charges. It can be concluded from **figure 3.4.3.2** that there are no N-H interactions in complex **D** and cyclic complex **E**. **Figure 3.4.3.3** shows noncovalent interactions between glycine betaine, $PhSiH_3$ and N-methylaniline.[82-84] In terms of complex **D**, the H atom in $PhSiH_3$ interacts with the H atom in glycine betaine instead of the N atom in glycine betaine.[82-84] The weak interaction is also indicated from the distance between the two H atoms and changes in the NPA charges. For complex **D** calculated from SMD(CH_3CN) ωB97XD/6-31+G(d,p), the distance between the H atom in $PhSiH_3$ and the H atom in glycine betaine is 2.5 Å. The NPA charges are shown in **figure 3.4.3.2**. In **figure 3.4.3.2**, the two hydrogen atoms in complex **D** have charges of -0.16 and 0.24 respectively. However, before complex **D** is formed, the two H atoms have charges of -0.16 and 0.22. By forming complex **D**, the charge of the H atom in glycine betaine changes about 8%. In terms of non-bonding interactions in cyclic complex **E**, the N atom in N-methylaniline interacts with the Si atom in $PhSiH_3$ instead of the H atom in $PhSiH_3$.[82-84] The interaction is also indicated from the distance between the N atom in N-methylaniline and the Si atom in $PhSiH_3$ and changes in the NPA charges. For cyclic complex **E** calculated from SMD(CH_3CN) ωB97XD/6-31+G(d,p), the distance between the N atom in N-methylaniline and the Si atom in $PhSiH_3$ is 4.3 Å. NPA charges are calculated in **figure 3.4.3.2**. In **figure 3.4.3.2**, the N atom and the Si atom in cyclic complex **E** have charges of -0.68 and 0.88. However, before cyclic complex **E** is formed, the N atom in N-methylaniline and the Si atom in $PhSiH_3$ have charges of -0.64 and 0.88. The charge of the N atom in N-methylaniline changes about 6%. Therefore, **figure 3.4.3.3** shows that no N-H interactions exist in complex **D** and cyclic complex **E**. Based on all the information, I think no N-H interaction exists in

the complex of $PhSiH_3$ and glycine betaine, and no oxygen-hydrogen interaction exists between glycine betaine and N-methylaniline.

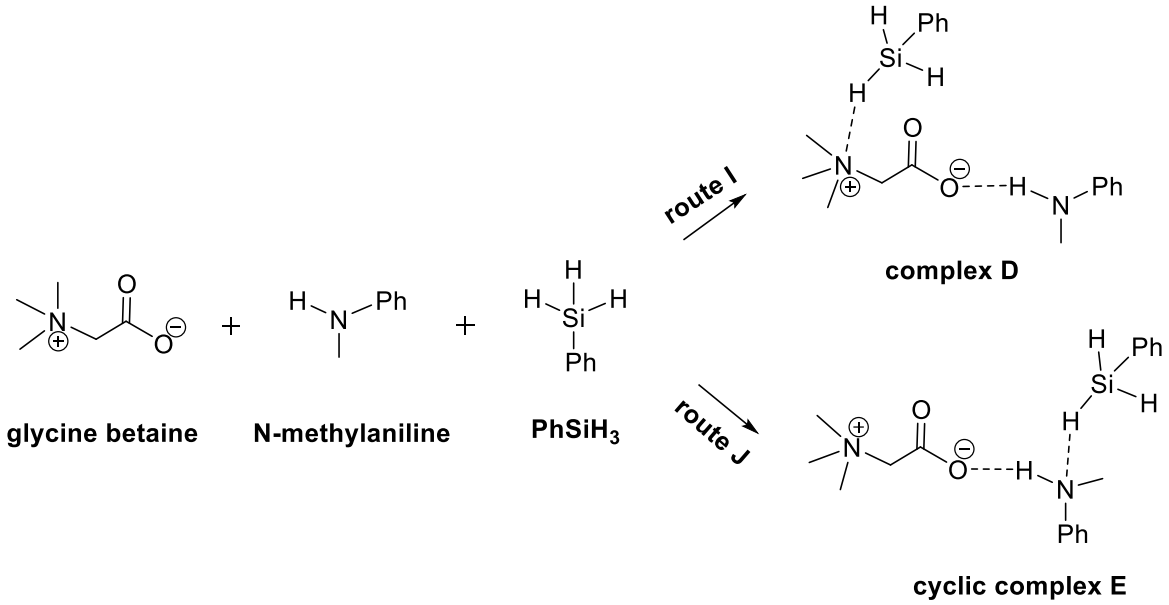

Figure 3.4.3.1. *Proposed comlexed D and E formed from $PhSiH_3$, N-methylaniline and glycine betaine*

Table 3.4.3.1. *DFT energetics of complex **D** and cyclic complex **E***

product	Calculation method	Δ*E* (kcal)	Δ*H* (kcal)	Δ*G* (kcal)	r_{NH} (Å)
complex **D**	SMD(CH_3CN) ωB97XD/6-31+G(d,p)	-15.6	-12.7	10.2	4.0
	SMD(CH_3CN) M06-2X/6-31+G(d,p)	-12.6	-8.8	13.8	3.9
	SMD(CH_3CN) B3LYP-D3(BJ)/6-31+G(d,p)	-15.1	-12.1	10.8	4.1
	SMD(CH_3CN) B3LYP/6-31+G(d,p)	-3.4	-1.4	15.8	5.1
cyclic complex **E**	SMD(CH_3CN) ωB97XD/6-31+G(d,p)	-14.4	-11.1	12.0	3.1
	SMD(CH_3CN) M06-2X/6-31+G(d,p)	-10.0	-7.8	13.4	3.0
	SMD(CH_3CN) B3LYP-D3(BJ)/6-31+G(d,p)	-14.3	-11.3	11.7	4.1
	SMD(CH_3CN) B3LYP/6-31+G(d,p)	-3.4	-0.7	15.1	3.3

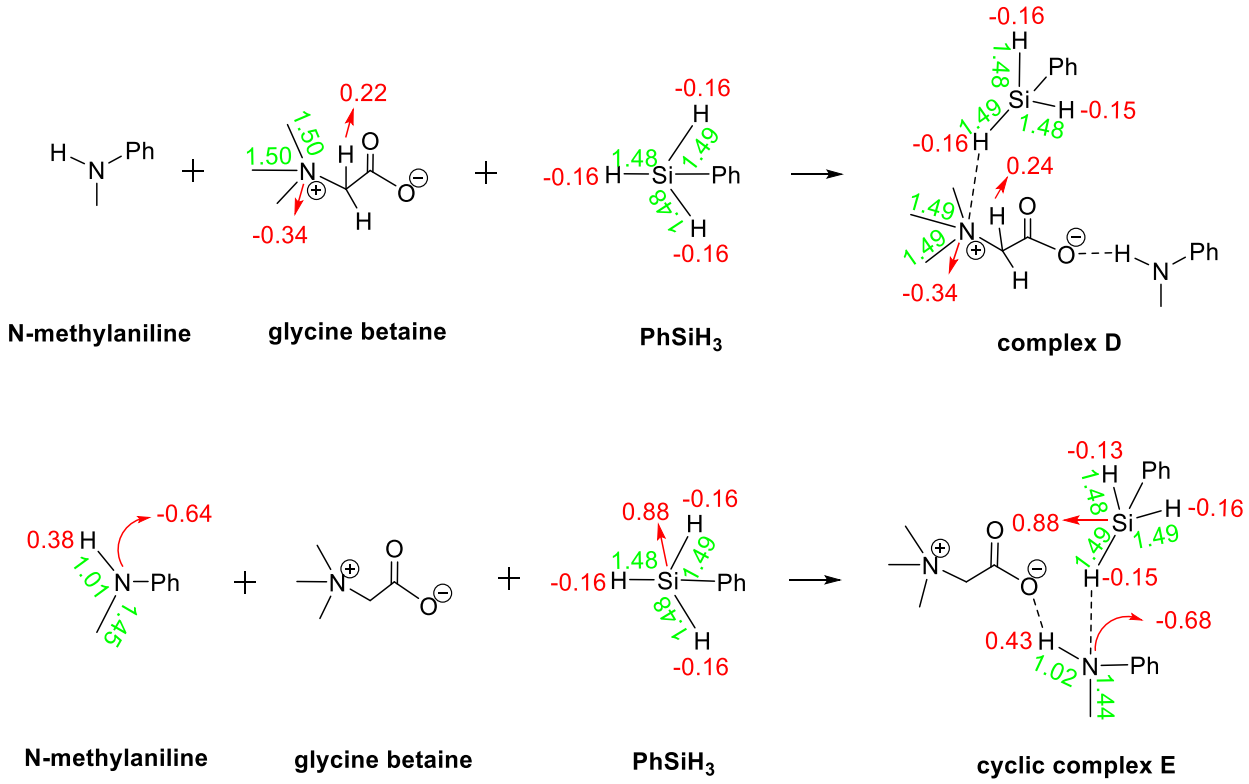

Figure 3.4.3.2. *NPA charges for glycine betaine, N-methylaniline, $PhSiH_3$, and their complexes. Data were predicted by NBO 6.0 using ωB97XD/6-311++G(d,p) (bond lengths in angstroms are shown in green; charges are shown in red).*

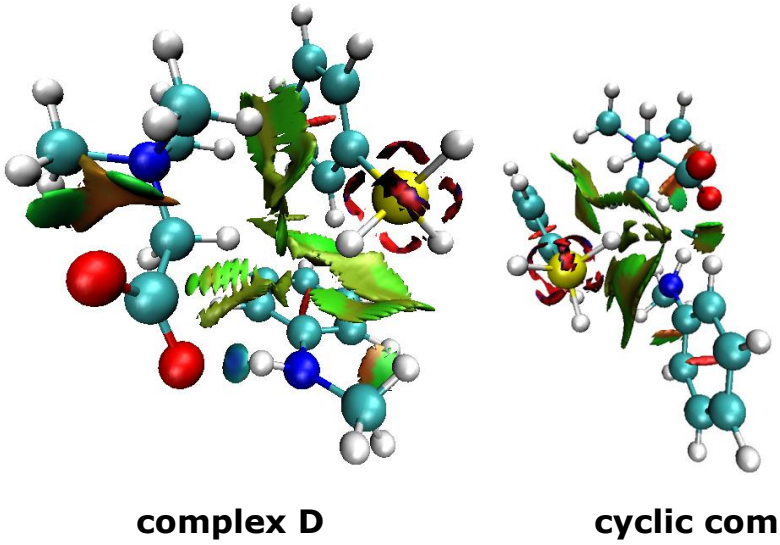

Figure 3.4.3.3. *Glycine betaine, N-methylaniline and $PhSiH_3$ complexes optimised in SMD(CH_3CN) ωB97XD/6-31+G(d,p) level of theory. NCI isosurfaces highlight noncovalent interactions (blue = attractive; green = weakly interacting; red = repulsive). Graphics were produced by CYLview and VMD.*[85, 86]

3.4.4 The interaction between CO_2 and glycine betaine

Han and co-workers did experiments to compare the NMR spectra of glycine betaine with the NMR spectra of the mixture of CO_2 and glycine betaine.[58] They found that there was no new signal or chemical shift in the ^{1}H and ^{13}C NMR spectra. Based on the experimental results, Han and co-workers think glycine betaine cannot activate CO_2 noticeably.[58] **Figure 3.4.4.1** shows the formation of complex **F**. **Table 3.4.4.1** shows the energy differences for the formation of complex **F**, and the distances between the N atom and the O atom in complex **F**. In **table 3.4.4.1**, complex **F** calculated from the four functionals have negative values of ΔE and an average length of the N-O interaction of 4.8 Å. Since the N-O bond provided from the Gaussian software is 1.4 Å, the average length of the N-O interaction calculated from **table 3.4.4.1** is too long for the weak interaction to exist. Therefore, DFT calculations fail to indicate the non-bonding interaction between glycine betaine and CO_2. **Figure 3.4.4.2** explains how the NPA charges change in isolated structures and their complex. Since the N atom in glycine betaine and the O atom in CO_2 have negative charges in complex **F**, there cannot be weak interactions between the N atom and the O atom. Therefore, **figure 3.4.4.2** shows that no weak interactions exist in complex **F**. In **figure 3.4.4.3**, the O atom in CO_2 interacts with the H atom in glycine betaine instead of the N atom in glycine betaine.[82-84] The interaction is also shown from the distance between the O atom in CO_2 and the H atom in glycine betaine, and changes in the NPA charges. For complex **F** calculated from SMD(CH_3CN) ωB97XD/6-31+G(d,p), the distance between the O atom and H atom is 3.3 Å. As shown in **figure 3.4.4.2**, although the charge of the H atom in glycine betaine does not change before and after forming complex **F**, the charge of the O atom in CO_2 changes from -0.51 to -0.53 after complex **F** is formed. The charge of the O atom in CO_2 changes about 4% and this change is an indication of the O-H interaction in complex **F**. Therefore, **figure 3.4.4.3** shows no weak interaction

between the N atom and the O atom in complex **F**. In conclusion, there is no non-bonding interactions between the N atom in glycine betaine and the O atom in CO_2.

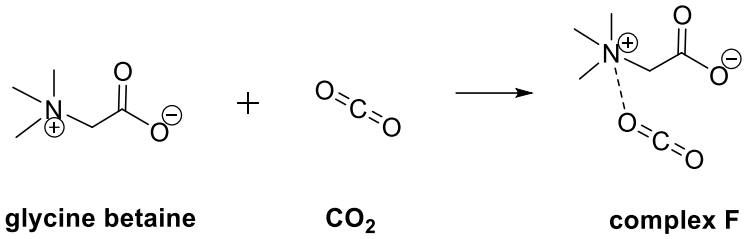

Figure 3.4.4.1. *Complex F formed from CO_2 and glycine betaine*

Table 3.4.4.1. *DFT energetics of complex* ***F***

Calculation method	Δ*E* (kcal)	Δ*H* (kcal)	Δ*G* (kcal)	r_{NO} (Å)
SMD(CH_3CN) ωB97XD/6-31+G(d,p)	-0.8	0.3	6.0	4.4
SMD(CH_3CN) M06-2X/6-31+G(d,p)	-0.5	0.5	6.5	4.5
SMD(CH_3CN) B3LYP-D3(BJ)/6-31+G(d,p)	-3.3	-2.3	4.3	4.3
SMD(CH_3CN) B3LYP/6-31+G(d,p)	-0.1	0.9	5.6	6.1

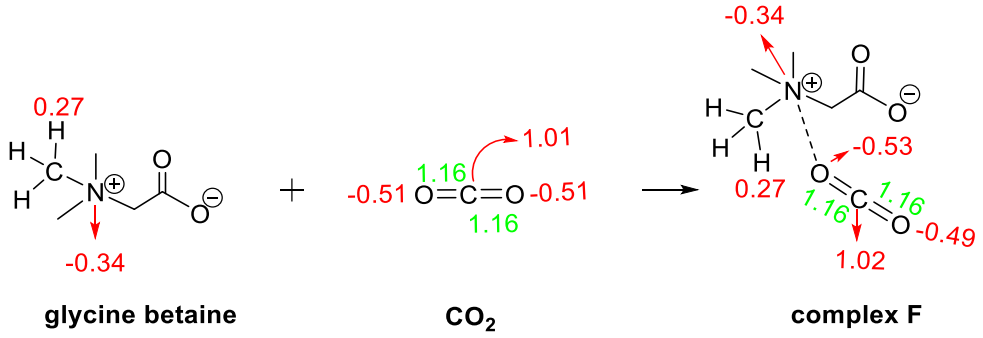

Figure 3.4.4.2. *NPA charges for glycine betaine, CO_2, and their complex. Data were predicted by NBO 6.0 using ωB97XD/6-311++G(d,p) (bond lengths in angstroms are shown in green; charges are shown in red).*

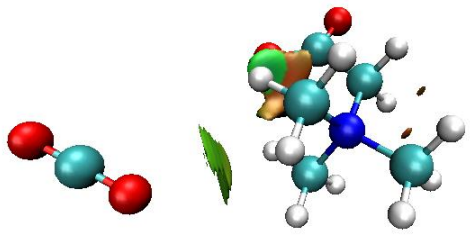

Figure 3.4.4.3. *Glycine betaine and CO_2 complex optimised in SMD(CH_3CN) ωB97XD/6-31+G(d,p) level of theory. NCI isosurfaces highlight noncovalent interactions (blue = attractive; green = weakly interacting; red = repulsive). Graphics were produced by CYLview and VMD.*[85, 86]

Chapter 4 Reaction pathway without catalysts

4.0 Synopsis

This chapter introduces the reaction mechanism of the model reactions between CO_2, $PhSiH_3$ and N-methylaniline under no catalysts. Three possible reaction pathways were proposed and studied (see Figure 4.1). As the Gibbs free energy activation barriers for all the three pathways are great than 40 kcal/mol, we conclude that a catalyst would be needed to promote this transformation.

Kim and co-workers analysed the mechanism of methylation of N-methylaniline with CO_2 and $PhSiH_3$ using DFT at the M05-2X(THF, SMD)/6-311++G**//M05-2X/6-31G* level.[60] Their reactions are model reactions with no catalyst and I recalculated part of these reactions at SMD(CH_3CN)[73] ωB97XD[74]/6-311++G(d,p)//ωB97XD[74]/6-31+G(d,p) level of theory. The reaction mechanism from my calculations is shown in **figure 4.1**. In **figure 4.1**, there are three reaction pathways: pathway 1, pathway 2 and pathway 3. Energy profiles of the three pathways are shown from **figure 4.2** to **figure 4.4**. In energy profiles, the Gibbs free energy of reference points are set to be zero and the reference points contain isolated reactants (i.e., CO_2, $PhSiH_3$ and N-methylaniline). **Figure 4.2** shows the two reactions in pathway 1. $PhSiH_3$ first reacts with CO_2 to form a four membered ring. Then the O atom and the H atom in the four membered ring in **TS'$_{1-2}$** are added to the Si atom

and the C atom respectively. The product becomes formoxysilane (**II'**). Next, the reaction between formoxysilane and $PhSiH_3$ produces another four membered ring. In the new four membered ring in **TS'$_{3-5}$**, the O atom and the H atom are added to the Si atom and the C atom separately. The product from **TS'$_{3-5}$** is bis(silyl)-acetal (**IV'**) and the activation free energy barrier ($\Delta G^{\ddagger}_{sol}$) of **TS'$_{3-5}$** is 52.2 kcal/mol. The rate-determining step (RDS) of pathway 1 is step involving **TS'$_{3-5}$**. **Figure 4.3** shows the reactions in pathway 2. Initially, CO_2 reacts with N-methylaniline to form the carbamic acid **XI'** *via* **TS'$_{10-11}$** with a Gibbs free energy activation barrier of 45.7 kcal/mol. Then carbamic acid reacts with $PhSiH_3$ to form either **TS'$_{12-14}$** or **TS'$_{12-13}$**. The difference between **TS'$_{12-14}$** and **TS'$_{12-13}$** is that a different O atom is added to the Si atom in the four membered rings. However, both four membered rings have the same H atom added to the C atom. The products from **TS'$_{12-14}$** and **TS'$_{12-13}$** are a complex of the formamide and phenylsilanol (**XIV'**) and **XIII'** respectively. The Gibbs free energy barriers of **TS'$_{12-14}$** and **TS'$_{12-13}$** are 73.2 and 59.6 kcal/mol. Because **TS'$_{12-14}$** has a higher activation free energy barrier than **TS'$_{12-13}$**, pathway 2 prefers to go through **TS'$_{12-13}$**, although both pathways are with high activation barriers. The RDS in pathway 2 is **TS'$_{12-13}$**. **Figure 4.4** presents the two reactions in pathway 3. Firstly, the reaction between $PhSiH_3$ and CO_2 forms **II'** and this reaction is the same as the first reaction in pathway 1. Secondly, **II'** reacts with N-methylaniline to form **TS'$_{22-14}$**. In the four membered ring in **TS'$_{22-14}$**, the H atom and the C atom are added to the O atom and the N atom separately. The product from **TS'$_{22-14}$** is a complex of the formamide and phenylsilanol (**XIV'**). Since **TS'$_{1-2}$** and **TS'$_{22-14}$** have Gibbs free energiesof 49.3 and 36.4 kcal/mol, **TS'$_{1-2}$** is the RDS in pathway 3. Because the activation free energy barriers of the rate-determining steps in the three pathways are more than 40 kcal/mol, none of the three pathways are feasible.

Based on my calculations, **TS'$_{1\text{-}2}$** have two conformers and they are shown in **figure 4.5**. There are many differences between **TS'$_{1\text{-}2\_2}$** and **TS'$_{1\text{-}2}$**, for example, the activation free energy barriers and the bond lengths of the four membered rings. These differences exist due to different positions where CO_2 comes towards $PhSiH_3$. Because **TS'$_{1\text{-}2}$** has a lower $\Delta G^{\ddagger}_{sol}$ than **TS'$_{1\text{-}2\_2}$**, **TS'$_{1\text{-}2}$** is more favourable and selected as the transition state in the reaction to produce **II'**.

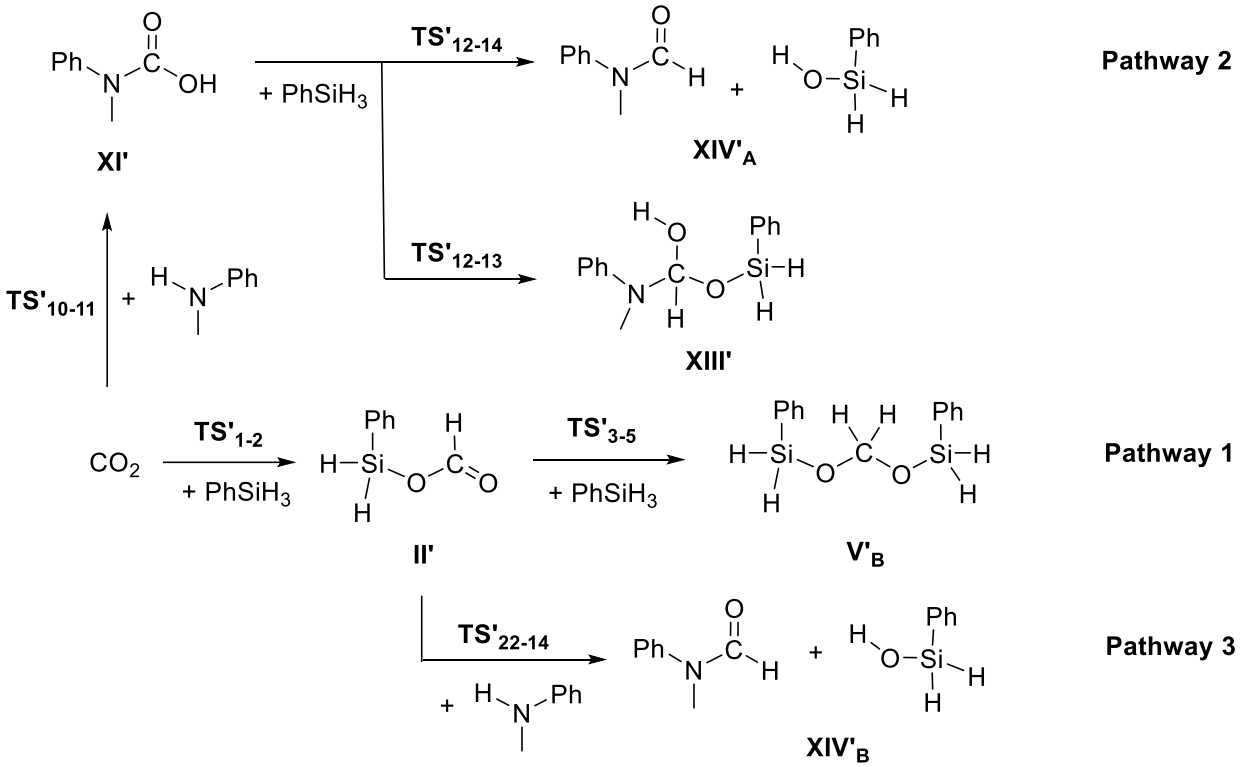

Figure 4.1. *The proposed reaction mechanisms for the non-catalysed reaction between CO_2, $PhSiH_3$ and N-methylaniline*[60]

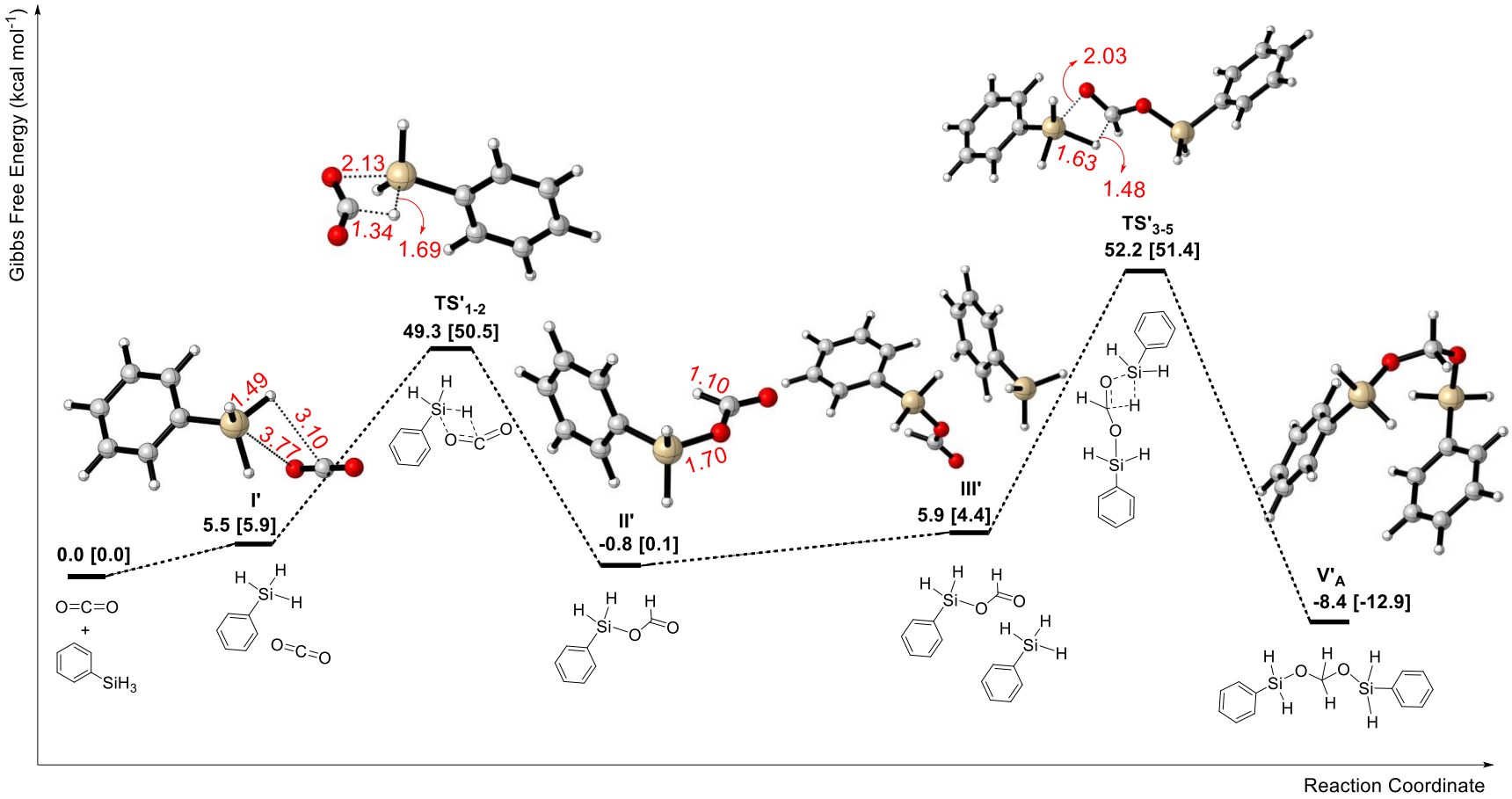

Figure 4.2. Computed free-energy profile for pathway 1. *The relative free energies given in kcal mol^{-1} are calculated with SMD(CH_3CN) ωB97XD/6-311++G(d,p)//ωB97XD/6-31+G(d,p). Free energies calculated in gas phase are quoted in square brackets. Bond distances are shown in Å in red. Molecular graphics were produced by CYLview.*

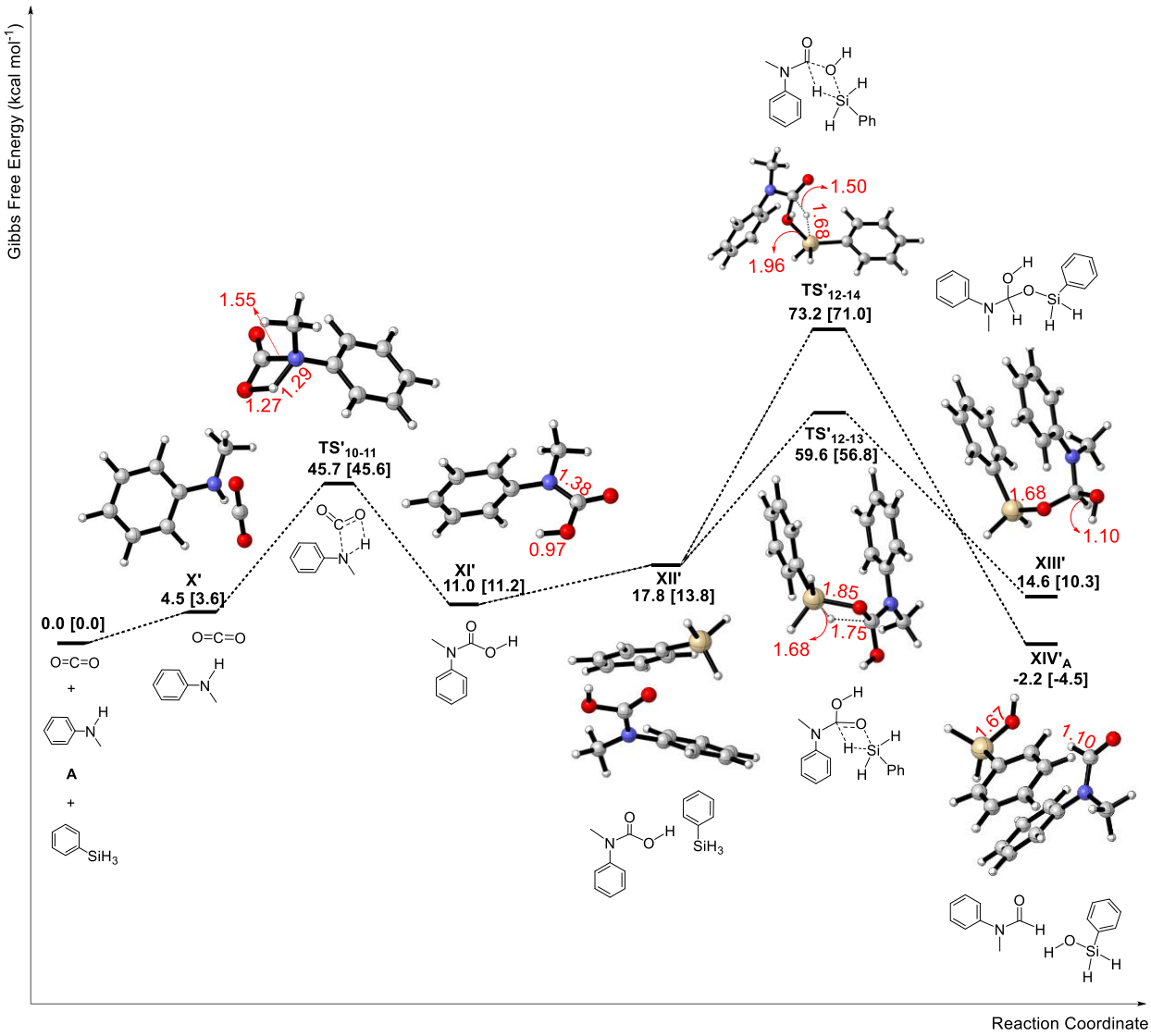

Figure 4.3. Computed free-energy profile for pathway 2. *The relative free energies given in kcal mol^{-1} are calculated by using SMD(CH_3CN) ωB97XD/6-311++G(d,p)//ωB97XD/6-31+G(d,p). Free energies calculated in gas phase are quoted in square brackets. Bond distances are shown in Å in red. Molecular graphics were produced by CYLview.*

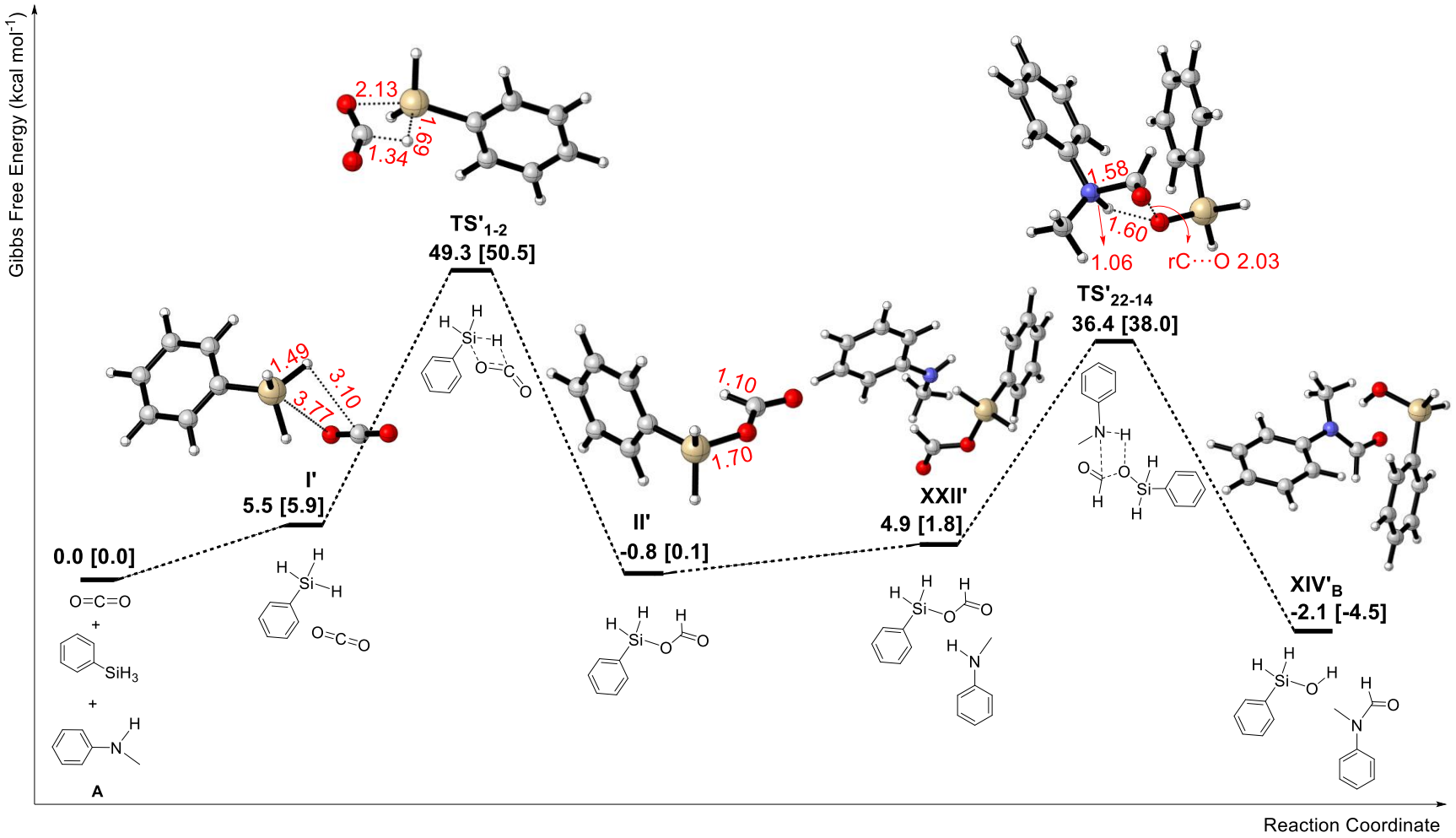

Figure 4.4. Computed free-energy profile for pathway 3. *The relative free energies given in kcal mol^{-1} are calculated by using SMD(CH_3CN) ωB97XD/6-311++G(d,p)//ωB97XD/6-31+G(d,p). Free energies calculated in gas phase are quoted in square brackets. Bond distances are shown in Å in red. Molecular graphics were produced by CYLview.*

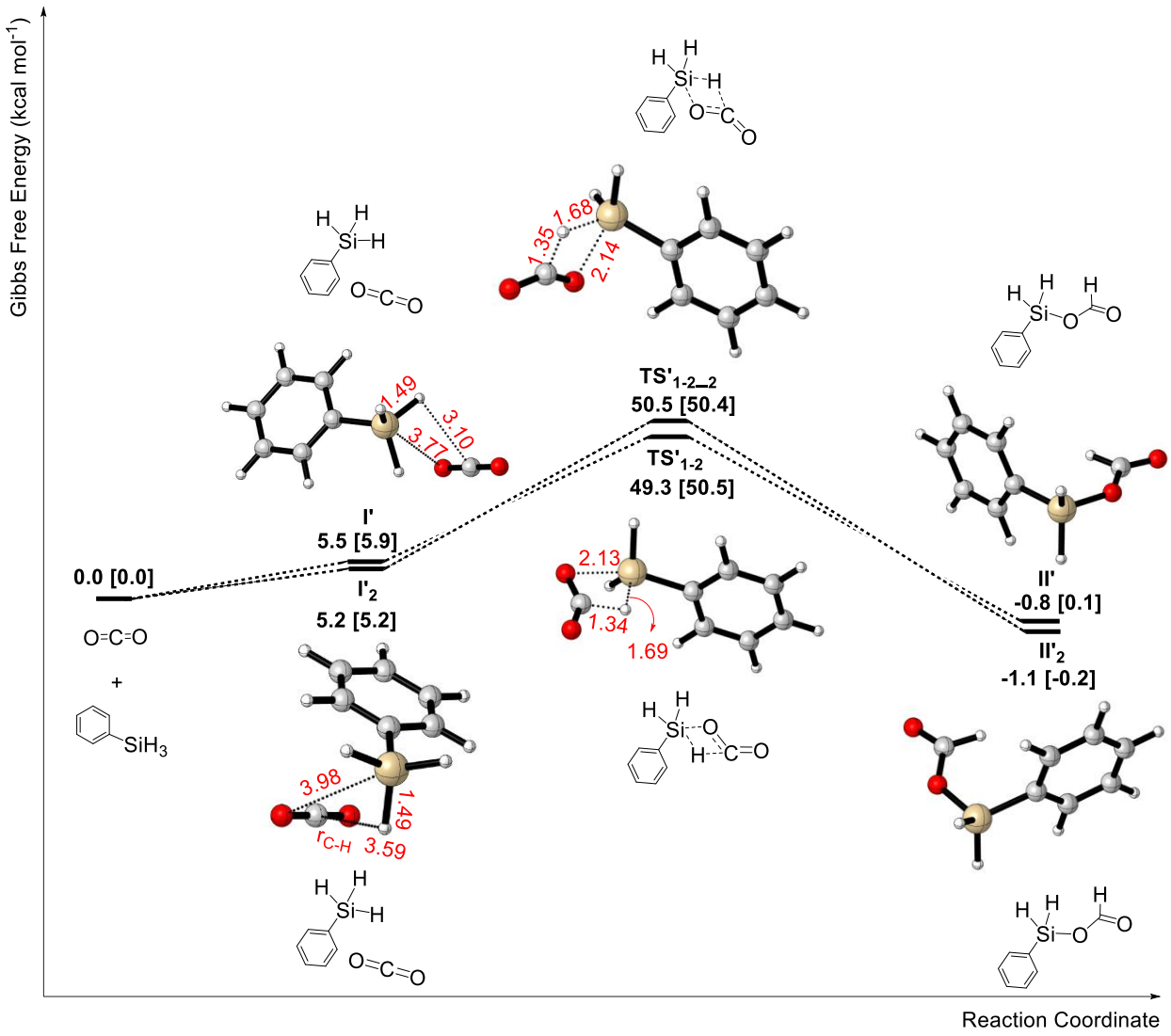

Figure 4.5. Conformers of $TS_{1\text{-}2}$. *The relative free energies given in kcal mol^{-1} are calculated with SMD(CH_3CN) ωB97XD/6-311++G(d,p)//ωB97XD/6-31+G(d,p). Free energies calculated in gas phase are quoted in square brackets. Bond distances are shown in Å in red. Molecular graphics were produced by CYLview.*

Chapter 5 Glycine betaine catalyzed CO_2 reduction

5.0 Synopsis

As discussed in Chapter 3, He and his co-workers, and Han and his co-workers reported respectively that amines can react with CO_2 and hydrosilanes to produce formamides, aminals and methylamines separately under the catalysis of glycine betaine.[37, 58] In **Chapter 5**, DFT calculations were carried out to understand the reaction mechanisms for these novel transformations. The reaction mechanisms are proposed in **Figure 5.0.1**. In **Figure 5.0.1**, there are three proposed pathways: pathway 1, pathway 2 and pathway 3. The energy profiles obtained from our calculations for these three pathways are presented in **5.1** to **5.3**. In **5.4**, several questions have been discussed, for example, the pathways that the reactions will go through in reality, how the reaction mechanism found from my DFT calculations accords with reaction conditions used in the experiments, and the comparison between the reaction mechanism under the catalysis of glycine betaine with the reaction mechanism under no catalyst. The functional and basis sets used in this chapter are SMD(CH_3CN)[73]-ωB97XD[74]/6-311++G(d,p)//ωB97XD[74]/6-31+G(d,p). Based on calculation results from **chapter 3.4**, ωB97XD, M06-2X and B3LYP-D3(BJ) can indicate weak interactions. Therefore, ωB97XD is chosen as the functional to analyse reaction mechanisms in **chapter 5**.

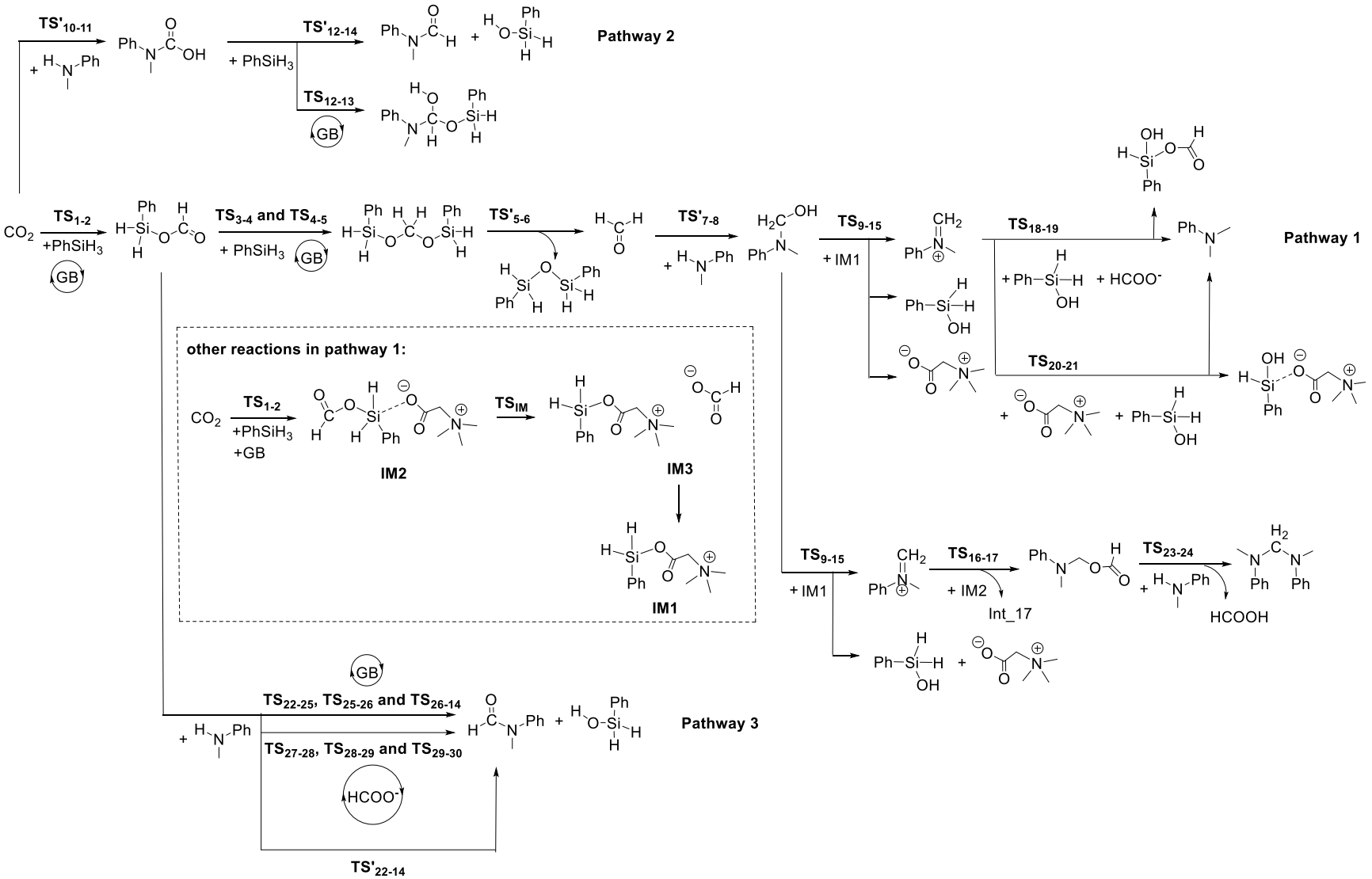

Figure 5.0.1. *The proposed reaction mechanism of the formylation, amination and methylation reactions under the catalysis of glycine betaine*

5.1 Calculated reaction pathway 1

Figure 5.1.1 to **Figure 5.1.6** show the energy profiles for the reactions in pathway 1. In the energy profiles in **Chapter 5**, the reference points are where reactants (*i.e.*, $PhSiH_3$, CO_2, N-methylaniline and glycine betaine) are isolated chemicals. The Gibbs free energy (G) for the reference points is zero. My DFT calculations started from the reaction between CO_2 and $PhSiH_3$ under the catalysis of GB. As shown in **Figure 5.1.1**, $PhSiH_3$ first reacts with CO_2 under the catalysis of glycine betaine to form formoxysilane (**II**) via $\mathbf{TS_{1\text{-}2}}$ with a Gibbs free energy activation barrier of 25.0 kcal/mol. In $\mathbf{TS_{1\text{-}2}}$, GB activates the Si-H bond in $PhSiH_3$ and thus helps the insertion of CO_2 into the activated Si-H bond. The new formed formoxysilane then reacts with $PhSiH_3$ under the catalysis of GB to form bis(silyl)-acetal ($\mathbf{V_A}$). This transformation involves two transition states: $\mathbf{TS_{3\text{-}4}}$ and $\mathbf{TS_{4\text{-}5}}$. In $\mathbf{TS_{3\text{-}4}}$, GB activates the Si-H bond in $PhSiH_3$ and promotes the transfer of the hydride to the C atom in formoxysilane. In $\mathbf{TS_{4\text{-}5}}$, a bond between the O atom from formoxysilane and the Si atom is formed. The activation free energy barriers of $\mathbf{TS_{3\text{-}4}}$ and $\mathbf{TS_{4\text{-}5}}$ are 37.8 and 26.0 kcal/mol. Next, bis(silyl)-acetal ($\mathbf{V_A}$) is converted to a complex of formaldehyde and $PhSiH_2OSiPhH_2$ **(VI'**) *via* $\mathbf{TS'_{5\text{-}6}}$. $\mathbf{TS'_{5\text{-}6}}$ has an activation free energy barrier of 18.7 kcal/mol. The addition between formaldehyde and N-methylaniline produces **VIII'** through $\mathbf{TS'_{7\text{-}8}}$. The following reaction of **VIII'** requires **IM1** and **IM1** is produced from reactions between GB, CO_2 and $PhSiH_3$ *via* two transition states: $\mathbf{TS_{1\text{-}2}}$ and $\mathbf{TS_{IM}}$. Since $\mathbf{TS_{1\text{-}2}}$ has already been discussed, the interaction between GB and formoxysilane forms **IM3** which is a complex of **IM1** and $HCOO^-$. Next **IM1** reacts with **VIII'** to form **XV** that is a complex of GB, phenylsilanol and a carbocation. The transition state involved in this reaction is $\mathbf{TS_{9\text{-}15}}$ with an activation free energy barrier of 4.3 kcal/mol. In $\mathbf{TS_{9\text{-}15}}$, there is an interaction between O and Si and the hydroxyl group transfers from the C atom to the Si atom. The next reaction is either to produce the methylamine or the aminal.

In terms of production of the methylamine, either $HCOO^-$ or GB can catalyse the reactions and the corresponding transition state is either **$TS_{18\text{-}19}$** or **$TS_{20\text{-}21}$** respectively. **$TS_{18\text{-}19}$** produces **XIX**, while **$TS_{20\text{-}21}$** forms **XXI**. The Gibbs free energies for **$TS_{18\text{-}19}$** and **$TS_{20\text{-}21}$** are 6.3 and 3.3 kcal/mol respectively. In terms of production of the aminal, another two transition states are required: **$TS_{16\text{-}17}$** and **$TS_{23\text{-}24}$**. **$TS_{16\text{-}17}$** and **$TS_{23\text{-}24}$** have the activation free energy barriers of -5.8 and -1.7 kcal/mol. To sum up, pathway 1 produces either the methylamine or the aminal under the catalysis of GB. The rate-determining step for productions of the two products is the same which is the reaction between formoxysilane and $PhSiH_3$ to produce bis(silyl)-acetal. The transition state of the rate-determining step (RDS) is **$TS_{3\text{-}4}$** with the activation free energy barrier of 37.8 kcal/mol.

In a contemporary study, He and his co-workers also carried out similar DFT calculations and also found that glycine betaine (GB) interacts with diphenylsilane through the nucleophilic oxygen centre of glycine betaine and the silicon centre of diphenylsilane, thus forming a hypervalent silicon species bearing an active hydride. They proposed that the new formed hypervalent silicon species can help the reaction between CO_2 and diphenylsilane.[37]

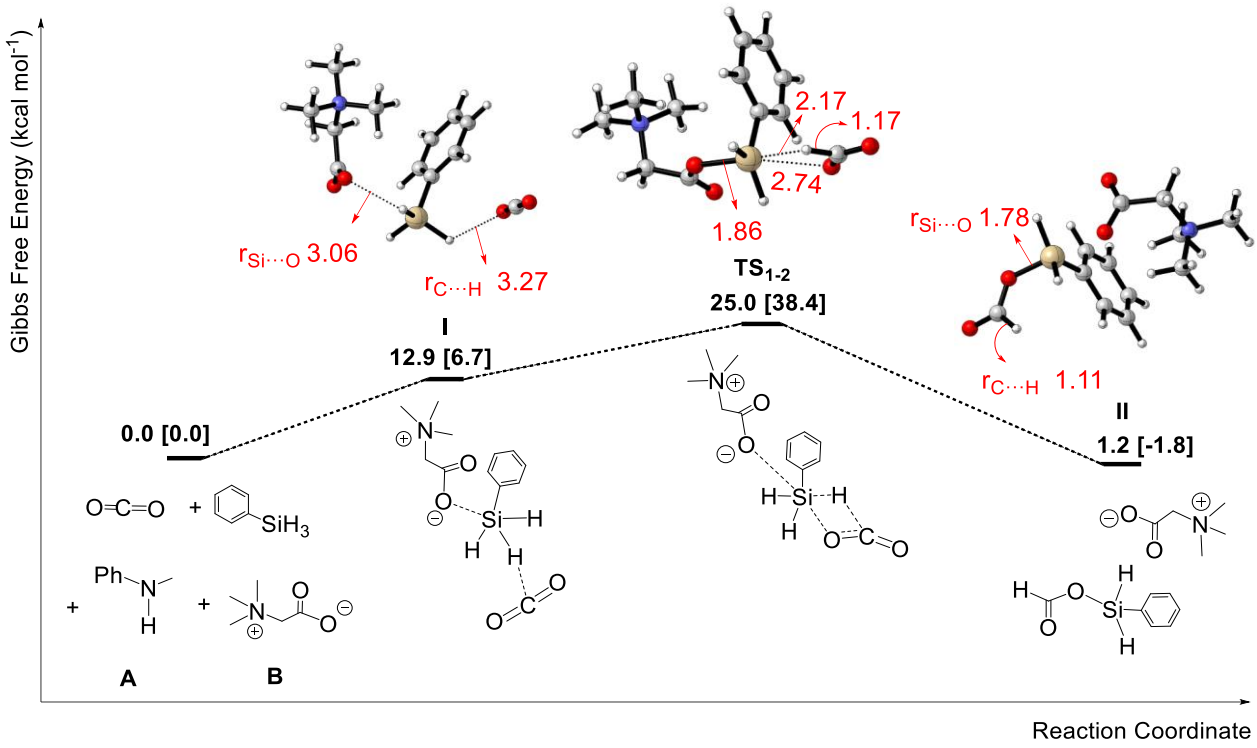

Figure 5.1.1. Computed free-energy profile for reactions in pathway 1 for the formation of intermediate II. *The relative free energies given in kcal mol^{-1} are calculated by using SMD(CH_3CN) ωB97XD/6-311++G(d,p)//ωB97XD/6-31+G(d,p). Free energies calculated in gas phase are quoted in square brackets. Bond distances are shown in Å in red. Molecular graphics were produced by CYLview.*

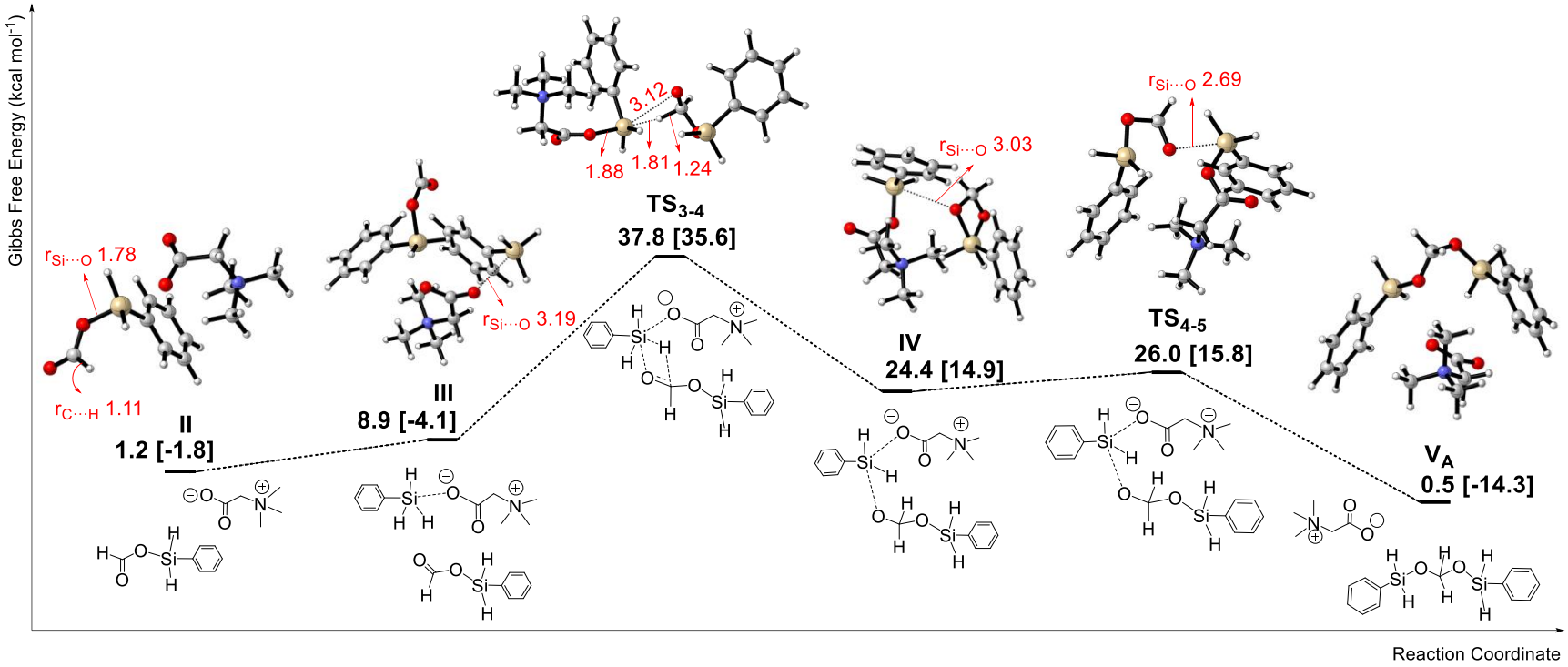

Figure 5.1.2. Computed free-energy profile for reactions in pathway 1 for the formation of intermediate V_A. *The relative free energies given in kcal mol^{-1} are calculated by using SMD(CH_3CN) ωB97XD/6-311++G(d,p)//ωB97XD/6-31+G(d,p). Free energies calculated in gas phase are quoted in square brackets. Bond distances are shown in Å in red. Molecular graphics were produced by CYLview.*

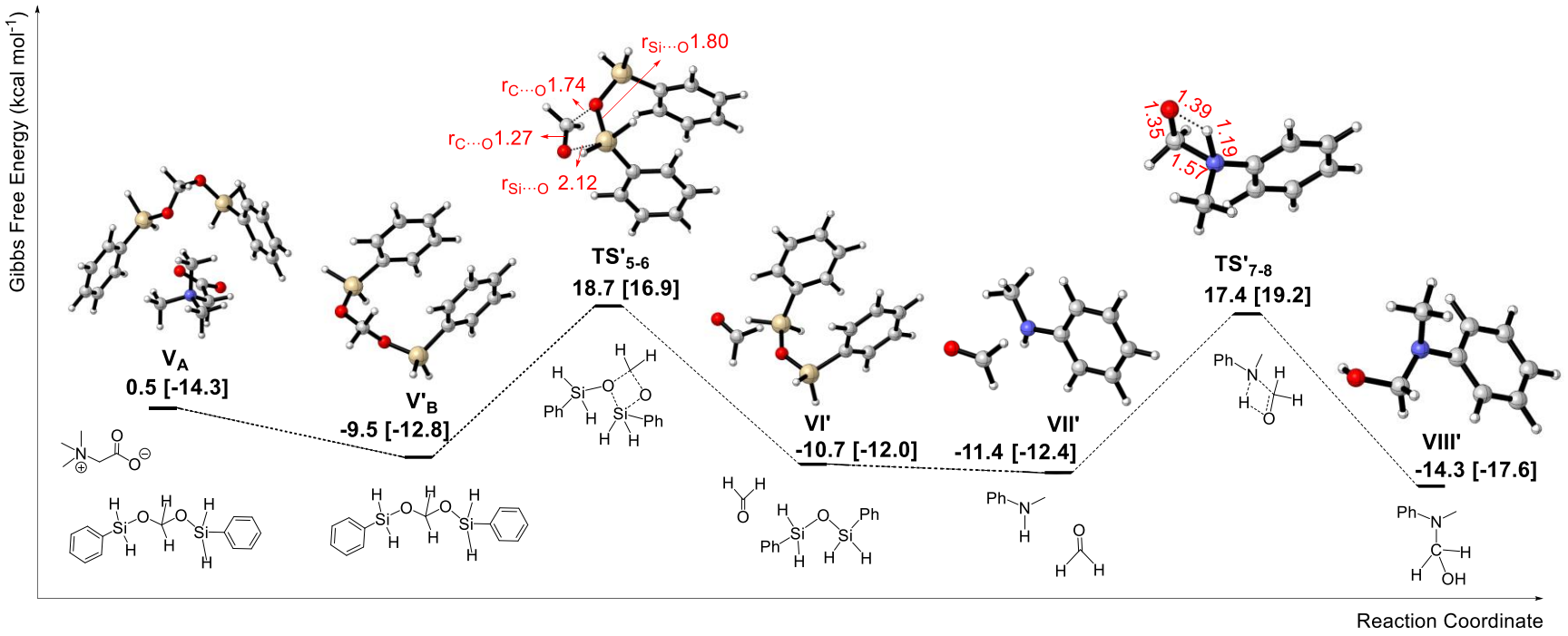

Figure 5.1.3. Computed free-energy profile for reactions in pathway 1 for the formation of intermediate VIII'. *The relative free energies given in kcal mol^{-1} are calculated by using SMD(CH_3CN) ωB97XD/6-311++G(d,p)//ωB97XD/6-31+G(d,p). Free energies calculated in gas phase are quoted in square brackets. Bond distances are shown in Å in red. Molecular graphics were produced by CYLview.*

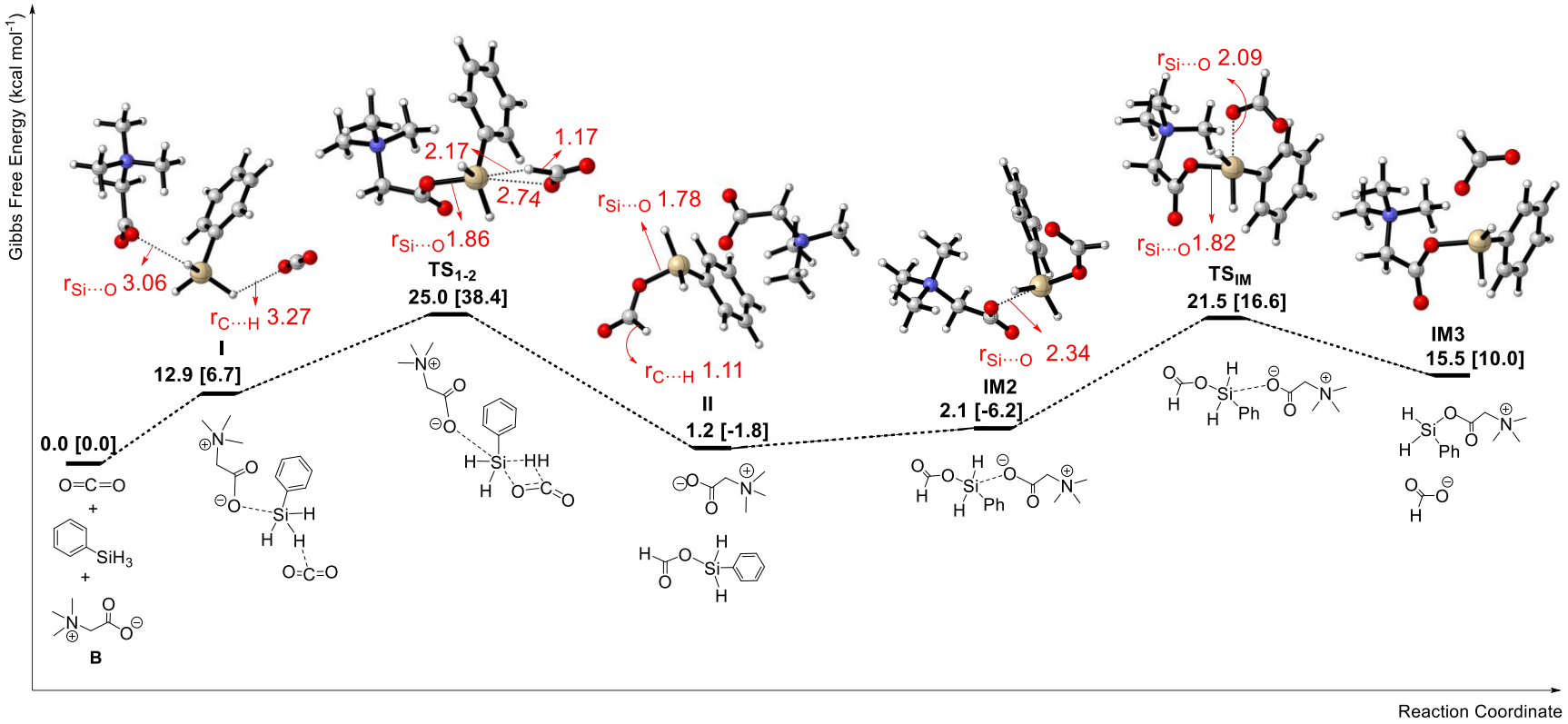

Figure 5.1.4. Computed free-energy profile for reactions in pathway 1 for the formation of intermediate IM3. *The relative free energies given in kcal mol^{-1} are calculated by using SMD(CH_3CN) ωB97XD/6-311++G(d,p)//ωB97XD/6-31+G(d,p). Free energies calculated in gas phase are quoted in square brackets. Bond distances are shown in Å in red. Molecular graphics were produced by CYLview.*

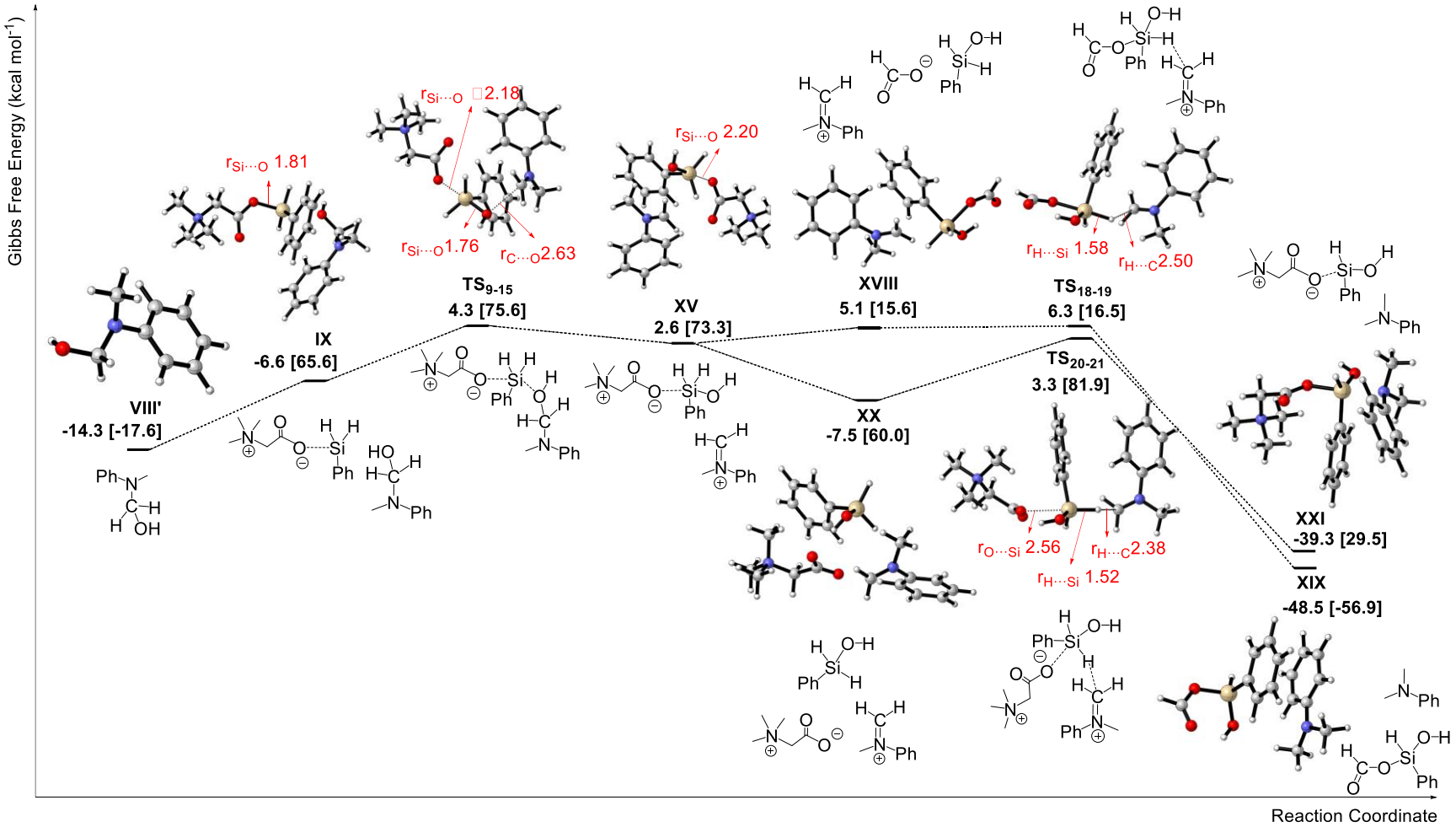

Figure 5.1.5. Computed free-energy profile for reactions in pathway 1 for the formation of intermediate XXI. *The relative free energies given in kcal mol^{-1} are calculated by using SMD(CH_3CN) ωB97XD/6-311++G(d,p)//ωB97XD/6-31+G(d,p). Free energies calculated in gas phase are quoted in square brackets. Bond distances are shown in Å in red. Molecular graphics were produced by CYLview.*

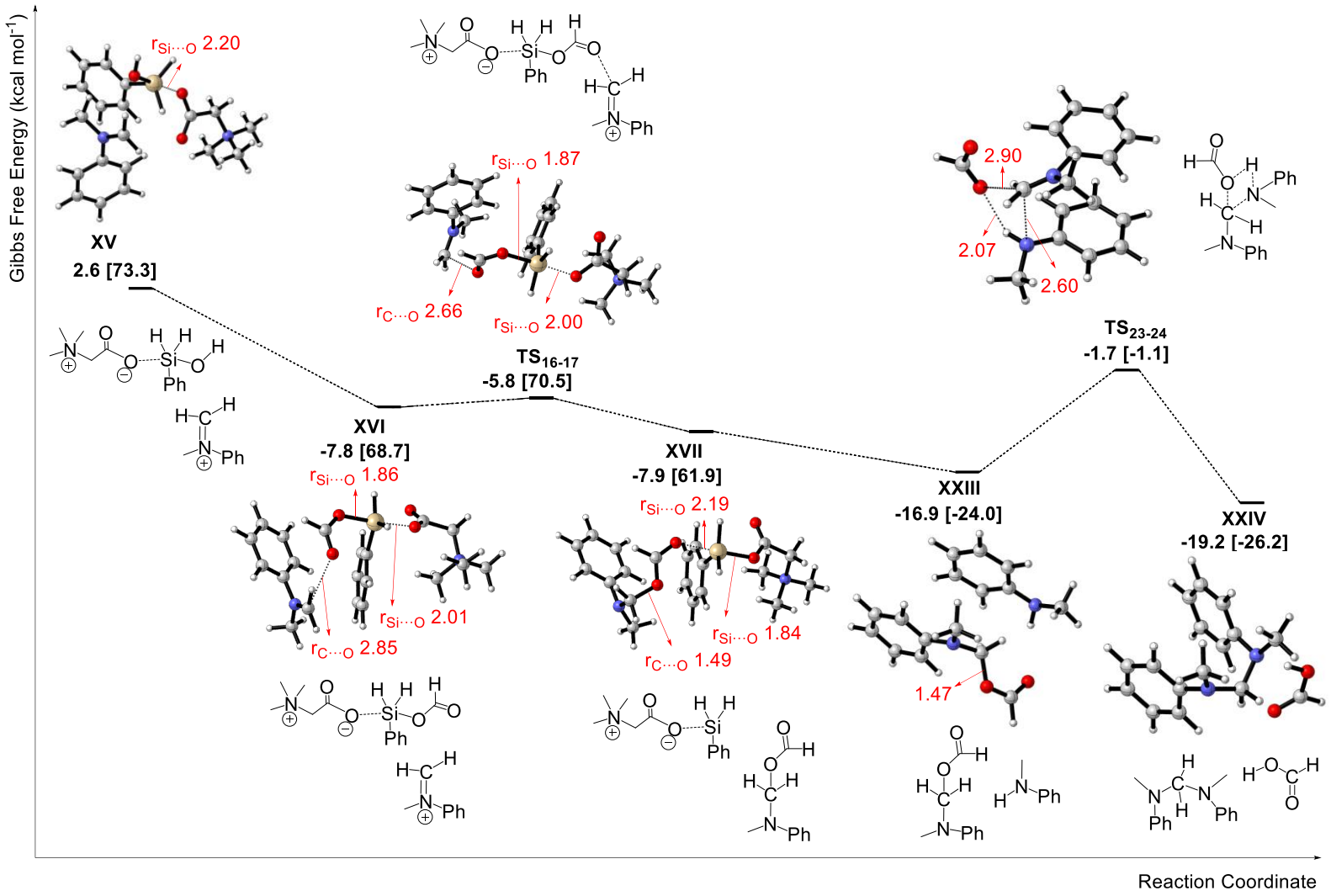

Figure 5.1.6. Computed free-energy profile for reactions in pathway 1 for the formation of intermediate XXIV. *The relative free energies given in kcal mol^{-1} are calculated by using SMD(CH_3CN) ωB97XD/6-311++G(d,p)//ωB97XD/6-31+G(d,p). Free energies calculated in gas phase are quoted in square brackets. Bond distances are shown in Å in red. Molecular graphics were produced by CYLview.*

During my DFT calculations, there are some trails where I failed to get transition states or I found conformers of the transition states mentioned in **figure 5.1.1** to **figure 5.1.6**. **Figure 5.1.7** presents four possible activation modes for **TS_{1-2}** and **TS_{3-5}**, naming from mode **K** to mode **N**. In mode **K** and mode **L** for **TS_{1-2}**, GB may activate either $PhSiH_3$ or CO_2. DFT calculations show that only mode **K** is feasible. **TS_{1-2}** in **figure 5.1.1** is calculated based on mode **K**. In terms of mode **M** and mode **N** for TS_{3-5}, GB might activate either $PhSiH_3$ or formoxysilane to help further reactions. Based on my DFT calculations, transition states from mode **M** and mode **N** are obtained and they are conformers of TS_{3-5}. These conformers are discussed in **figure 5.1.8**, **figure 5.1.9** and **figure 5.1.10**. In **figure 5.1.8**, the reaction between formoxysilane, $PhSiH_3$ and GB can be either a one-step reaction or a two-step reaction. The one-step reaction involves one transition state that is **TS_{3-5_4}**, while the two-step reaction involves two transition states which are **TS_{3-4}** and **TS_{4-5}**. In the one-step reaction, GB activates the Si-H bond in $PhSiH_3$. Then the active hydride from the activated Si-H bond transfers to the C atom, and a new O-Si bond is formed. The product from **TS_{3-5_4}** is **V_4** that is a complex of GB and bis(silyl)-acetal. In the two-step reaction, GB first activates the Si-H bond in $PhSiH_3$ and thus helps the hydride transfer to the C atom. In the second transition state (**TS_{4-5}**) of the two-step reaction, the Si-O bond is formed and the corresponding product is **V_A** which is a complex of GB and bis(silyl)-acetal. **Figure 5.1.9** and **figure 5.1.10** present seven conformers of **TS_{3-5}**, named as **TS_{3-4}** and **TS_{4-5}**, **TS_{3-5_2}**, **TS_{3-5_3}**… and **TS_{3-5_7}**. Among the seven conformers, **TS_{3-5_7}** is calculated based on mode **N**, while the rest are calculated based on mode **M**. **TS_{3-4}** has the lowest $\Delta G^{\ddagger}_{sol}$ (37.8 kcal/mol) compared to the other six conformers. In **TS_{3-4}**, the Si atom and the phenyl ring in $PhSiH_3$ interact with the O atom and the N atom in GB. The two interactions in **TS_{3-4}** make its activation free energy barrier ($\Delta G^{\ddagger}_{sol}$) reduced from 52.2 kcal/mol (**TS'_{3-5}**) to 37.8 kcal/mol. In terms of **TS_{3-5_2}**, three

hydrogen atoms and the Si atom in $PhSiH_3$ are approximately in one plane. **$TS_{3\text{-}5\_2}$** has the highest $\Delta G^{\ddagger}_{sol}$ compared to the other six conformers of **$TS_{3\text{-}5}$**. In terms of **$TS_{3\text{-}5\_3}$**, the positively charged N atom in GB seems to have π-cation interaction with the phenyl ring in formoxysilane instead of the phenyl ring in $PhSiH_3$. This difference may be the reason why **$TS_{3\text{-}5\_3}$** has a larger $\Delta G^{\ddagger}_{sol}$ than **$TS_{3\text{-}4}$**. Regarding to **$TS_{3\text{-}5\_4}$**, the Si atom in $PhSiH_3$ might interact with the phenyl ring in formoxysilane and this interaction may increase the $\Delta G^{\ddagger}_{sol}$. In **$TS_{3\text{-}5\_5}$**, the O atom in the C=O bond in formoxysilane is close to the N atom in GB and this result may explain why **$TS_{3\text{-}5\_5}$** has a higher $\Delta G^{\ddagger}_{sol}$ than **$TS_{3\text{-}4}$**. Similar to **$TS_{3\text{-}4}$**, the reaction involving **$TS_{3\text{-}4\_6}$** is a two-step reaction. In **$TS_{3\text{-}4\_6}$**, the interaction between GB and $PhSiH_3$ is worse than that in **$TS_{3\text{-}4}$** and this difference may explain the increase of $\Delta G^{\ddagger}_{sol}$. The interaction between GB and formoxysilane in **$TS_{3\text{-}5\_7}$** does not seem to be as efficient as the interaction between GB and $PhSiH_3$. The $\Delta G^{\ddagger}_{sol}$ of **$TS_{3\text{-}5\_7}$** is 52.5 kcal/mol which is similar to that of the un-catalysed transition state **$TS'_{3\text{-}5}$** (52.2 kcal/mol).

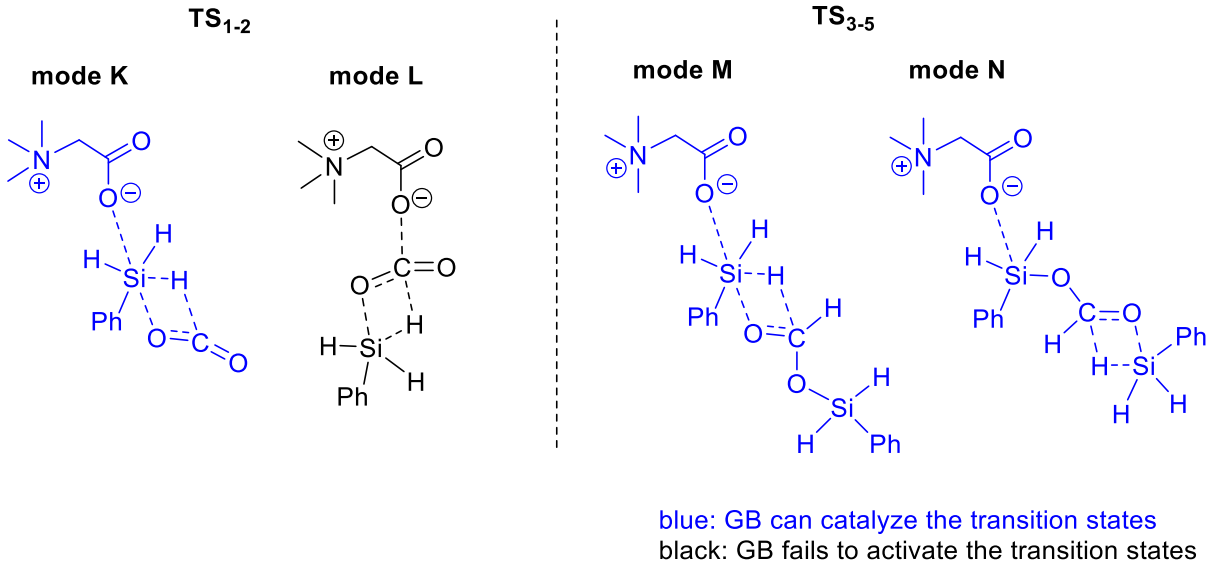

Figure 5.1.7. *Other trials for transition states in pathway 1*

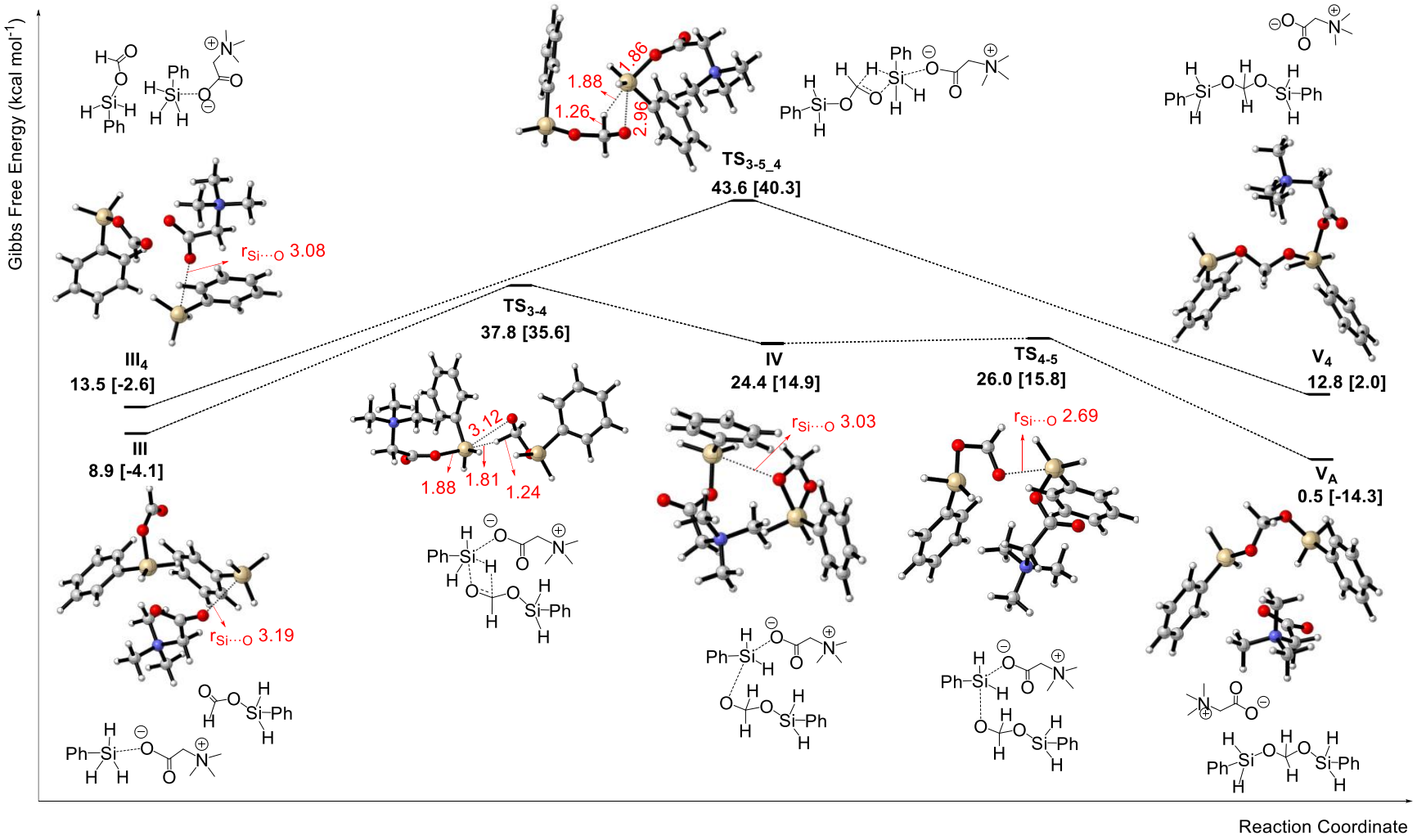

Figure 5.1.8. Computed free-energy profile for the reaction between formoxysilane, $PhSiH_3$ and glycine betaine. *The relative free energies given in kcal mol^{-1} are calculated by using SMD(CH_3CN) ωB97XD/6-311++G(d,p)//ωB97XD/6-31+G(d,p). Free energies calculated in gas phase are quoted in square brackets. Bond distances are shown in Å in red. Molecular graphics were produced by CYLview.*

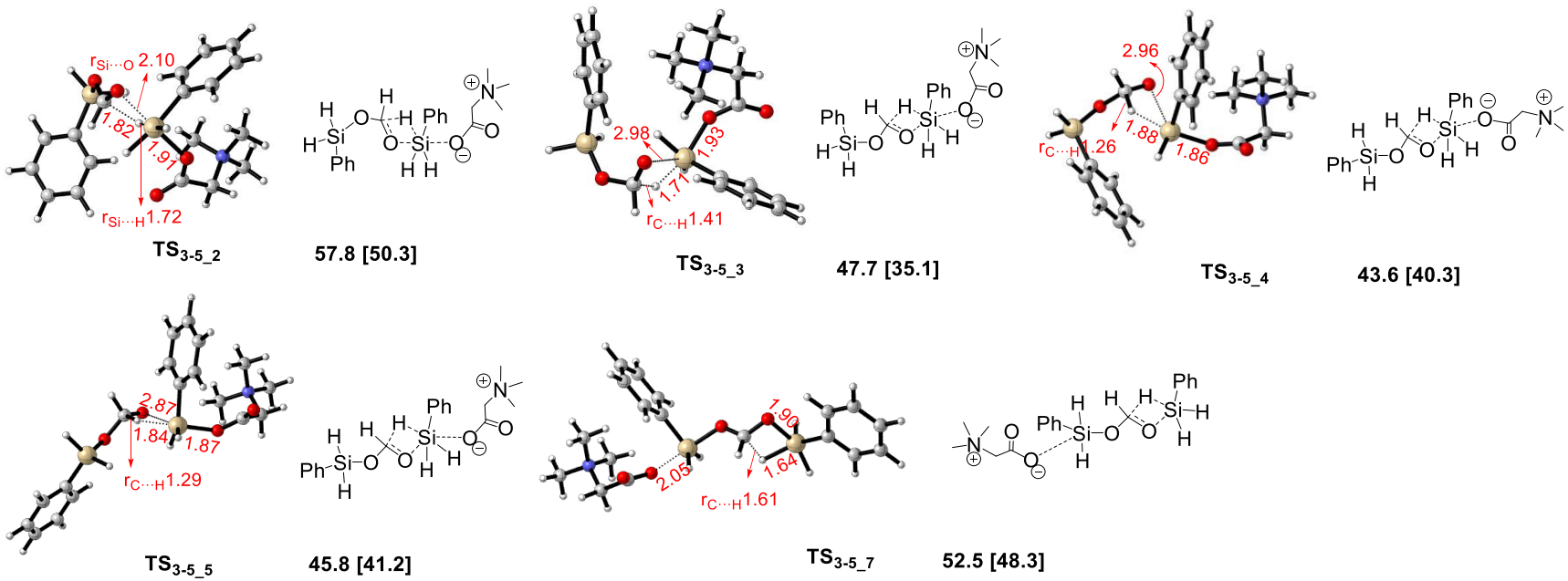

Figure 5.1.9. Conformers of $TS_{3\text{-}5}$. *The relative free energies given in kcal mol^{-1} are calculated by using SMD(CH_3CN) ωB97XD/6-311++G(d,p)//ωB97XD/6-31+G(d,p). Free energies calculated in gas phase are quoted in square brackets. Bond distances are shown in Å in red. Molecular graphics were produced by CYLview.*

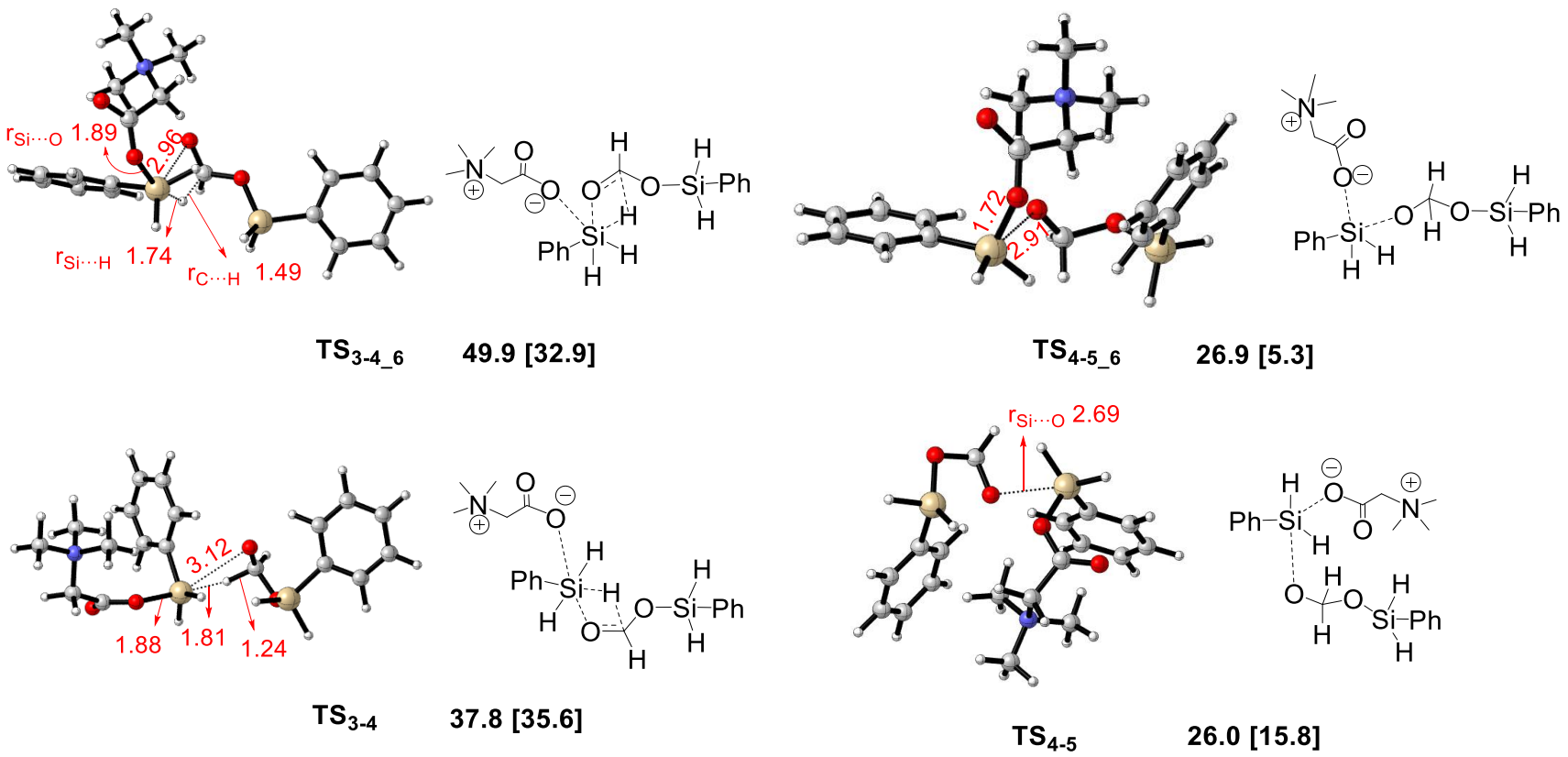

Figure 5.1.10. Conformers of $TS_{3\text{-}5}$. *The relative free energies given in kcal mol^{-1} are calculated by using SMD(CH_3CN) ωB97XD/6-311++G(d,p)//ωB97XD/6-31+G(d,p). Free energies calculated in gas phase are quoted in square brackets. Bond distances are shown in Å in red. Molecular graphics were produced by CYLview.*

During my DFT calculations, both **TS'$_{5\text{-}6}$** and **TS$_{5\text{-}6}$** are found and the two transition states are shown in **figure 5.1.11**. **TS$_{5\text{-}6}$** is the transition state under the catalysis of glycine betaine, while **TS'$_{5\text{-}6}$** has no catalyst. In **TS'$_{5\text{-}6}$**, bis(silyl)-acetal (**V'$_B$**) converts to **VI'** via a four-membered ring. In **TS$_{5\text{-}6}$**, glycine betaine seems to interact with bis(silyl)-acetal to form **VI**. The activation free energy barrier of **TS$_{5\text{-}6}$** is 19.3 kcal/mol, while the activation free energy barrier of **TS'$_{5\text{-}6}$** is 18.7 kcal/mol. Since the activation free energy barrier of **TS$_{5\text{-}6}$** is higher than that of **TS'$_{5\text{-}6}$**, glycine betaine cannot help reduce the energy barrier of the reaction. Therefore, **TS'$_{5\text{-}6}$** is chosen as the transition states in **figure 5.1.3**. During my DFT calculations, two conformers of **TS$_{IM}$** are found and they are **TS$_{IM}$** and **TS$_{IM_2}$**. **Figure 5.1.12** presents the two transition states. Both transition states are catalysed by glycine betaine and produce complexes of $HCOO^-$ and **IM1** in the same reaction mechanism. The activation free energy barrier of **TS$_{IM}$** is 21.5 kcal/mol, while the activation free energy barrier of **TS$_{IM_2}$** is 24.8 kcal/mol. Therefore, **TS$_{IM}$** is selected as the transition state in **figure 5.1.4**.

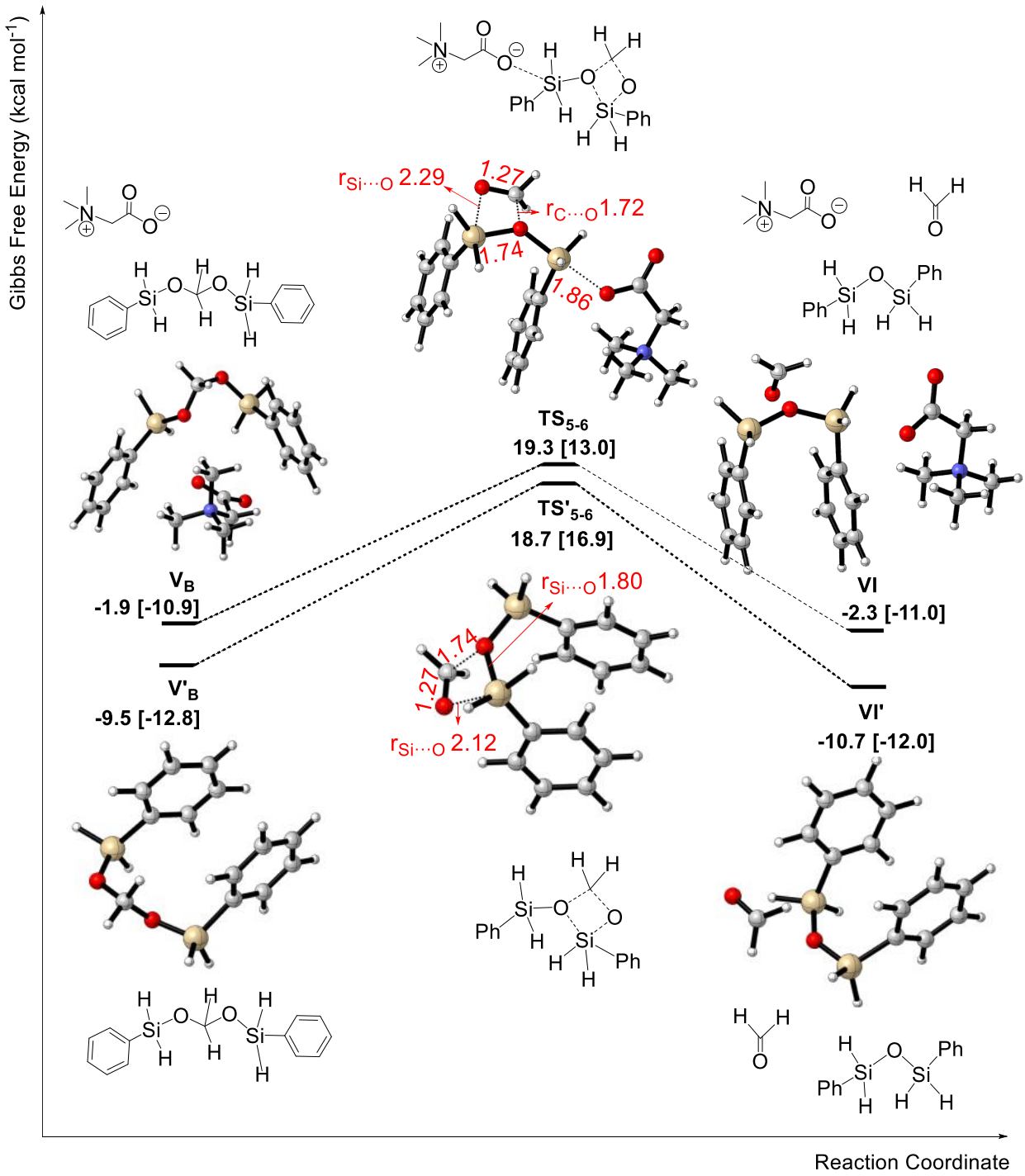

Figure 5.1.11. Comparison of the reactions involving TS'$_{5-6}$ and TS$_{5-6}$. *The relative free energies given in kcal mol^{-1} are calculated by using SMD(CH$_3$CN) ωB97XD/6-311++G(d,p)//ωB97XD/6-31+G(d,p). Free energies calculated in gas phase are quoted in square brackets. Bond distances are shown in Å in red. Molecular graphics were produced by CYLview.*

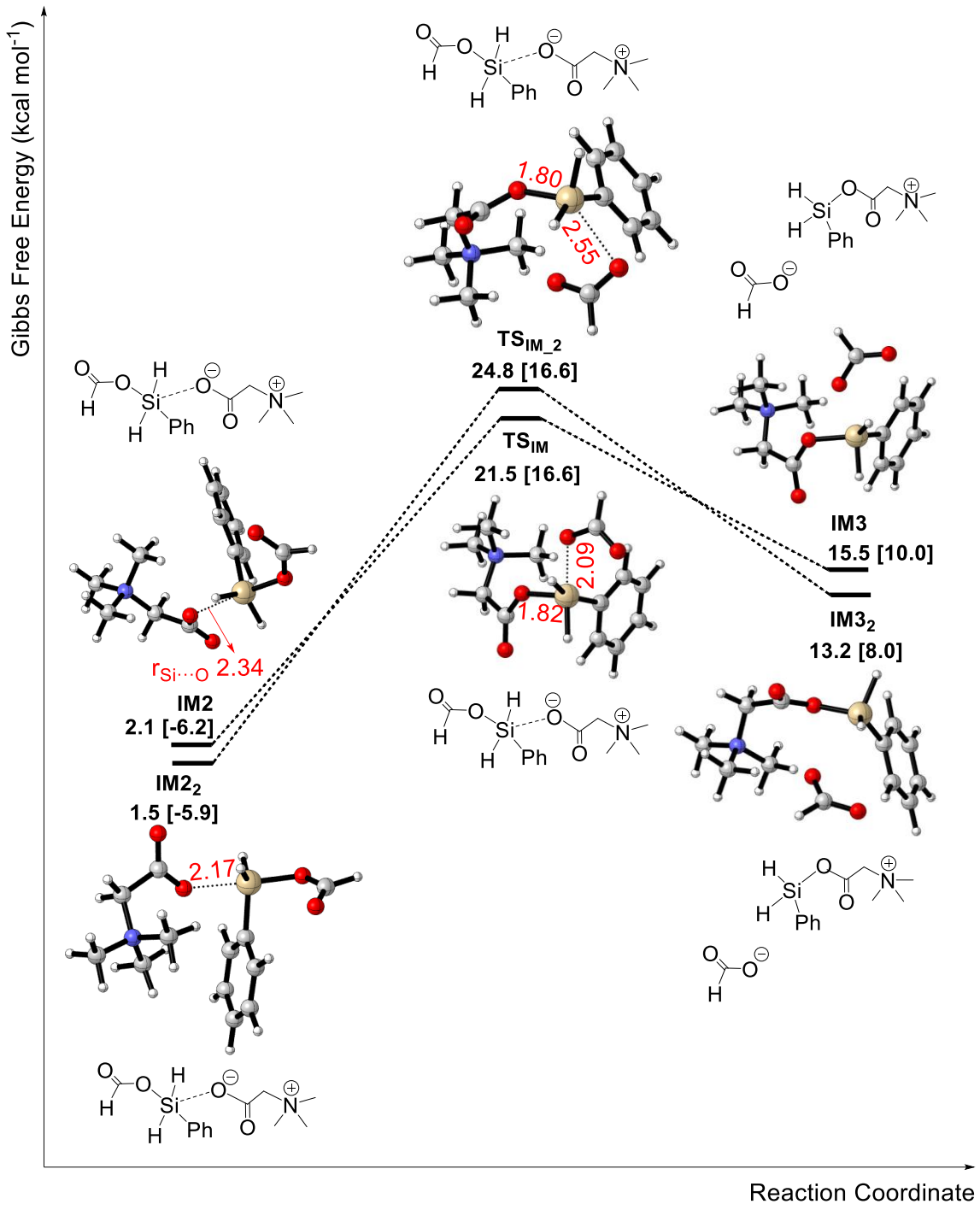

Figure 5.1.12. Conformers of TS_{IM}. *The relative free energies given in kcal/mol are calculated by using SMD(CH_3CN) ωB97XD/6-311++G(d,p)//ωB97XD/6-31+G(d,p). Free energies calculated in gas phase are quoted in square brackets. Bond distances are shown in Å in red. Molecular graphics were produced by CYLview.*

5.2 Calculated reaction pathway 2

Figure 5.2.1 presents the energy profile of the reactions in pathway 2. Initially, the reaction between CO_2 and N-methylaniline produces carbamic acid (**XI'**) *via* a four-membered ring in **TS'$_{10\text{-}11}$**. In **TS'$_{10\text{-}11}$**, the C atom from CO_2 is added to the N atom from N-methylaniline, and the H atom from N-methylaniline is added to the O atom from CO_2. The $\Delta G^{\ddagger}_{sol}$ of **TS'$_{10\text{-}11}$** is 45.7 kcal/mol. Next, **XI'** is converted to either **XIII** or **XIV'** via either **TS$_{12\text{-}13}$** or **TS'$_{12\text{-}14}$**. In **TS$_{12\text{-}13}$**, glycine betaine activates the Si-H bond in $PhSiH_3$, and thus helps the active hydride transfer to the C atom in carbamic acid. Meanwhile, a new bond connecting the O atom from carbamic acid and the Si atom in $PhSiH_3$ is formed. In **TS'$_{12\text{-}14}$**, carbamic acid reacts with $PhSiH_3$ *via* a four membered ring to produce a complex of the formamide and phenylsilanol. The activation free energy barrier of **TS$_{12\text{-}13}$** is 53.5 kcal/mol, while the activation free energy barrier of **TS'$_{12\text{-}14}$** is 73.2 kcal/mol. Since the activation free energy barrier of **TS$_{12\text{-}13}$** is lower than that of **TS'$_{12\text{-}14}$**, the reaction prefers to go through **TS$_{12\text{-}13}$** and produces **XIII**. The rate-determining step for pathway 2 is the reaction with **TS$_{12\text{-}13}$** as the transition state.

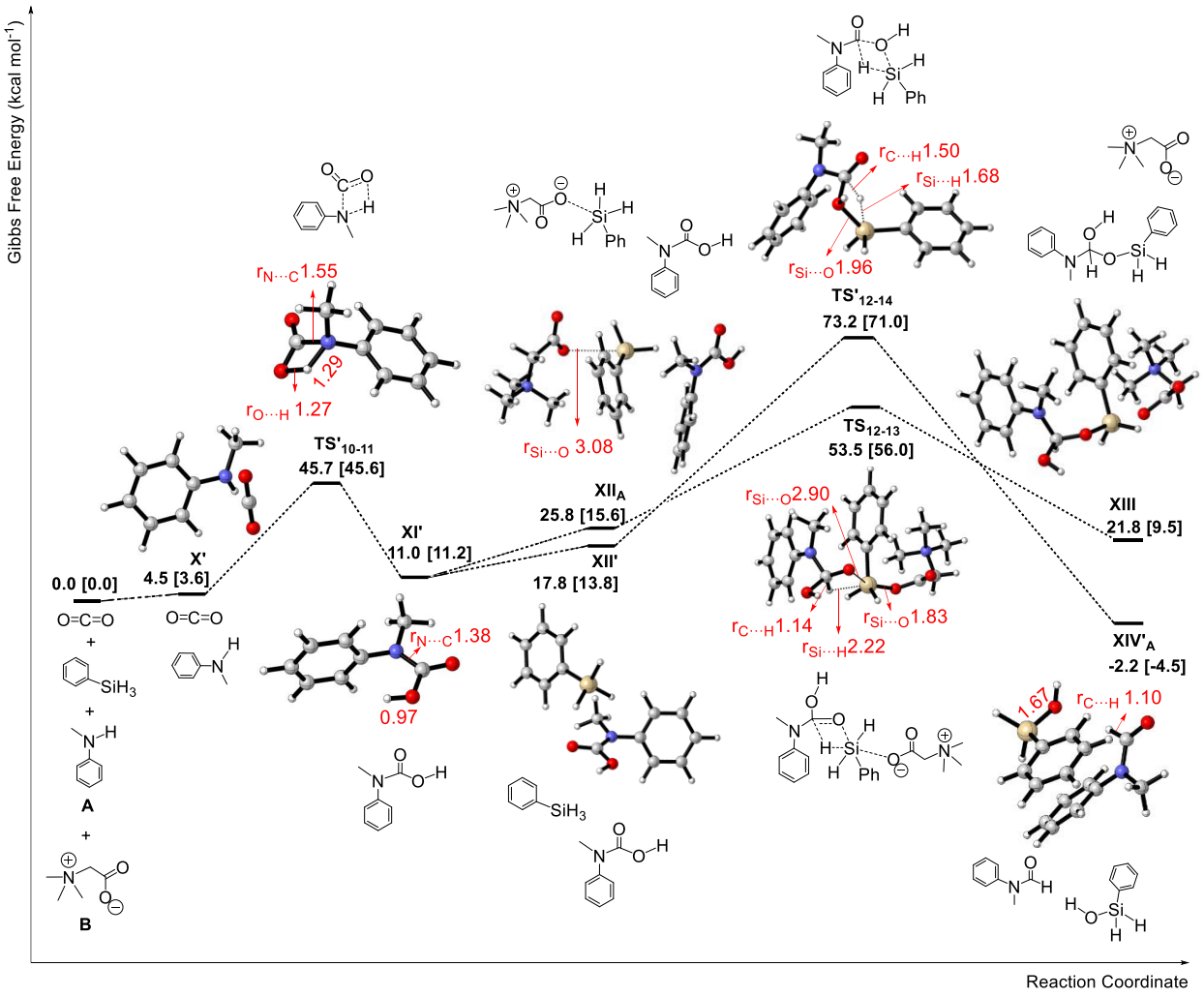

Figure 5.2.1. Computed free-energy profile for the reactions in pathway 2. *The relative free energies given in kcal mol^{-1} are calculated by using SMD(CH_3CN) ωB97XD/6-311++G(d,p)//ωB97XD/6-31+G(d,p). Free energies calculated in gas phase are quoted in square brackets. Bond distances are shown in Å in red. Molecular graphics were produced by CYLview.*

Pathway 2 has three transition states which are **TS_{10-11}**, **TS_{12-13}** and **TS_{12-14}**. During my DFT calculations, I tried six activation modes for the three transition states, ranging from mode **O** to mode **T**. **Figure 5.2.2** shows the six activation modes. Mode **O** and mode **P** are proposed for **TS_{10-11}**. In the two activation modes, GB may activate either CO_2 or N-methylaniline to reduce the activation barriers of the transition states. However, neither of the activation modes works. **Figure 5.2.3** presents **TS_{10-11}** and **TS'_{10-11}**. Both transition states produce carbamic acid *via* a four membered ring. There is

glycine betaine in **$TS_{10\text{-}11}$**, while **$TS'_{10\text{-}11}$** does not have glycine betaine. Glycine betaine in **$TS_{10\text{-}11}$** seems to have no interaction with the two reactants. The activation free energy barrier of **$TS_{10\text{-}11}$** is 54.8 kcal/mol, while the activation free energy barrier of **$TS'_{10\text{-}11}$** is 45.7 kcal/mol. By looking at the structure at the transition state and comparing the activation free energy barriers of the two transition states, it can be concluded that GB cannot activate **$TS_{10\text{-}11}$**. Therefore, **$TS'_{10\text{-}11}$** is selected as the transition state in **figure 5.2.1**.

In **figure 5.2.2**, two activation modes are proposed for **$TS_{12\text{-}14}$**: mode **Q** and mode **R**. Glycine betaine is proposed to activate $PhSiH_3$ in mode **Q**, while glycine betaine is proposed to activate carbamic acid in mode **R**. My DFT calculations show the existence of mode **Q**, but fail to find mode **R**. **Figure 5.2.4** presents two conformers of **$TS_{12\text{-}14}$**: **$TS_{12\text{-}14}$** and **$TS_{12\text{-}14\_2}$**. Both transition states produce a complex of phenylsilanol and the formamide *via* a four membered ring. Glycine betaine in **$TS_{12\text{-}14\_2}$** seems to have no interaction with the reactants, while glycine betaine in **$TS_{12\text{-}14}$** catalyses the transition state in the form of mode **Q**. The activation free energy barrier of **$TS_{12\text{-}14}$** is 79.1 kcal/mol. However, the activation free energy barrier of **$TS'_{12\text{-}14}$** is 73.2 kcal/mol. Since glycine betaine cannot help reduce the activation free energy barrier of **$TS_{12\text{-}14}$**, **$TS'_{12\text{-}14}$** is used as the transition state in **figure 5.2.1**.

Figure 5.2.2 presents two proposed activation modes for **$TS_{12\text{-}13}$**: mode **S** and mode **T**. Glycine betaine activates $PhSiH_3$ or carbamic acid in mode **S** or mode **R**. My DFT calculations show that both activation modes exist. Transition states based on mode **S** and mode **T** are conformers of **$TS_{12\text{-}13}$**, and they are presented in **Figure 5.2.5** and **Figure 5.2.6**. In **figure 5.2.5**, energy profiles of the reactions involving **$TS_{12\text{-}13}$** and **$TS_{12\text{-}13\_2}$** are shown. Both conformers produce the same product via a four membered ring. **Figure 5.2.6** shows four conformers of **$TS_{12\text{-}13}$**, ranging from **$TS_{12\text{-}13}$** to **$TS_{12\text{-}13\_4}$**. Mode **S** applies to

both **$TS_{12\text{-}13}$** and **$TS_{12\text{-}13\_2}$**, while mode **T** applies to **$TS_{12\text{-}13\_3}$**. In **$TS_{12\text{-}13\_4}$**, glycine betaine seems to have no interaction with any of the reactants. Therefore, neither of the activation modes applies in **$TS_{12\text{-}13\_4}$**. Among the four conformers of **$TS_{12\text{-}13}$**, **$TS_{12\text{-}13}$** has the lowest activation free energy barrier which is 53.5 kcal/mol. As shown in **figure 4.3**, **$TS'_{12\text{-}13}$** has an activation free energy barrier of 59.6 kcal/mol. By adding the catalyst, the activation free energy barrier of the transition state is reduced. Therefore, it can be concluded that GB acts as a catalyst in **$TS_{12\text{-}13}$**. Since the interaction between GB and $PhSiH_3$ in **$TS_{12\text{-}13}$** is much better than that in **$TS_{12\text{-}13\_2}$**, the activation free energy barrier of **$TS_{12\text{-}13}$** is lower than that of **$TS_{12\text{-}13\_2}$**. The interaction between GB and carbamic acid in **$TS_{12\text{-}13\_3}$** helps to reduce the activation free energy barrier from 59.6 kcal/mol (**$TS'_{12\text{-}13}$**) to 55.0 kcal/mol. In terms of **$TS_{12\text{-}13\_4}$**, GB seems to interact with neither of the reactants and its activation free energy barrier is higher than that of the transition state with no catalyst (**$TS'_{12\text{-}13}$**).

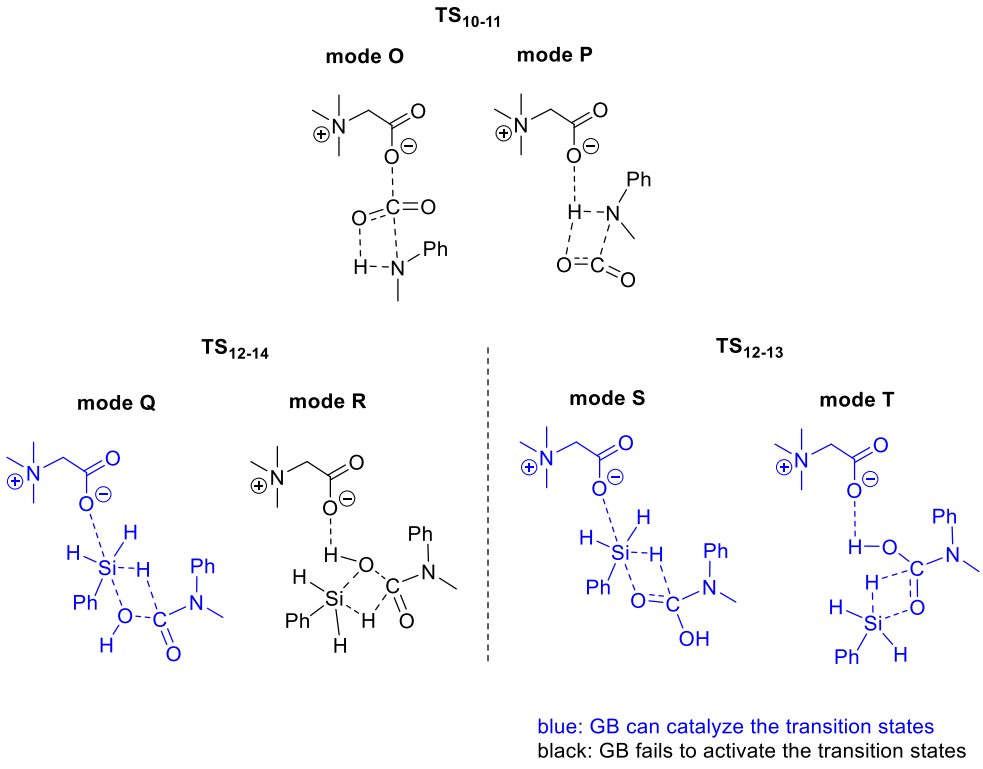

Figure 5.2.2. *Other trials for transition states in pathway 2*

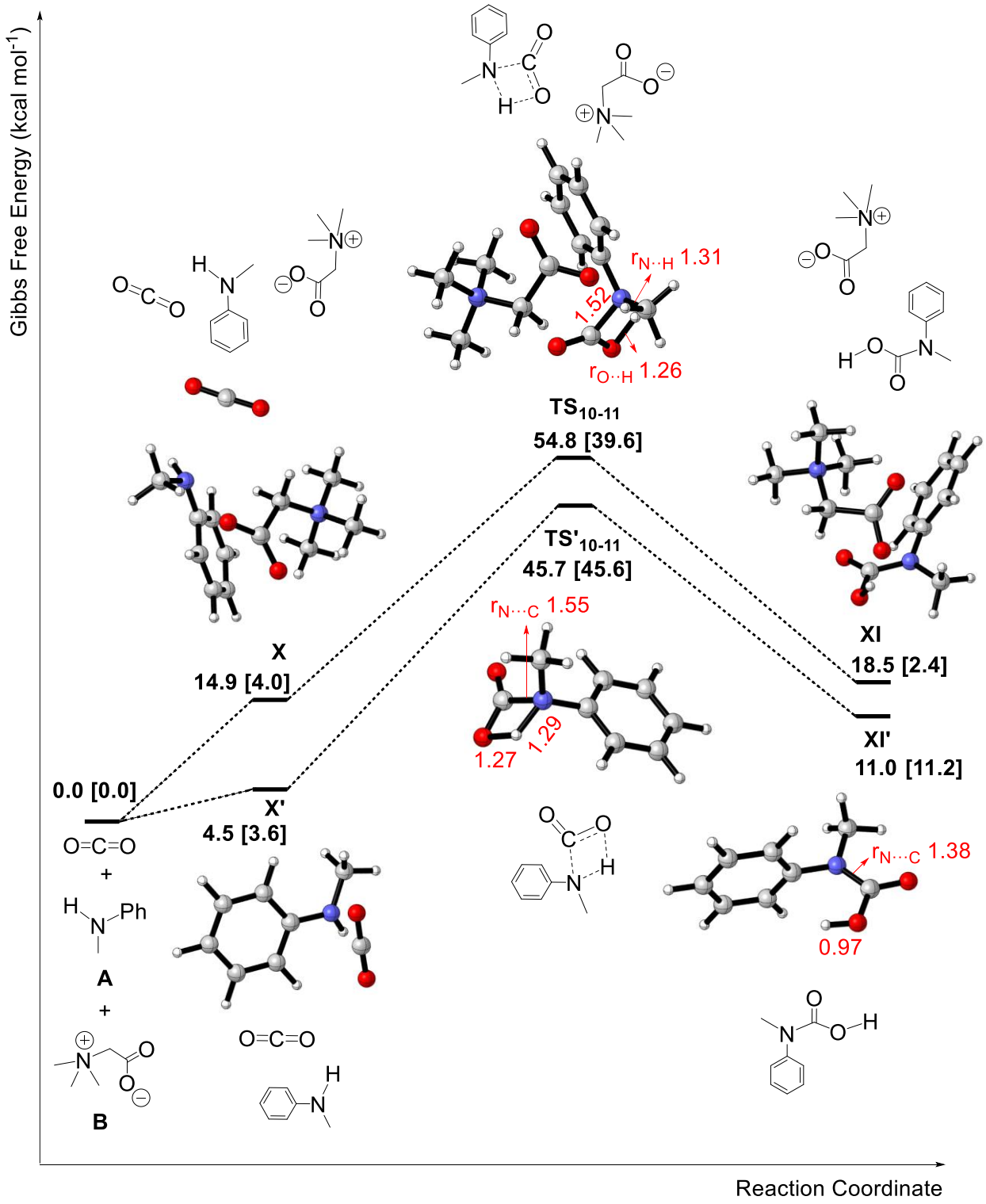

Figure 5.2.3. Computed free-energy profile for the two reactions involving $TS_{10\text{-}11}$ and $TS'_{10\text{-}11}$. *The relative free energies given in kcal mol^{-1} are calculated by using SMD(CH_3CN) ωB97XD/6-311++G(d,p)//ωB97XD/6-31+G(d,p). Free energies calculated in gas phase are quoted in square brackets. Bond distances are shown in Å in red. Molecular graphics were produced by CYLview.*

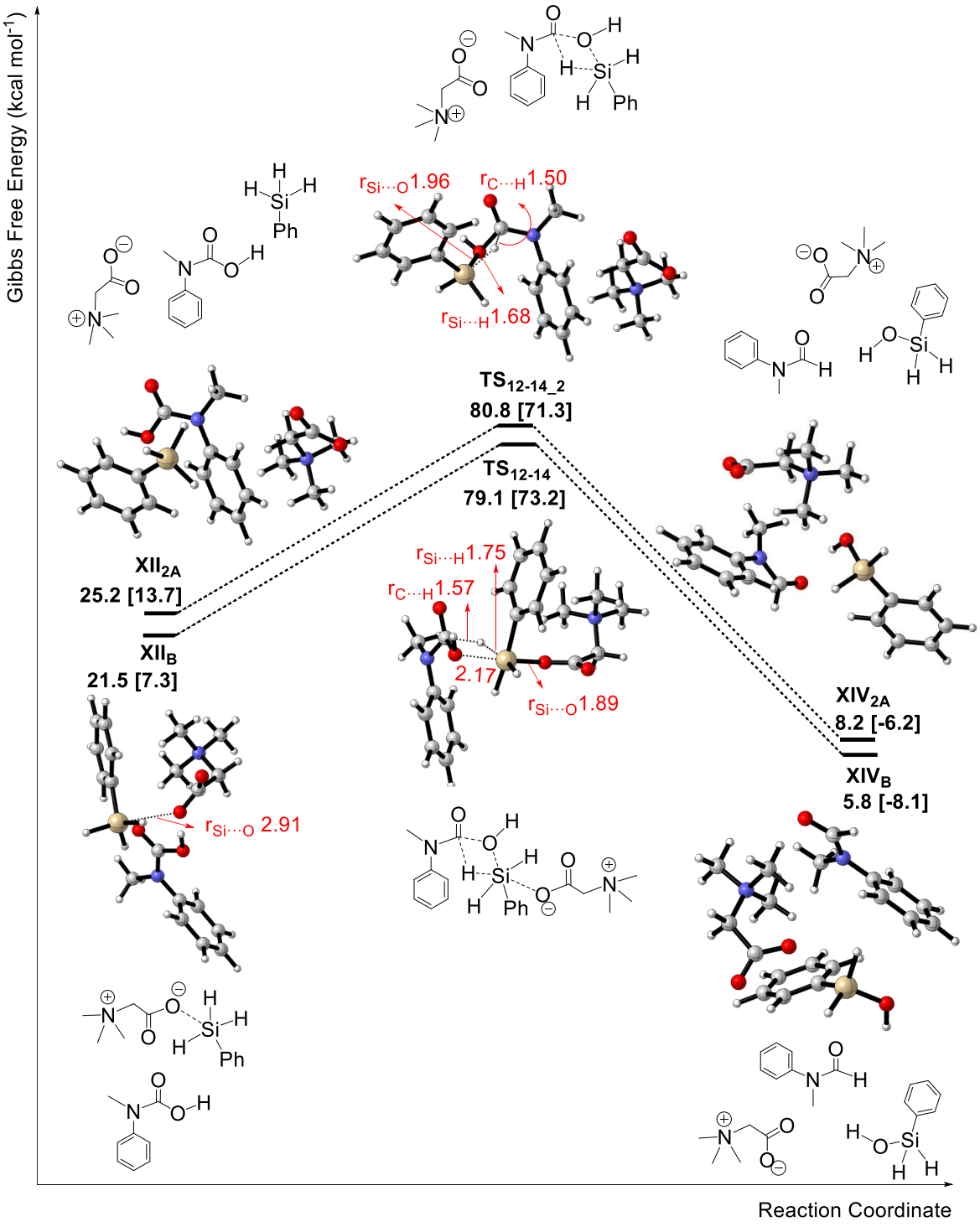

Figure 5.2.4. Conformers of $TS_{12\text{-}14}$. *The relative free energies given in kcal/mol are calculated by using SMD(CH_3CN) ωB97XD/6-311++G(d,p)//ωB97XD/6-31+G(d,p). Free energies calculated in gas phase are quoted in square brackets. Bond distances are shown in Å in red. Molecular graphics were produced by CYLview.*

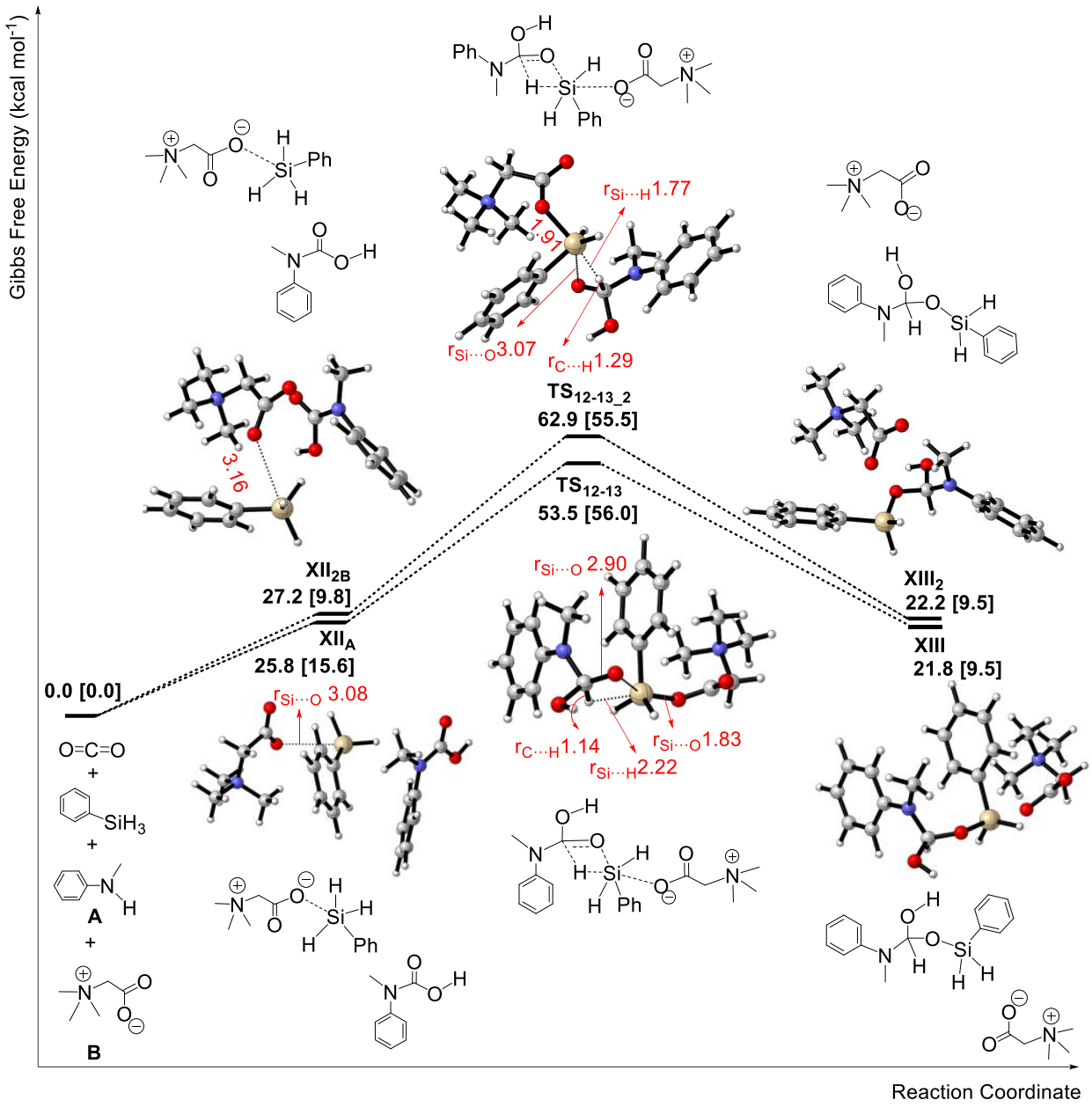

Figure 5.2.5. Computed free-energy profile for the reactions involving conformers of $TS_{12\text{-}13}$. *The relative free energies given in kcal mol^{-1} are calculated by using SMD(CH_3CN) ωB97XD/6-311++G(d,p)//ωB97XD/6-31+G(d,p). Free energies calculated in gas phase are quoted in square brackets. Bond distances are shown in Å in red. Molecular graphics were produced by CYLview.*

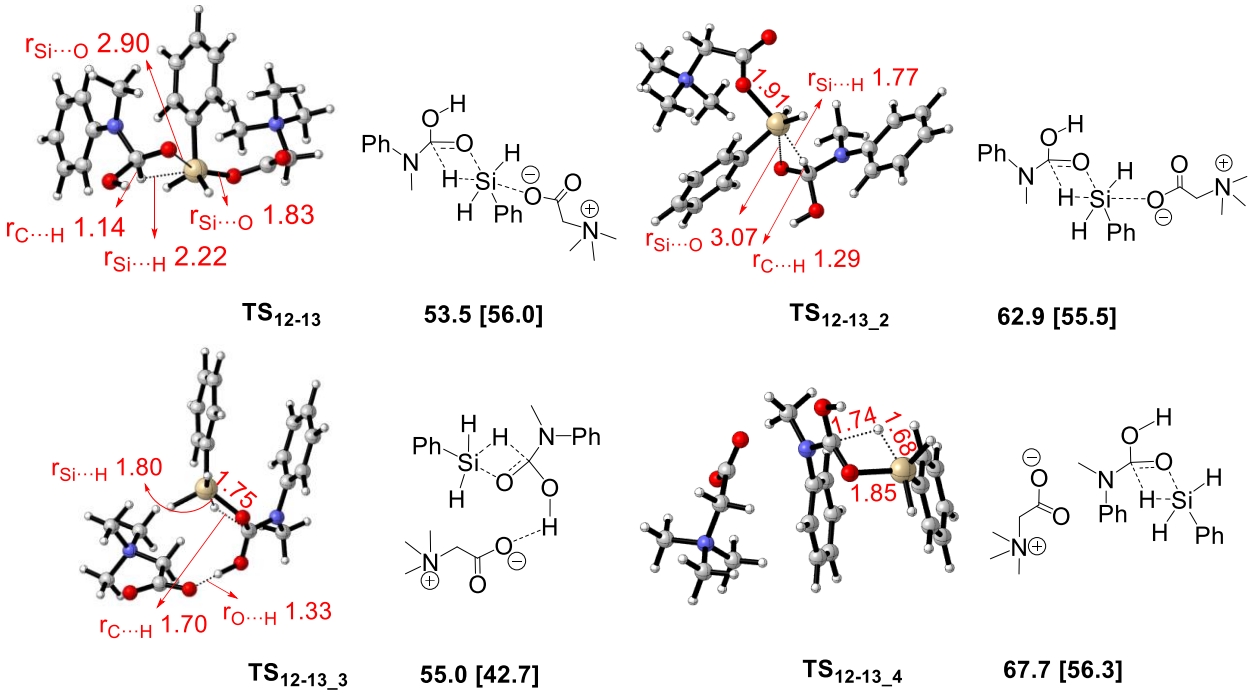

Figure 5.2.6. Conformers of $TS_{12\text{-}13}$. *The relative free energies given in kcal/mol are calculated by using SMD(CH_3CN) ωB97XD/6-311++G(d,p)//ωB97XD/6-31+G(d,p). Free energies calculated in gas phase are quoted in square brackets. Bond distances are shown in Å in red. Molecular graphics were produced by CYLview.*

5.3 Calculated reaction pathway 3

The final product from pathway 3 is the formamide and the product is produced under the catalysis of either glycine betaine or $HCOO^-$. **Figure 5.3.1**, **figure 5.3.2** and **figure 5.3.5** show the energy profiles for the reactions under the catalysis of glycine betaine in pathway 3. **Figure 5.3.3** and **figure 5.3.4** present the energy profile for the reactions under the catalysis of glycine betaine and $HCOO^-$ in pathway 3. In **figure 5.3.1**, CO_2 first reacts with $PhSiH_3$ under the catalysis of glycine betaine to produce formoxysilane. This reaction happens *via* **$TS_{1\text{-}2}$** and it is the same as the first reaction in pathway 1. Formoxysilane then reacts with N-methylaniline under the catalysis of glycine betaine to form **XIV** which is a complex of the formamide and phenylsilanol. The reaction involves three transition states: **$TS_{22\text{-}25}$**, **$TS_{25\text{-}26}$** and **$TS_{26\text{-}14}$**. In **$TS_{22\text{-}25}$**, the distance between the N atom in N-methylaniline and the C atom

in formoxysilane is reduced, and the distance between the H atom in N-methylaniline and the O atom in glycine betaine becomes shorter. In **TS_{25-26}**, the proton transfers from the N atom to the O atom. In **TS_{26-14}**, the Si-O bond and the C-O bond disconnect to form the formamide and phenylsilanol. The activation free energy barriers of **TS_{22-25}**, **TS_{25-26}** and **TS_{26-14}** are 25.8, 34.6 and 33.5 kcal/mol. The reaction mechanism in **figure 5.3.3** and **figure 5.3.4** is the same as the reaction mechanism in **figure 5.3.1** and **figure 5.3.2**. The only difference is that a complex of the formamide and phenylsilanol is formed under the catalysis of $HCOO^-$. Both glycine betaine and $HCOO^-$ have the carboxylate group. It is the carboxylate group catalyses the formation of **XIV** and **XXX**. In **figure 5.3.5**, CO_2 first reacts with $PhSiH_3$ under the catalysis of glycine betaine to produce formoxysilane. The reaction occurs via **TS_{1-2}**. Formoxysilane then reacts with N-methylaniline to form **XIV'_B** which is a complex of the formamide and phenylsilanol. The reaction occurs through **TS'_{22-14}** under no catalyst. To sum up, pathway 3 has three routes to form the formamide. Two of them are catalysed by glycine betaine, while the other route is catalysed by glycine betaine and $HCOO^-$. In terms of one of the reactions catalysed by glycine betaine, the rate-determining step is the reaction involving **TS_{25-26}** and the activation free energy barrier of the reaction is 34.6 kcal/mol. For the other reaction catalysed by glycine betaine, the rate-determining step is the reaction involving **TS'_{22-14}** and the activation free energy barrier of the reaction is 36.4 kcal/mol. When the catalysts are glycine betaine and $HCOO^-$, the rate-determining step is the reaction involving **TS_{28-29}** and the activation free energy barrier of the reaction is 32.2 kcal/mol. Since the route catalysed by glycine betaine and $HCOO^-$ has the lowest activation free energy barrier of the rate-determining step, this route is more preferred to produce the formamide. Therefore, the formamide is produced under the catalysis of glycine betaine and $HCOO^-$, and the activation free energy barrier of the rate-determining step is 32.2 kcal/mol.

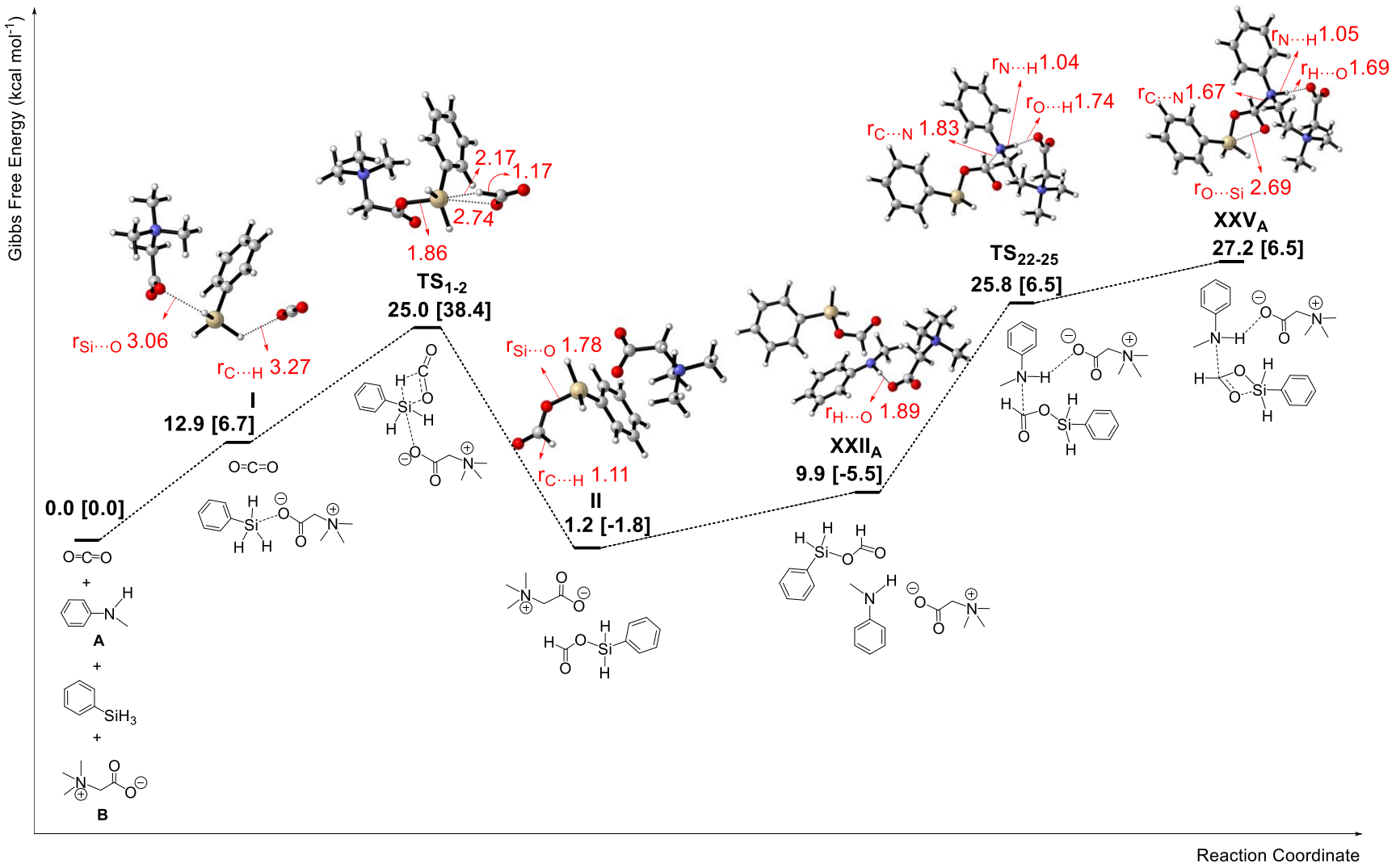

Figure 5.3.1. Computed free-energy profile for the reactions in pathway 3 for the formation of XXV_A. *The relative free energies given in kcal mol^{-1} are calculated by using SMD(CH_3CN) ωB97XD/6-311++G(d,p)//ωB97XD/6-31+G(d,p). Free energies calculated in gas phase are quoted in square brackets. Bond distances are shown in Å in red. Molecular graphics were produced by CYLview.*

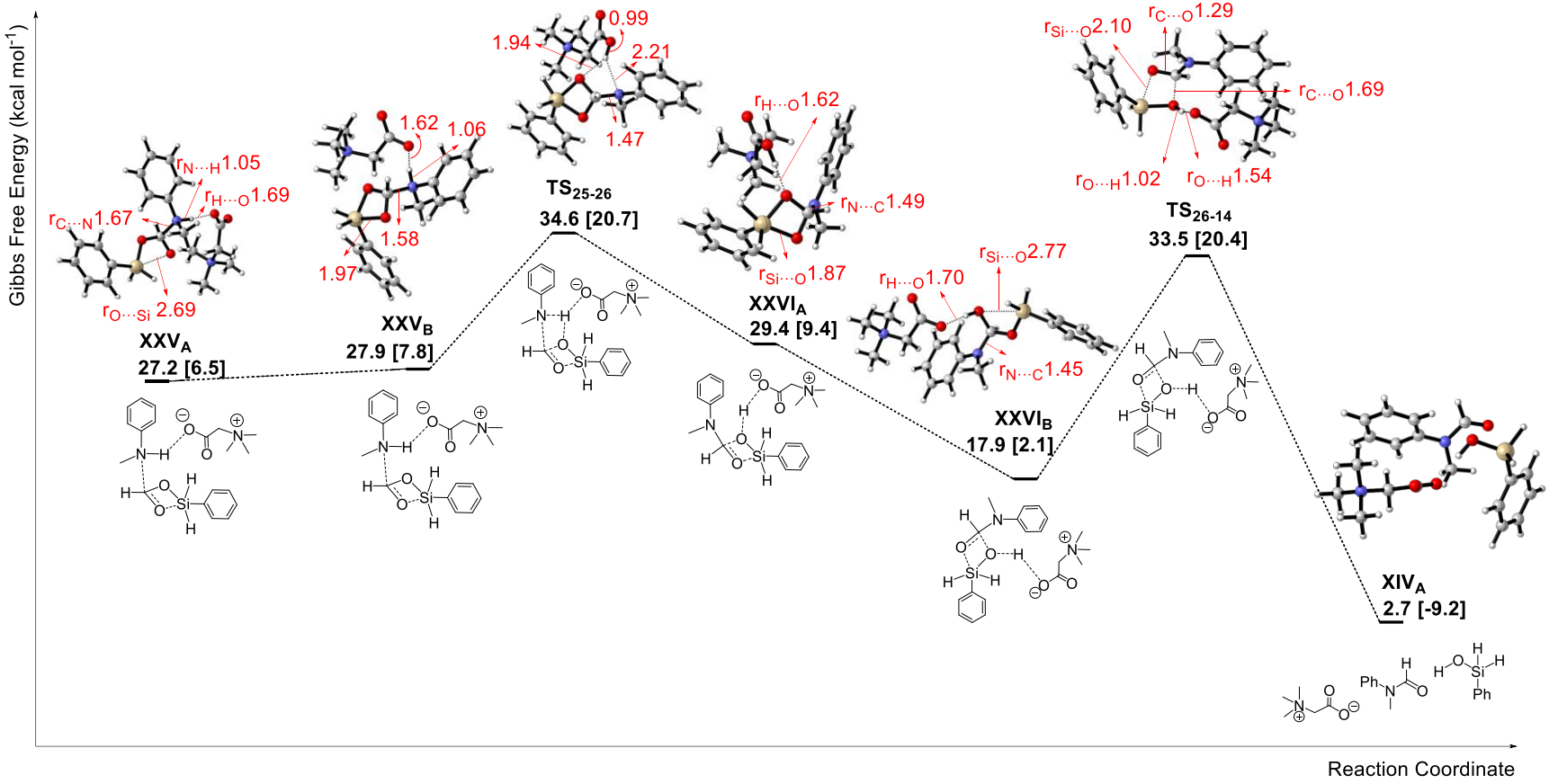

Figure 5.3.2. Computed free-energy profile for the reactions in pathway 3 for the formation of intermediate XIV$_A$. *The relative free energies given in kcal mol^{-1} are calculated by using SMD(CH$_3$CN) ωB97XD/6-311++G(d,p)//ωB97XD/6-31+G(d,p). Free energies calculated in gas phase are quoted in square brackets. Bond distances are shown in Å in red. Molecular graphics were produced by CYLview.*

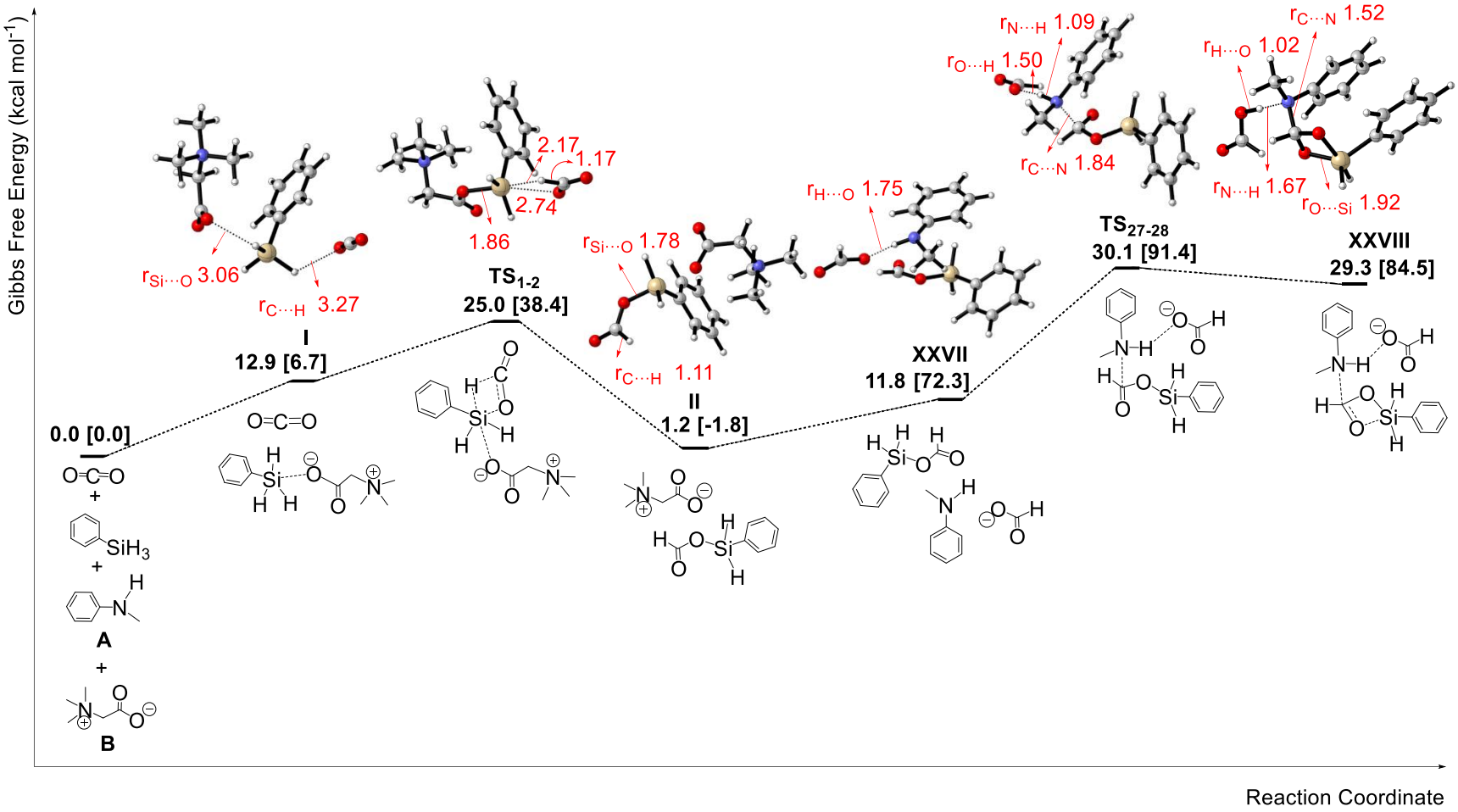

Figure 5.3.3. Computed free-energy profile for the reactions in pathway 3 for the formation of intermediate XXVIII. *The relative free energies given in kcal mol^{-1} are calculated by using SMD(CH_3CN) ωB97XD/6-311++G(d,p)//ωB97XD/6-31+G(d,p). Free energies calculated in gas phase are quoted in square brackets. Bond distances are shown in Å in red. Molecular graphics were produced by CYLview.*

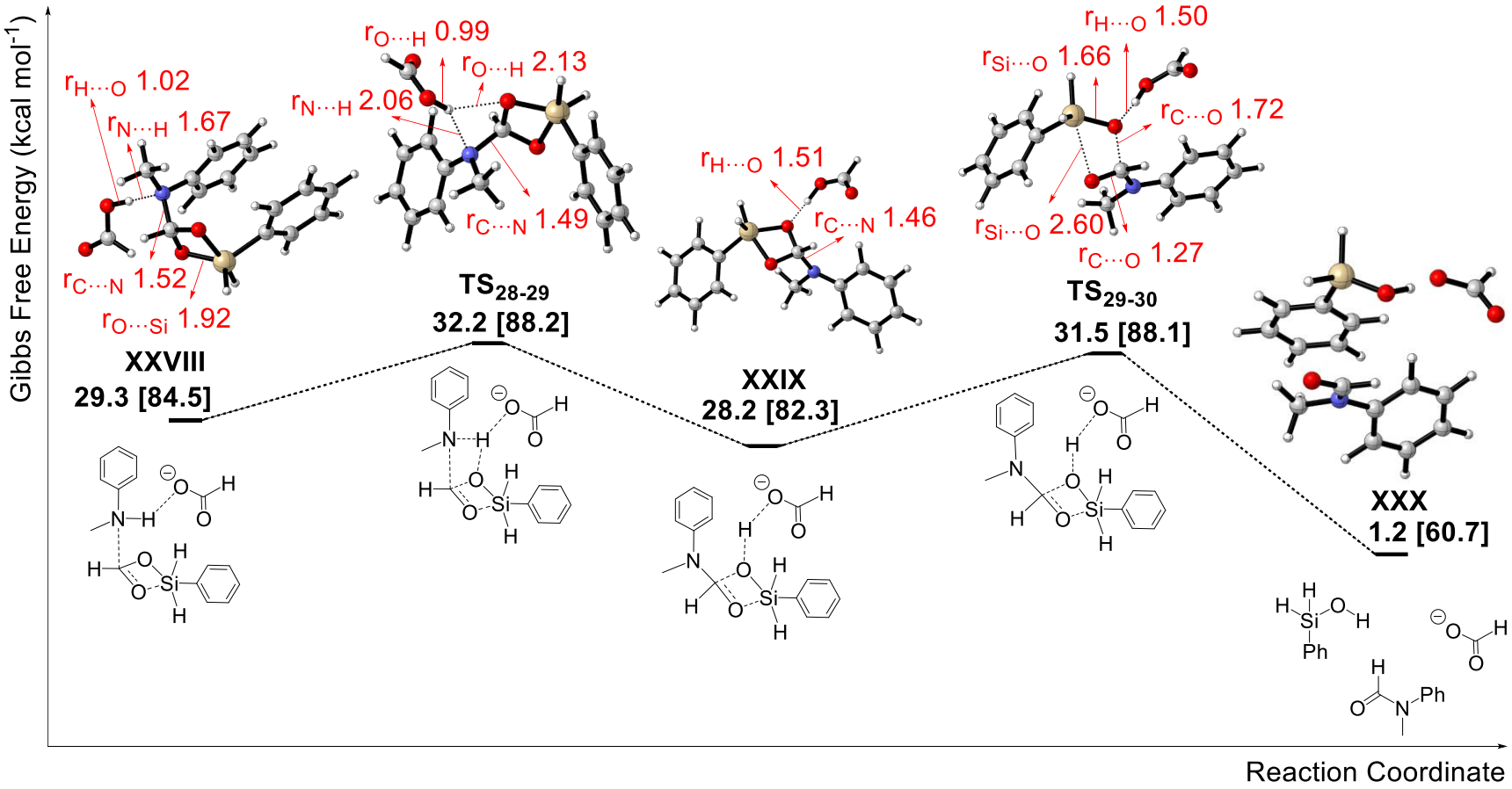

Figure 5.3.4. Computed free-energy profile for the reactions in pathway 3 for the formation of intermediate XXX. *The relative free energies given in kcal mol^{-1} are calculated by using SMD(CH_3CN) ωB97XD/6-311++G(d,p)//ωB97XD/6-31+G(d,p). Free energies calculated in gas phase are quoted in square brackets. Bond distances are shown in Å in red. Molecular graphics were produced by CYLview.*

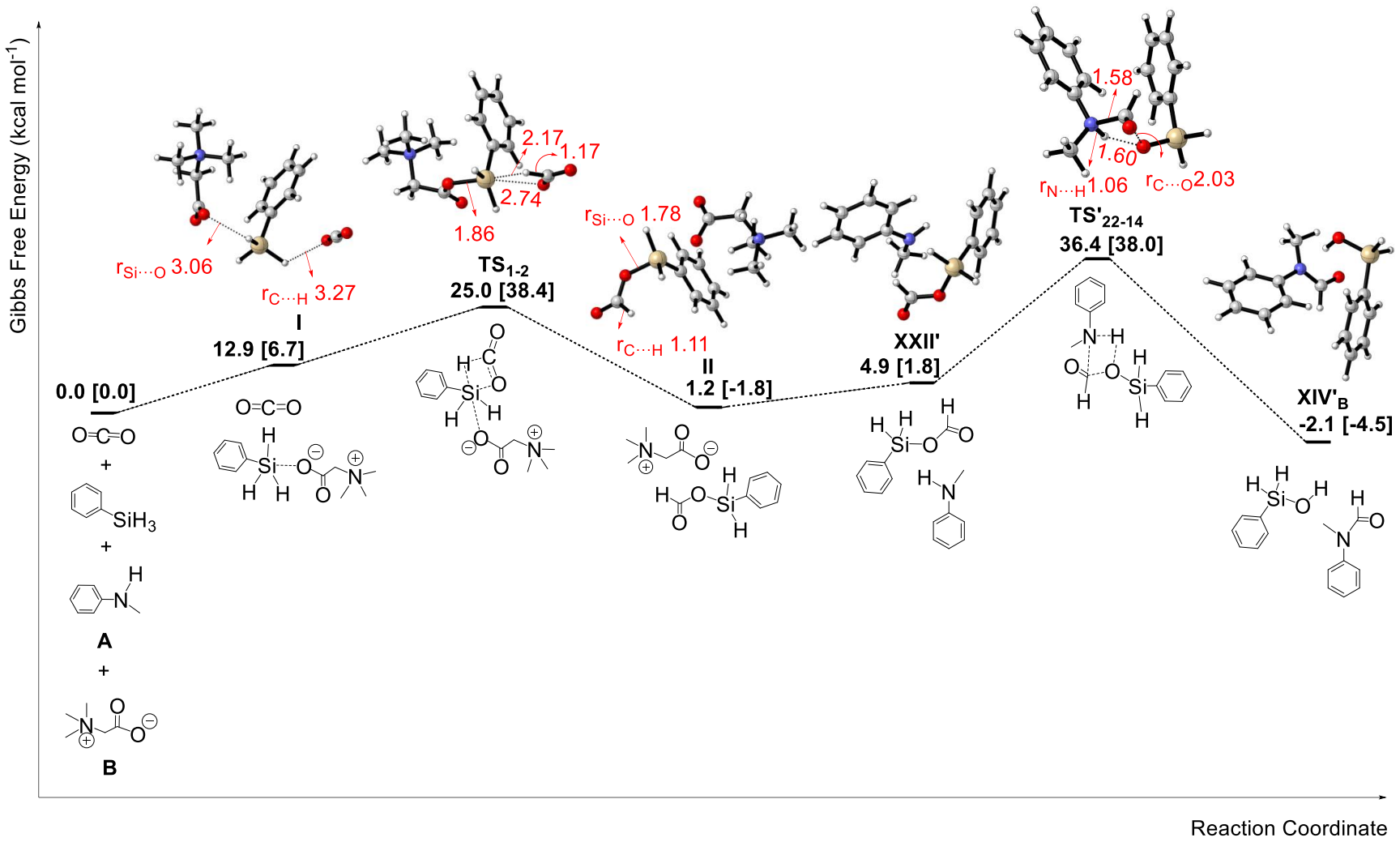

Figure 5.3.5. Computed free-energy profile for the reactions in pathway 3 for the formation of intermediate XIV'$_B$. *The relative free energies given in kcal mol^{-1} are calculated by using SMD(CH_3CN) ωB97XD/6-311++G(d,p)//ωB97XD/6-31+G(d,p). Free energies calculated in gas phase are quoted in square brackets. Bond distances are shown in Å in red. Molecular graphics were produced by CYLview.*

During my DFT calculations, conformers of **$TS_{28\text{-}29}$** and **$TS_{29\text{-}30}$** are found. They are presented in **figure 5.3.6** and **figure 5.3.7**. In **figure 5.3.6**, there are two conformers of **$TS_{28\text{-}29}$**: **$TS_{28\text{-}29}$** and **$TS_{28\text{-}29\_2}$**. The reaction mechanism of the two transition states are the same, which is to transfer the proton from N-methylaniline to formoxysilane via a four membered ring. The activation free energy barrier of $TS_{28\text{-}29}$ is 32.2 kcal/mol, while the activation free energy barrier of **$TS_{28\text{-}29\_2}$** is 33.4 kcal/mol. Since the activation free energy barrier of **$TS_{28\text{-}29}$** is lower than that of **$TS_{28\text{-}29\_2}$**, **$TS_{28\text{-}29}$** is used as the transition state in **figure 5.3.4**. **Figure 5.3.7** presents two conformers of **$TS_{29\text{-}30}$**: **$TS_{29\text{-}30}$** and **$TS_{29\text{-}30\_2}$**. Both transition states aim to produce the formamide using the same reaction mechanism where the Si-O bond and the C-O bond in the four membered ring are disconnected. The activation free energy barrier of **$TS_{29\text{-}30}$** is 31.5 kcal/mol, while the activation free energy barrier of **$TS_{29\text{-}30\_2}$** is 33.4 kcal/mol. Since the activation free energy barrier of $TS_{29\text{-}30}$ is lower than that of **$TS_{29\text{-}30\_2}$**, **$TS_{29\text{-}30}$** is used as the transition state in **figure 5.3.4**.

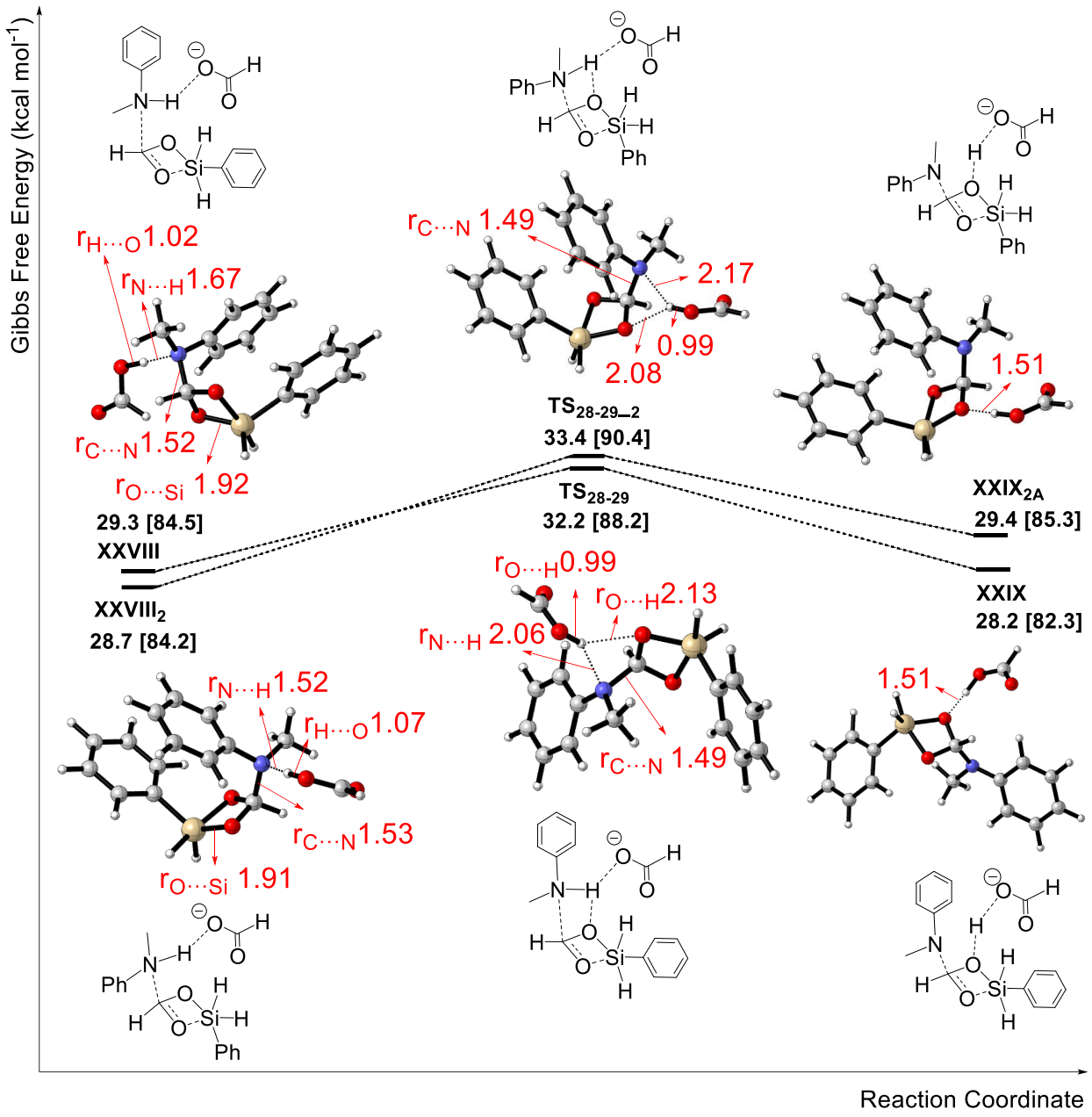

Figure 5.3.6. Conformers of $TS_{28\text{-}29}$. *The relative free energies given in kcal/mol are calculated by using SMD(CH_3CN) ωB97XD/6-311++G(d,p)//ωB97XD/6-31+G(d,p). Free energies calculated in gas phase are quoted in square brackets. Bond distances are shown in Å in red. Molecular graphics were produced by CYLview.*

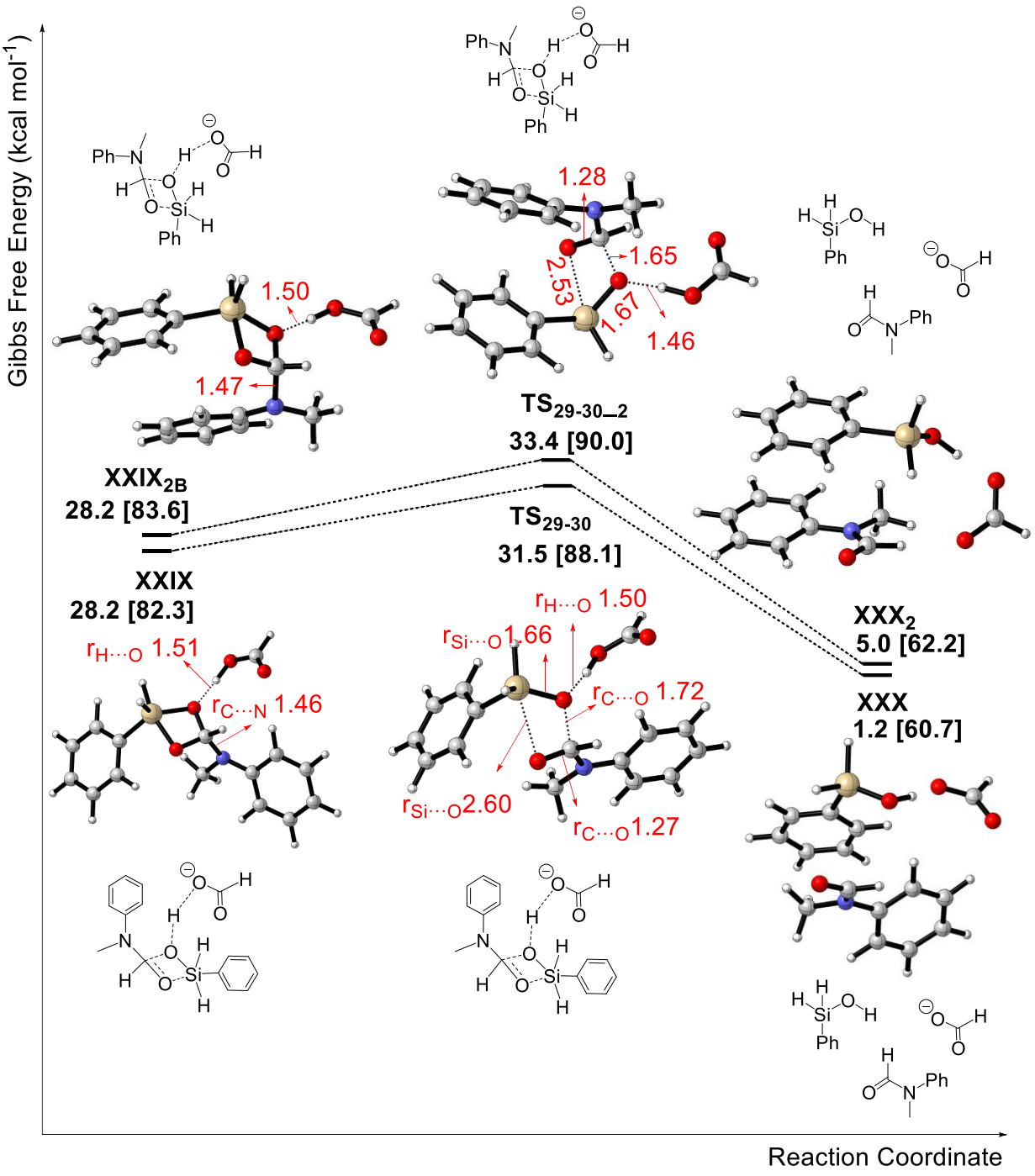

Figure 5.3.7. Conformers of $TS_{29\text{-}30}$. *The relative free energies given in kcal/mol are calculated by using SMD(CH_3CN) ωB97XD/6-311++G(d,p)//ωB97XD/6-31+G(d,p). Free energies calculated in gas phase are quoted in square brackets. Bond distances are shown in Å in red. Molecular graphics were produced by CYLview.*

During my DFT calculations, whether **TS'$_{22\text{-}14}$** can be catalysed by glycine betaine is tried. Two activation modes for **TS$_{22\text{-}14}$** are proposed in **figure 5.3.8**, which are mode **U** and mode **V**. In the two activation modes, glycine betaine may activate either the amine or formoxysilane in mode **U** or mode **V**. However, neither of the activation modes are obtained. **Figure 5.3.9** presents two conformers of **TS$_{22\text{-}14}$**, which are **TS$_{22\text{-}14}$** and **TS$_{22\text{-}14_2}$**. It seems like **TS$_{22\text{-}14_2}$** is based on mode **V**. However, the distance between the O atom in glycine betaine and the Si atom in $PhSiH_3$ is 3.21 Å. Since the distance is long, there is no interaction between glycine betaine and $PhSiH_3$. Therefore, the transition state based on mode **V** is not found. Glycine betaine in **TS$_{22\text{-}14}$** has no interaction with any of the reactants. Therefore, neither mode **U** nor mode **V** applies in **TS$_{22\text{-}14}$**. The activation free energy barrier of **TS$_{22\text{-}14_2}$** is 47.2 kcal/mol, while the activation free energy barrier of **TS$_{22\text{-}14}$** is 43.4 kcal/mol. As mentioned in **figure 4.4**, the activation free energy barrier of **TS'$_{22\text{-}14}$** is 36.4 kcal/mol when there is no catalyst. Thus, compared to **TS$_{22\text{-}14}$** and **TS$_{22\text{-}14_2}$**, **TS'$_{22\text{-}14}$** is more preferred and chosen as the transition state in **figure 5.3.5**.

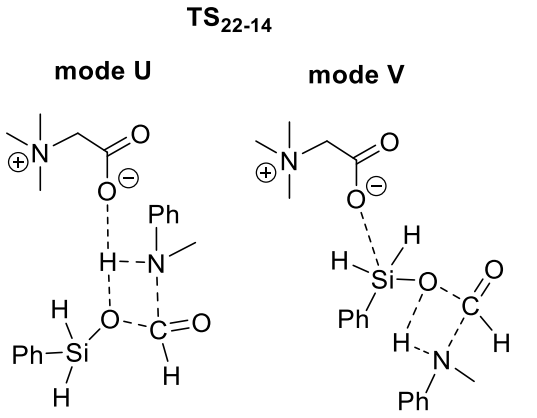

Figure 5.3.8. *Other trials for transition states in pathway 3*

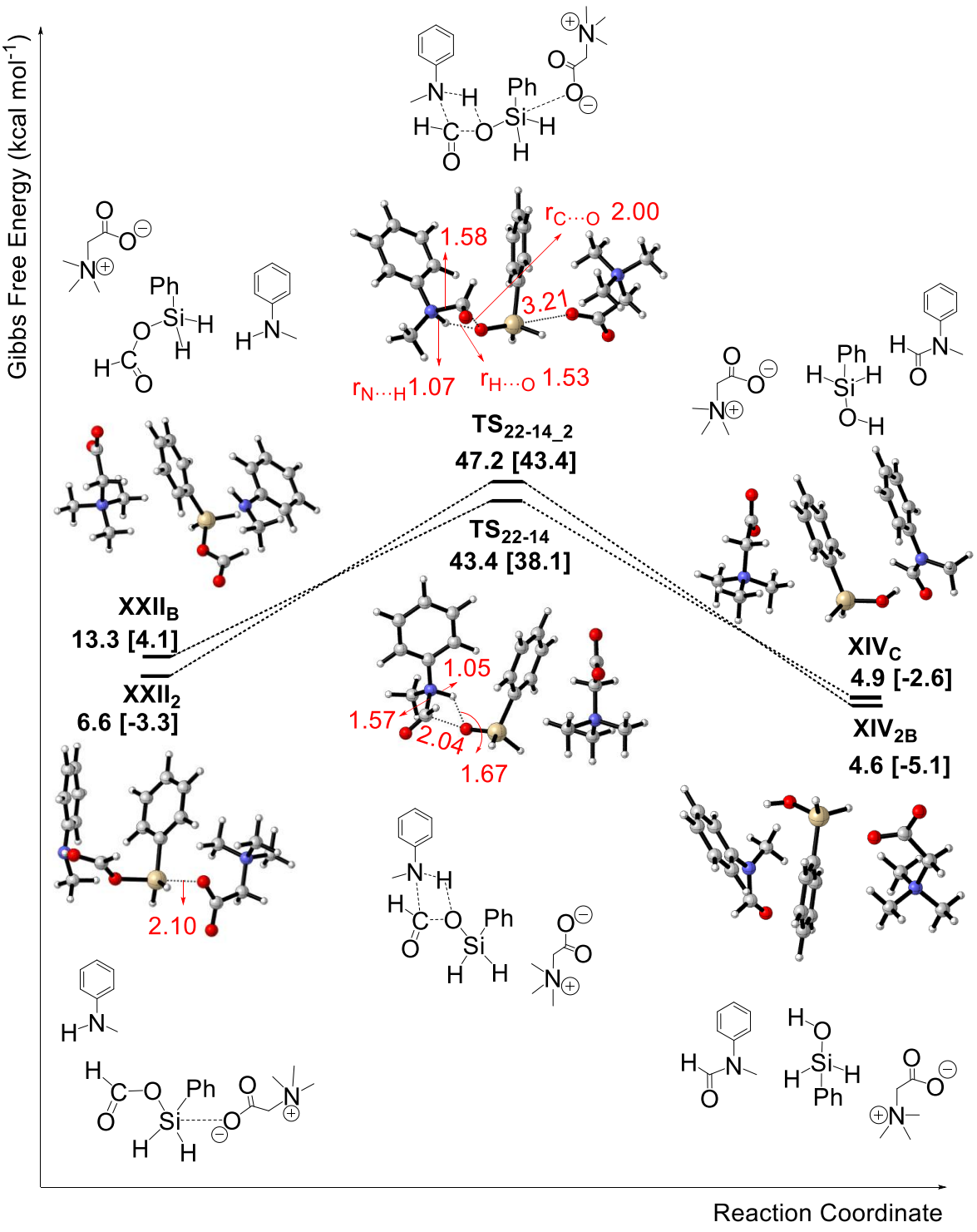

Figure 5.3.9. Conformers of $TS_{22\text{-}14}$. *The relative free energies given in kcal/mol are calculated by using SMD(CH_3CN) ωB97XD/6-311++G(d,p)//ωB97XD/6-31+G(d,p). Free energies calculated in gas phase are quoted in square brackets. Bond distances are shown in Å in red. Molecular graphics were produced by CYLview.*

5.4 Summary of the most likely reaction pathway

Up to now, two papers have mentioned glycine betaine catalysed CO_2 reduction. One is the experiments by Han and co-workers, the other is the experiments by He and co-workers.[37, 58] Since my DFT calculations have shown the formation of the formamide, the methylamine and the aminal, **table 5.4.0.1** presents my DFT calculation results and reaction conditions found by Han and co-workers.[58] In **table 5.4.0.1**, pathway 1 produces either the aminal or the methylamine under the catalysis of glycine betaine (GB). The rate-determining step (RDS) to produce the two products is the same and the activation free energy barrier ($\Delta G^{\ddagger}_{sol}$) of the rate-determining step is 37.8 kcal/mol. Since the two products are produced at 100 °C from experiments, the activation free energy barrier found from my DFT calculations is reasonable. From my DFT calculations, the input ratio of N-methylaniline:CO_2:$PhSiH_3$ to produce the aminal is 2:2:3. However, the input ratio from the experiments was 1:2:2. In terms of the production of the methylamine, the input ratio of N-methylaniline:CO_2:$PhSiH_3$ from my DFT calculations is 1:2:3, while the input ratio from the experiments is 1:6:4. There are some deviations between the input ratios from my DFT calculations and the input ratios from the experiments. The deviations may due to experimental errors. For pathway 2, the $\Delta G^{\ddagger}_{sol}$ of the RDS is 53.5 kcal/mol. Since the experiments occur under mild conditions, the activation free energy barrier for pathway 2 is too high. Therefore, pathway 2 is not worth exploring further although it is incomplete. Pathway 3 produces the formamide and both GB and $HCOO^-$ work as the catalysts in the reactions. The $\Delta G^{\ddagger}_{sol}$ of the RDS of pathway 3 is 32.2 kcal/mol. In experiments, the reaction took place at 25 °C. Therefore, the activation free energy barrier found from my DFT calculations is reasonable. The input ratio of N-methylaniline:CO_2:$PhSiH_3$ from my DFT calculations is 1:1:1, while the input ratio from the experiments is 1:10:2. The deviation may due to experimental errors. In conclusion, the proved

reaction mechanism of the formation of the formamide, the methylamine and the aminal is presented in **figure 5.4.0.1**.

Table 5.4.0.1. *Comparison between the DFT calculation results and experimental results*

results from my DFT calculations							experimental results by Han and co-workers	
reaction pathway	product	catalyst	RDS	$\Delta G^{\ddagger}_{sol}$ (kcal/mol)	input ratio (amine:CO_2:$PhSiH_3$)		T (°C)	P (MPa)
pathway 1	aminal	GB	reaction *via* **TS_{3-4}**	37.8	2:2:3	1:2:2	100	0.2
	methylamine				1:2:3	1:6:4	100	0.3
pathway 2	unnecessary to explore further	GB	reaction *via* **TS_{12-13}**	53.5				
pathway 3	formamide	$HCOO^-$ and GB	reaction *via* **TS_{28-29}**	32.2	1:1:1	1:10:2	25	0.5

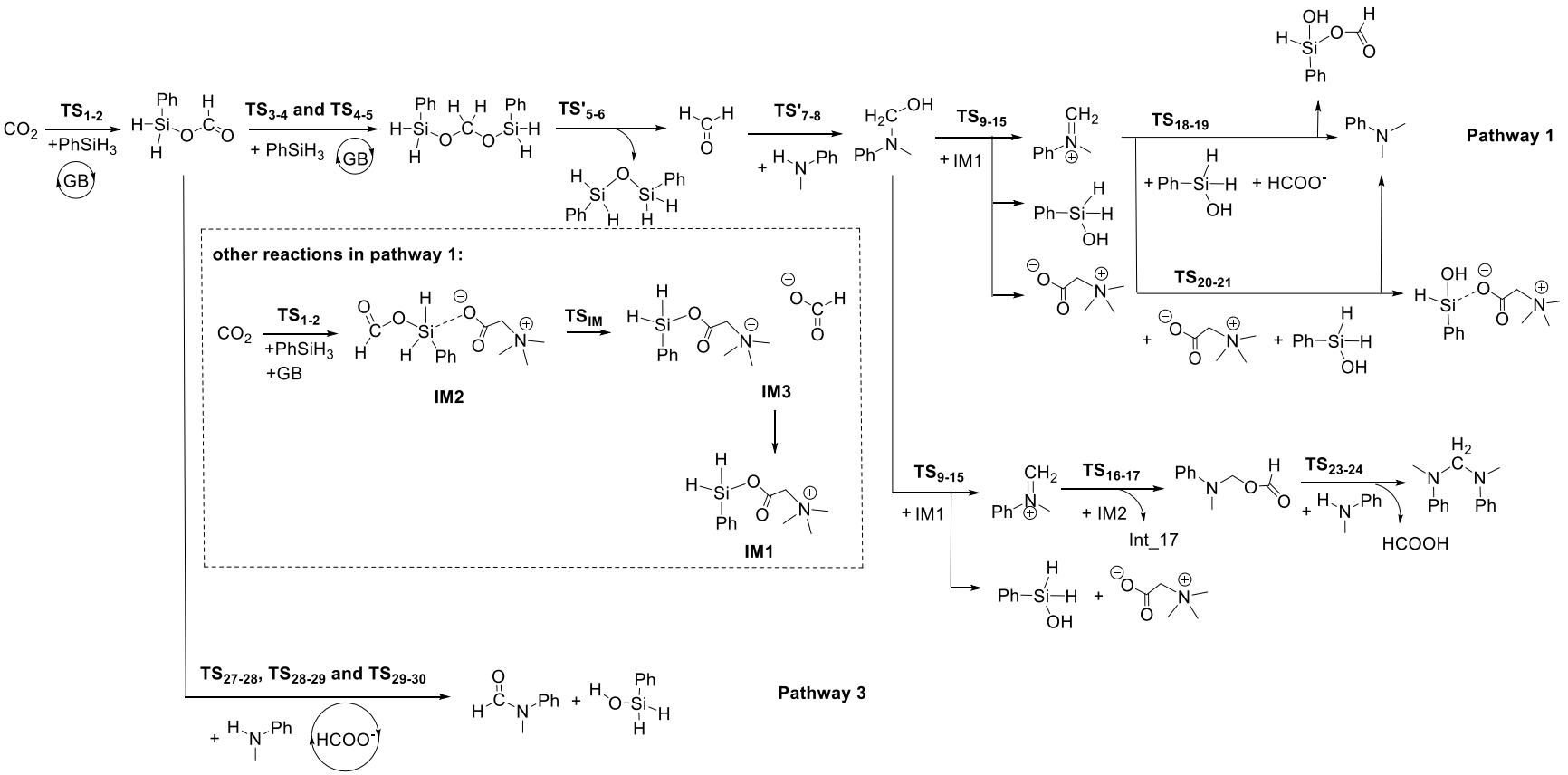

Figure 5.4.0.1. *The proved reaction mechanism of the formation of the formamide, the methylamine and the aminal*

My DFT calculations show that glycine betaine catalyses the reactions between CO_2, $PhSiH_3$ and N-methylaniline. **Table 5.4.0.2** compares the activation free energy barriers of the reactions under the catalysis of glycine betaine with the activation free energy barriers of the reactions under no catalyst. It can be concluded from **table 5.4.0.2** that GB helps reduce the activation free energy barriers of the reactions in the three pathways.

Table 5.4.0.2. *Comparison between the reactions catalysed by GB and the reactions with no catalyst*

	Reactions under no catalyst	$\Delta G^{\ddagger}_{sol}$ (kcal/mol)	GB catalysed reactions	$\Delta G^{\ddagger}_{sol}$ (kcal/mol)
pathway 1	**TS'$_{1\text{-}2}$**	49.3	**TS$_{1\text{-}2}$**	25.0
	TS'$_{3\text{-}5}$	52.2	**TS$_{3\text{-}4}$**	37.8
			TS$_{4\text{-}5}$	26.0
pathway 2	**TS'$_{10\text{-}11}$**	45.7	**TS'$_{10\text{-}11}$**	45.7
	TS'$_{12\text{-}13}$	59.6	**TS$_{12\text{-}13}$**	53.5
	TS'$_{12\text{-}14}$	73.2	**TS'$_{12\text{-}14}$**	73.2
pathway 3	**TS'$_{1\text{-}2}$**	49.3	**TS$_{1\text{-}2}$**	25.0

5.4.1 Benchmark/validation study

He and co-workers used SMD(CH_3CN) M06-2X/6-311++G(d,p)//B3LYP/6-31+G(d) to calculate the reaction mechanism shown in **figure 5.4.1.1**.[61] In **figure 5.4.1.1**, the reaction between formoxysilane (IM1a) and Si-1a produces **IM2a** *via* **TS$_{2a}$**. CH_3COO^- acts as a catalyst in this reaction. To double check their calculations, I recalculated the reaction using the same functional and basis set. My calculation results are shown in **figure 5.4.1.2**. In **figure 5.4.1.2**, there is a black energy profile and a red energy profile. In order to calculate the black energy profile, **TS$_{2a}$** was obtained from the literature and recalculated with TS optimisation. In terms of the red energy profile, **TS$_{2a}$** was obtained from the literature and recalculated without TS optimisation. By comparing the energy profiles in **figure 5.4.1.1** and **figure 5.4.1.2**, it can be concluded that the three structures of **TS$_{2a}$** in the two figures are the same.

The final products in the two figures are **IM2a**, **IM2a_2** and **IM2a_3**. The difference between **IM2a** and **IM2a_3** results from the rotation of the Si-O bond on the left. The difference between **IM2a_2** and **IM2a_3** is the coordination around the Si atom on the right. The coordination around the Si atom in **IM2a_2** is a trigonal bipyramid, while the coordination around the Si atom in **IM2a_3** is a square pyramid. The two figures show the same **TS_{2a}** but different reaction pathways. This phenomenon shows that one transition state can lead to different products using the same functional and basis set.

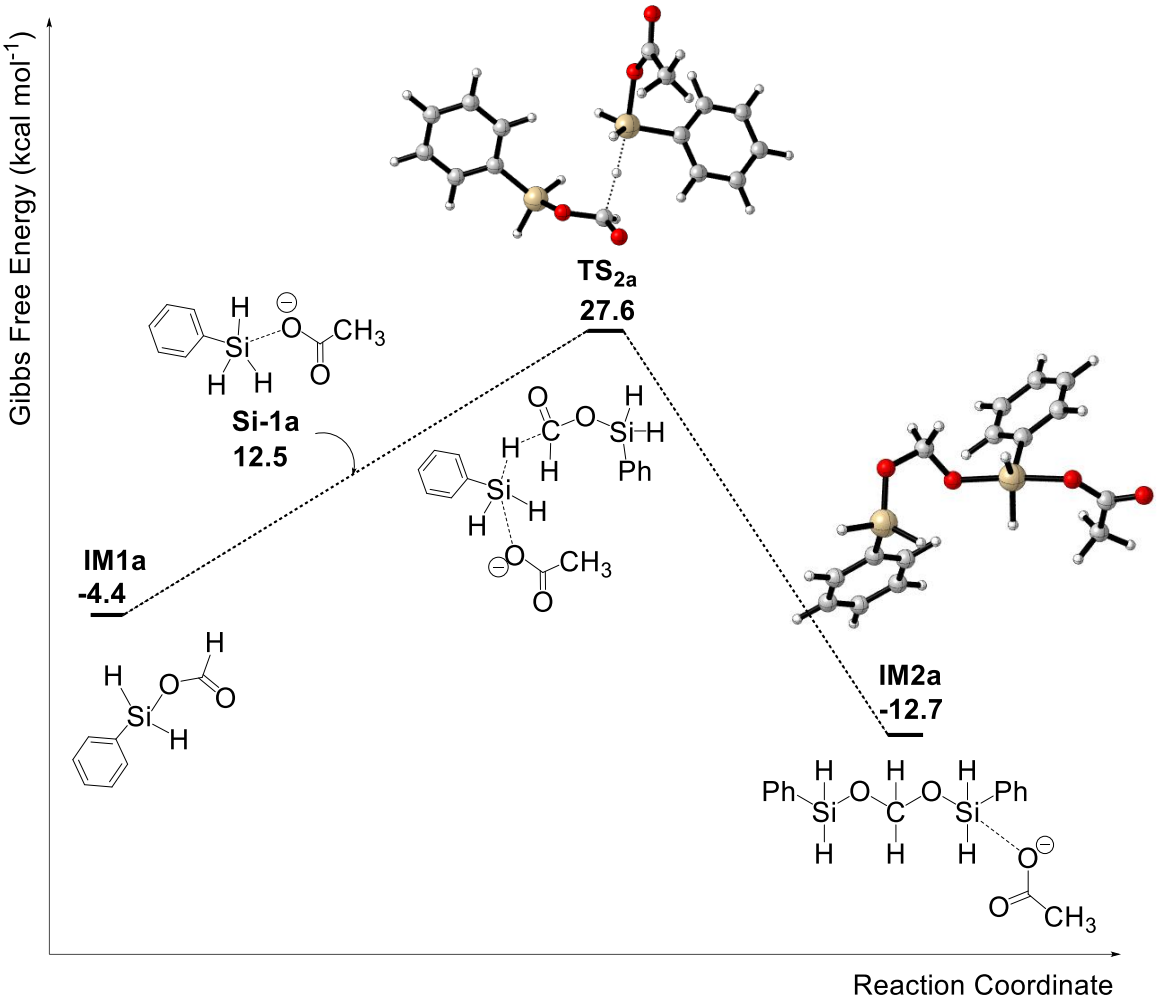

Figure 5.4.1.1. The reaction mechanism calculated by He and co-workers.[61] *The relative free energies given in kcal mol^{-1} are calculated by using SMD(CH_3CN) M06-2X/6-311++G(d,p)//B3LYP/6-31+G(d). Molecular graphics were produced by CYLview.*

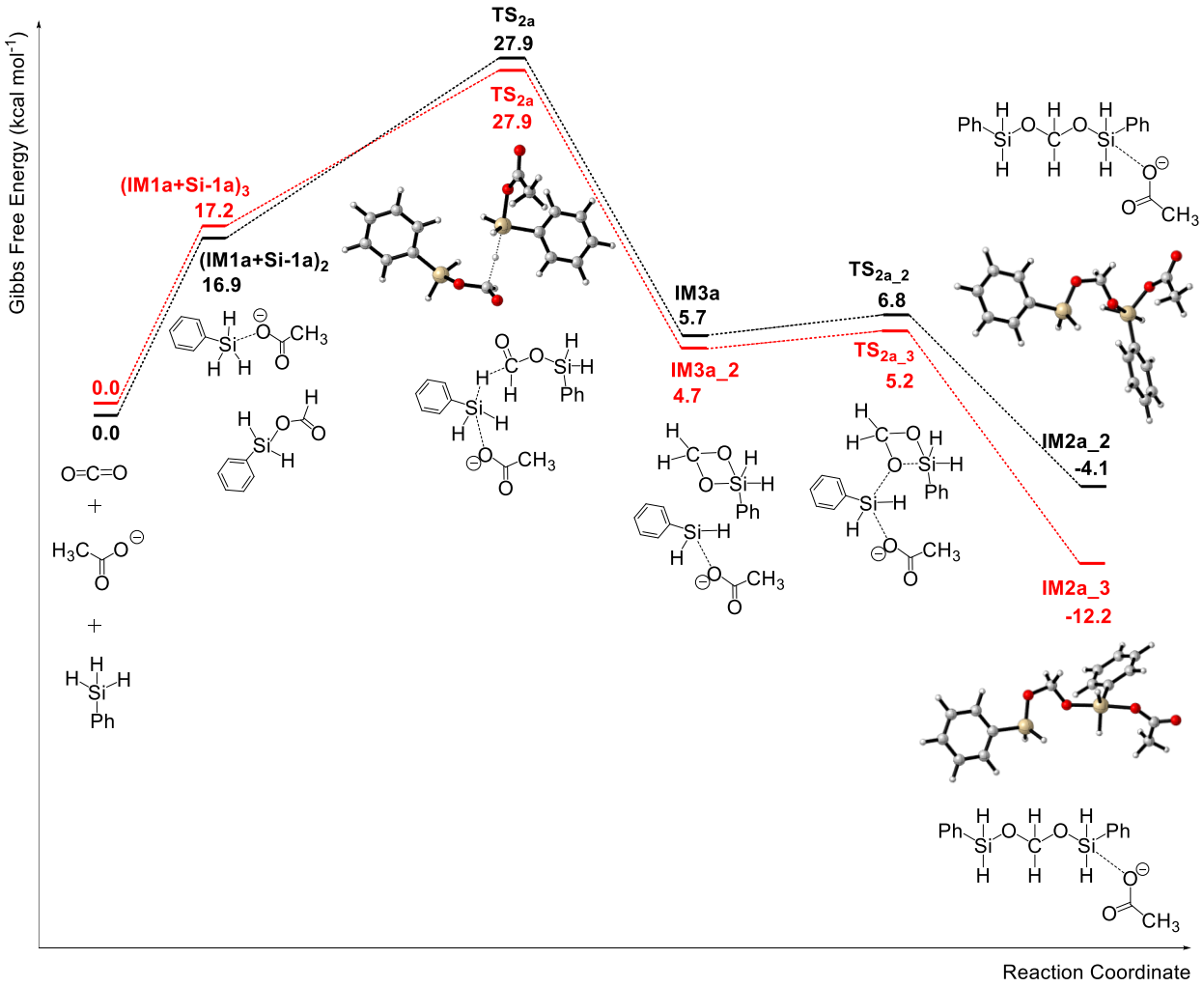

Figure 5.4.1.2. The recalculated reaction mechanism. *The relative free energies given in kcal mol^{-1} are calculated by using SMD(CH_3CN) M06-2X/6-311++G(d,p)//B3LYP/6-31+G(d). Molecular graphics were produced by CYLview.*

5.4.2 The effect of different functionals on single point calculations

Chapter 5.1 to **5.3** used ωB97XD for single point calculations. To see if a different functional will influence the calculation results, M06-2X is used for single point calculations in this section. **Figure 5.4.2.1** to **figure 5.4.2.12** present energy profiles for the three pathways in **figure 5.0.1**. **Figure 5.4.2.1** to **figure 5.4.2.6** shows the energy profiles of the reactions in pathway 1. It can be concluded from **figure 5.4.2.1** to **figure 5.4.2.6** that pathway 1 produces two different products: the methylamine and the aminal. The rate-determining step (RDS) to produce the two products is the same, which is the reaction with the transition state of **TS_{3-4}**. The activation free energy barrier ($\Delta G^{\ddagger}_{sol}$) of the RDS is 28.9 kcal/mol. **Figure 5.4.2.7** presents the energy profile of the reactions in pathway 2. The RDS of pathway 2 is the reaction through **TS_{12-13}** with the activation free energy barrier of 45.0 kcal/mol. **Figure 5.4.2.8** to **figure 5.4.2.12** present the energy profiles of the reactions in pathway 3. In **figure 5.4.2.8** and **figure 5.4.2.9**, reactions are catalysed by glycine betaine and the RDS is the reaction via **TS_{25-26}**. The $\Delta G^{\ddagger}_{sol}$ of the RDS is 26.7 kcal/mol. In **figure 5.4.2.10** and **figure 5.4.2.11**, reactions are first catalysed by glycine betaine and then catalysed by $HCOO^-$. The RDS in **figure 5.4.2.10** and **figure 5.4.2.11** is the reaction through TS_{1-2} with the $\Delta G^{\ddagger}_{sol}$ of 20.1 kcal/mol. In **figure 5.4.2.12**, the first reaction is catalysed by glycine betaine, while the second reaction has no catalyst. The RDS in **figure 5.4.2.12** is the reaction *via* **TS'_{22-14}** with the $\Delta G^{\ddagger}_{sol}$ of 33.4 kcal/mol. After comparing the activation free energy barriers of the rate-determining steps in **figure 5.4.2.8** to **figure 5.4.2.12**, it can be concluded that the formamide is more preferred to be produced *via* the reactions presented in **figure 5.4.2.10** and **figure 5.4.2.11**. **Chapter 5.1** to **5.3** finds the reaction mechanism to produce the methylamine, the aminal and the formamide, which is shown in **figure 5.4.0.1**. After using a different functional for single point calculations, the reaction mechanism in **figure**

5.4.0.1 is still true. Therefore, it can be concluded that the reaction mechanism in **figure 5.4.0.1** shows how the methylamine, the aminal and the formamide are produced from experiments.

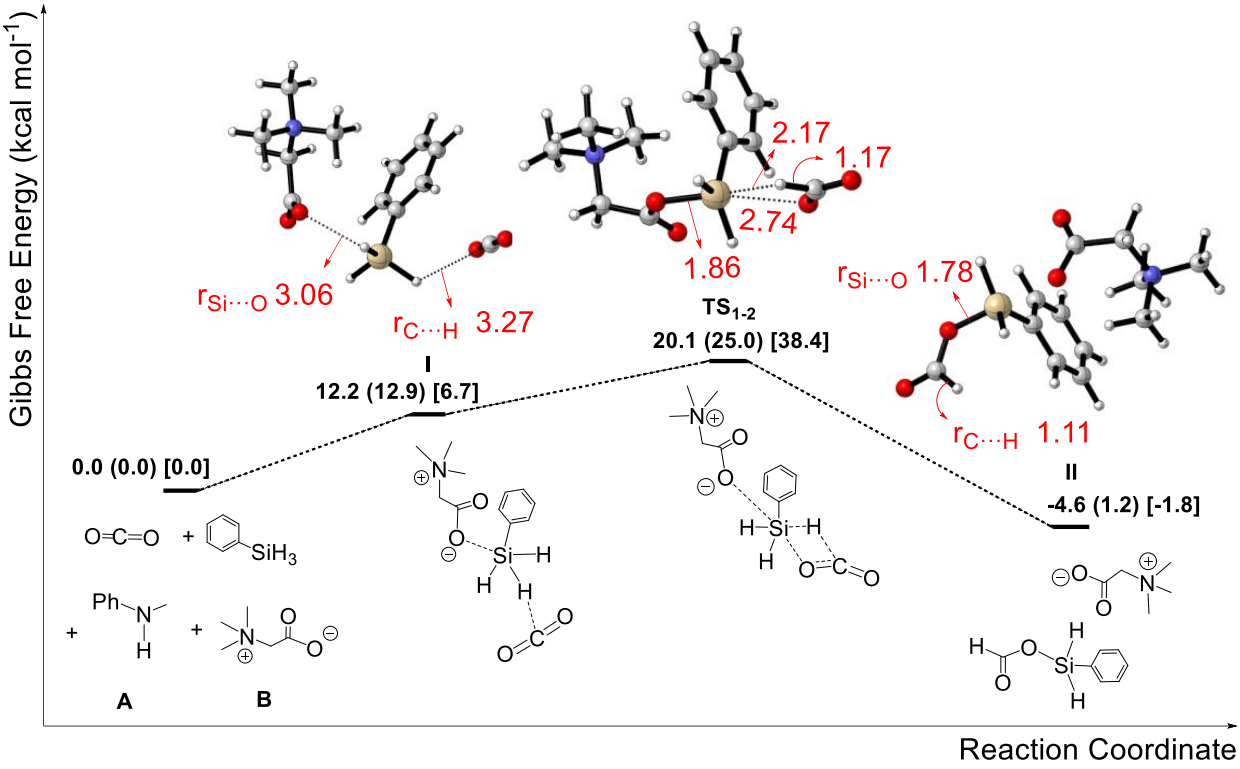

Figure 5.4.2.1. Computed free-energy profile for the reactions in pathway 1. *The relative free energies given in kcal mol^{-1} are calculated by using SMD(CH_3CN) M06-2X/6-311++G(d,p)//ωB97XD/6-31+G(d,p). The relative free energies given in kcal mol^{-1} in round brackets are calculated by using SMD(CH_3CN) ωB97XD/6-311++G(d,p)//ωB97XD/6-31+G(d,p). Free energies calculated in gas phase are quoted in square brackets. Bond distances are shown in Å in red. Molecular graphics were produced by CYLview.*

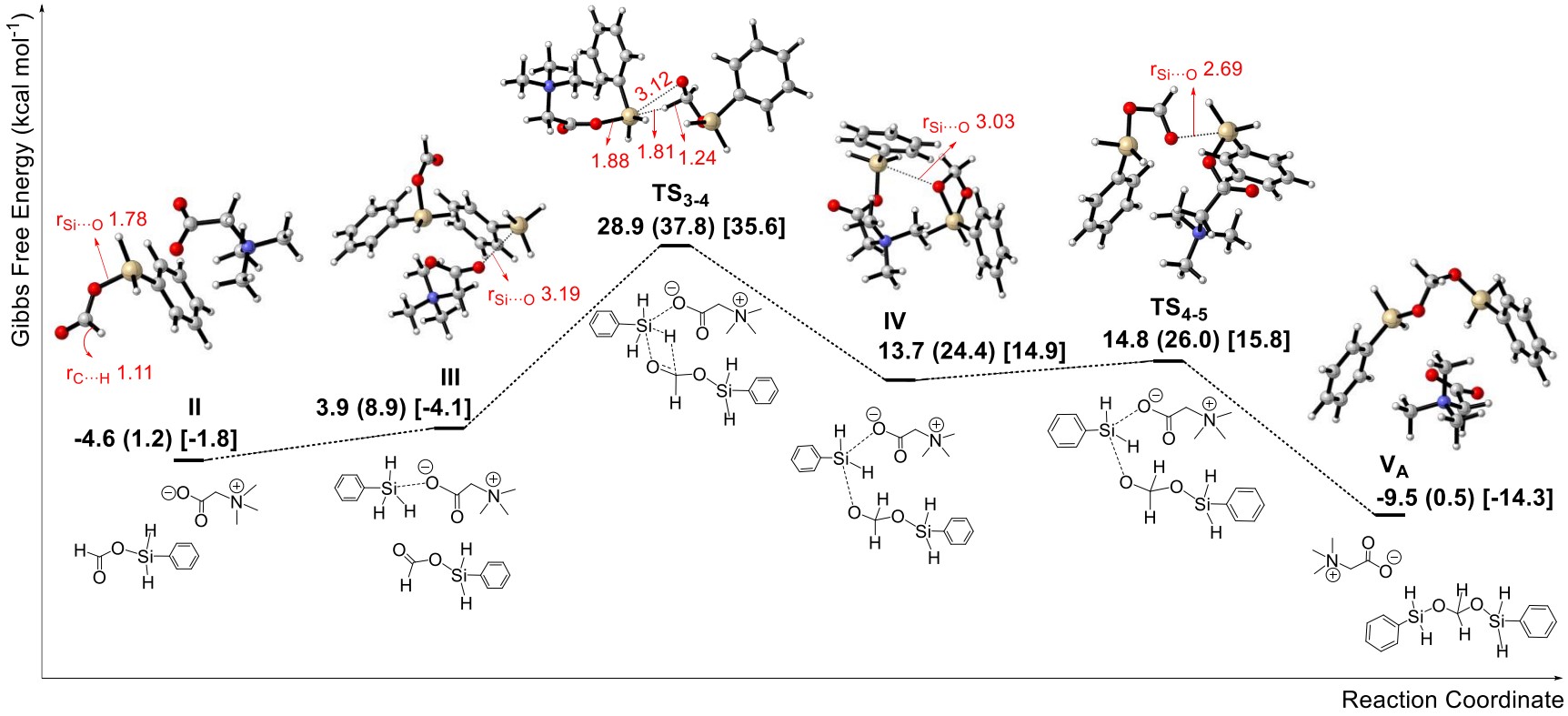

Figure 5.4.2.2. Computed free-energy profile for the reactions in pathway 1. *The relative free energies given in kcal mol^{-1} are calculated by using SMD(CH_3CN) M06-2X/6-311++G(d,p)//ωB97XD/6-31+G(d,p). The relative free energies given in kcal mol^{-1} in round brackets are calculated by using SMD(CH_3CN) ωB97XD/6-311++G(d,p)//ωB97XD/6-31+G(d,p). Free energies calculated in gas phase are quoted in square brackets. Bond distances are shown in Å in red. Molecular graphics were produced by CYLview.*

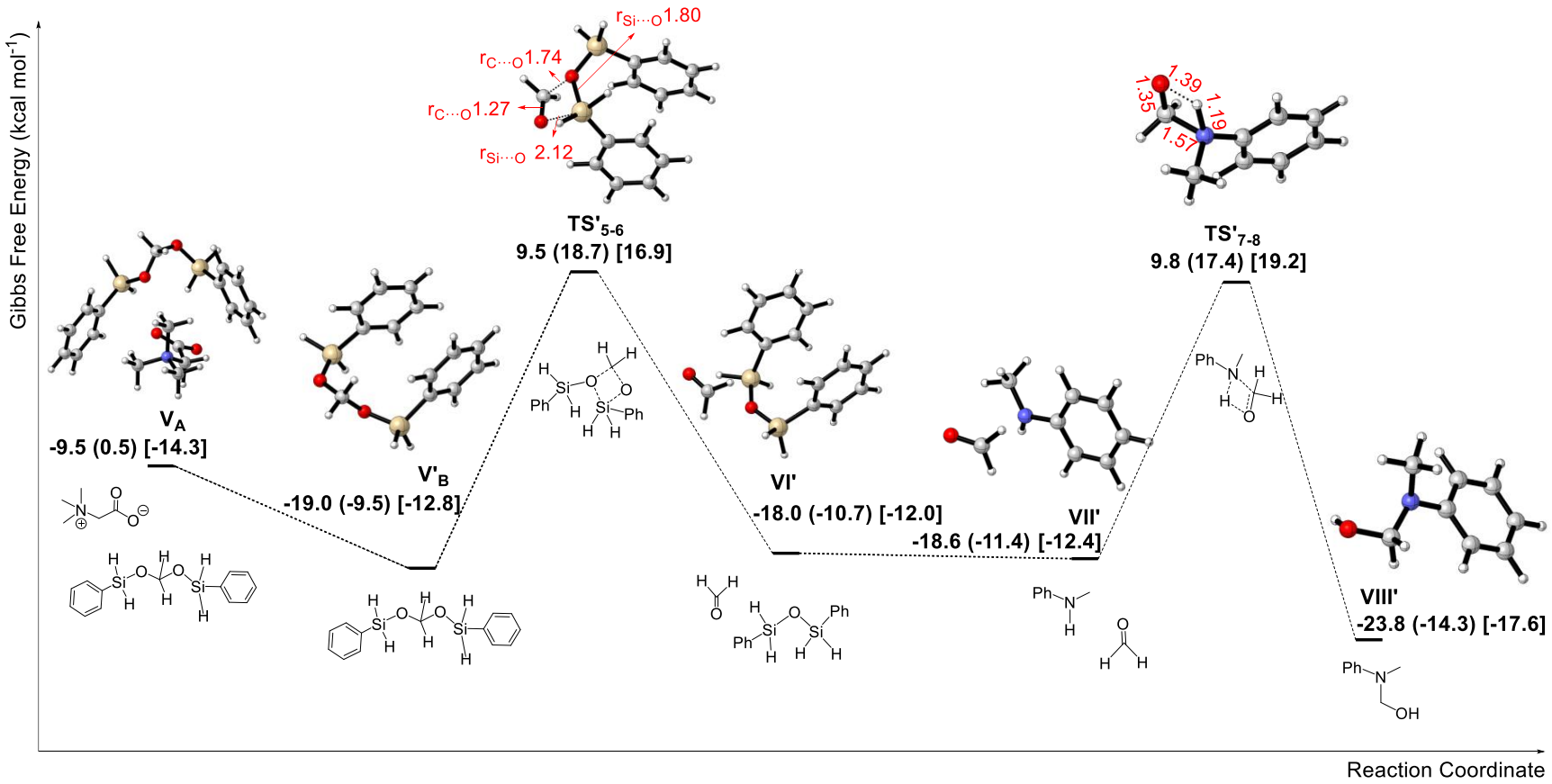

Figure 5.4.2.3. Computed free-energy profile for the reactions in pathway 1. *The relative free energies given in kcal mol^{-1} are calculated by using SMD(CH_3CN) M06-2X/6-311++G(d,p)//ωB97XD/6-31+G(d,p). The relative free energies given in kcal mol^{-1} in round brackets are calculated by using SMD(CH_3CN) ωB97XD/6-311++G(d,p)//ωB97XD/6-31+G(d,p). Free energies calculated in gas phase are quoted in square brackets. Bond distances are shown in Å in red. Molecular graphics were produced by CYLview.*

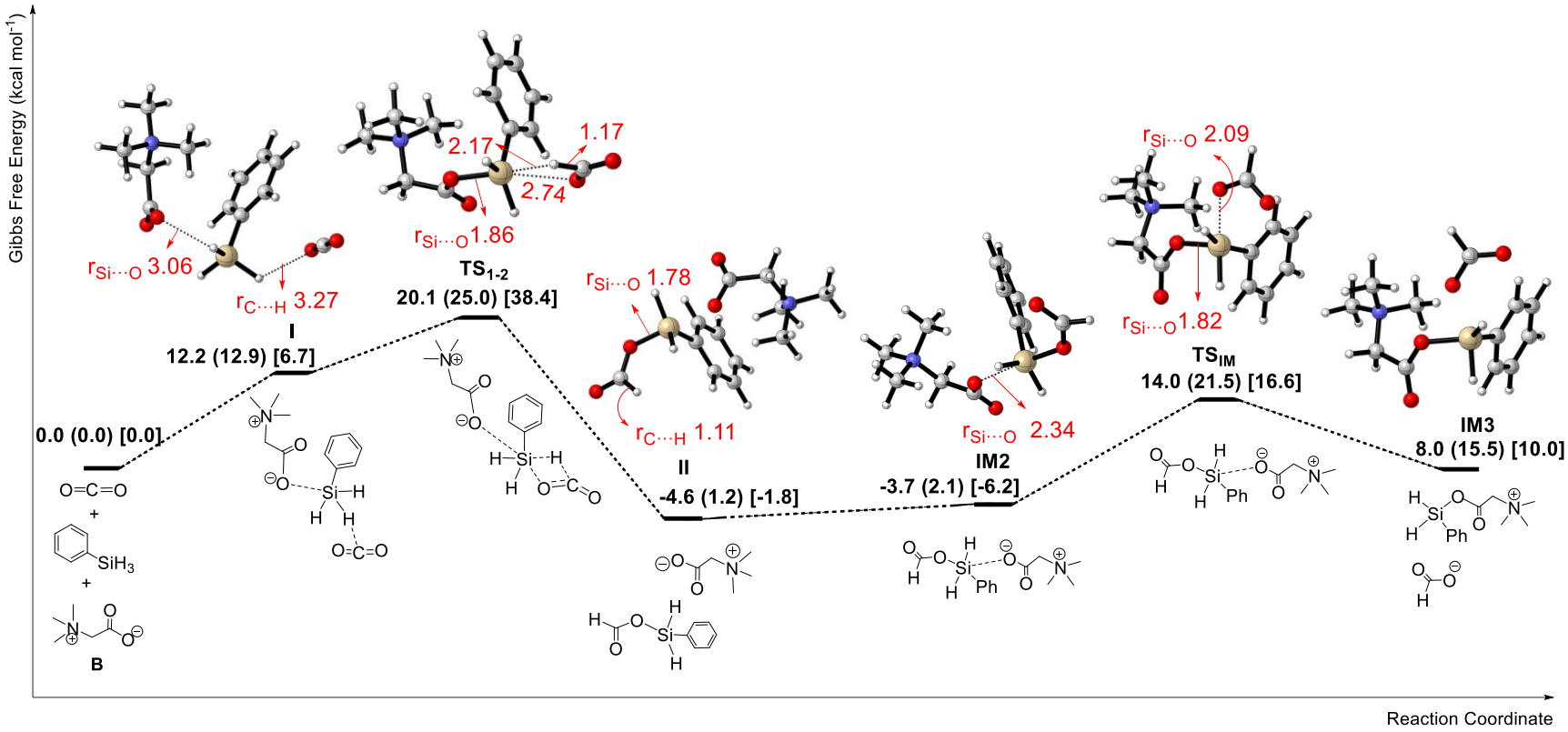

Figure 5.4.2.4. Computed free-energy profile for the reactions in pathway 1. *The relative free energies given in kcal mol^{-1} are calculated by using SMD(CH_3CN) M06-2X/6-311++G(d,p)//ωB97XD/6-31+G(d,p). The relative free energies given in kcal mol^{-1} in round brackets are calculated by using SMD(CH_3CN) ωB97XD/6-311++G(d,p)//ωB97XD/6-31+G(d,p). Free energies calculated in gas phase are quoted in square brackets. Bond distances are shown in Å in red. Molecular graphics were produced by CYLview.*

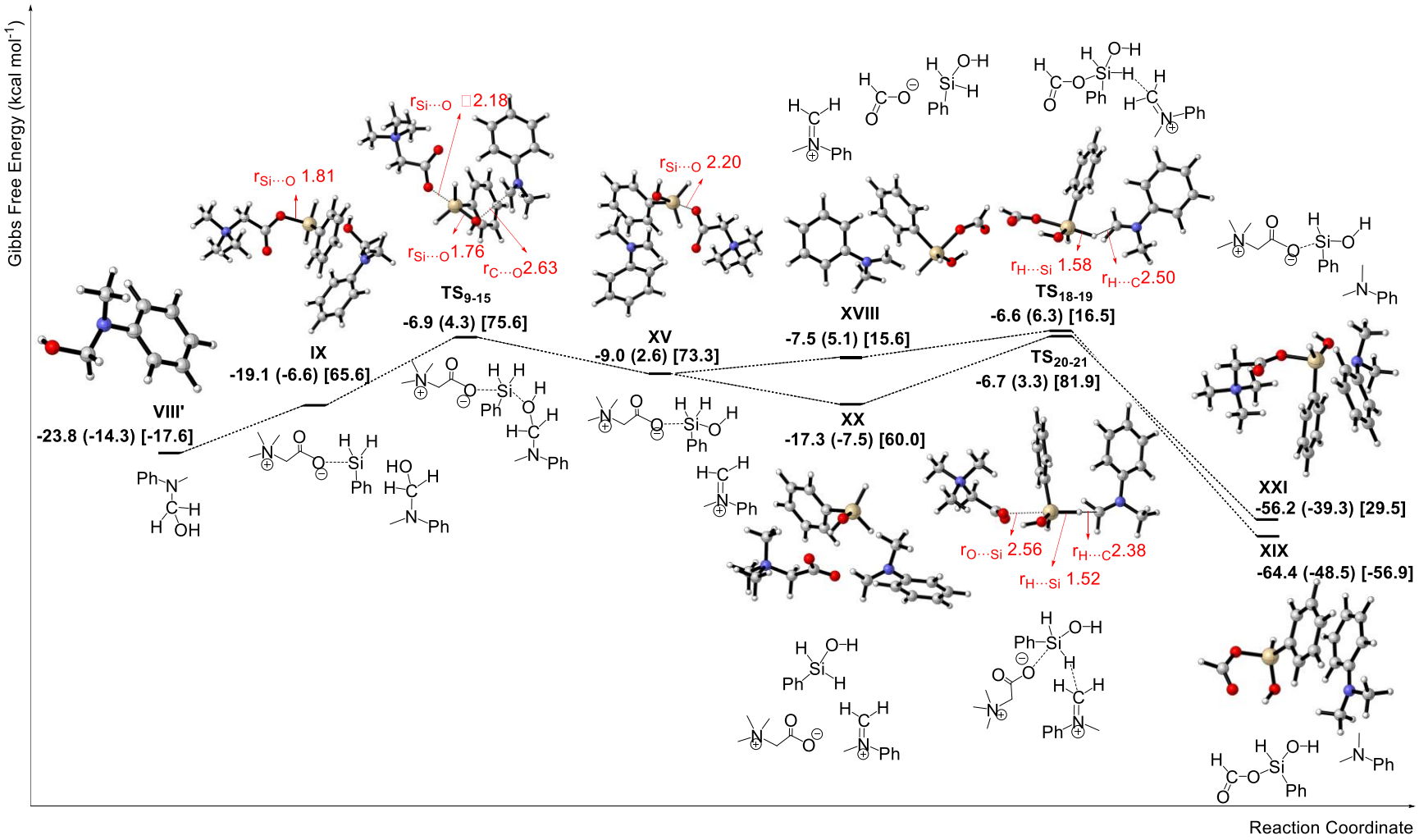

Figure 5.4.2.5. Computed free-energy profile for the reactions in pathway 1. *The relative free energies given in kcal mol^{-1} are calculated by using SMD(CH_3CN) M06-2X/6-311++G(d,p)//ωB97XD/6-31+G(d,p). The relative free energies given in kcal mol^{-1} in round brackets are calculated by using SMD(CH_3CN) ωB97XD/6-311++G(d,p)//ωB97XD/6-31+G(d,p). Free energies calculated in gas phase are quoted in square brackets. Bond distances are shown in Å in red. Molecular graphics were produced by CYLview.*

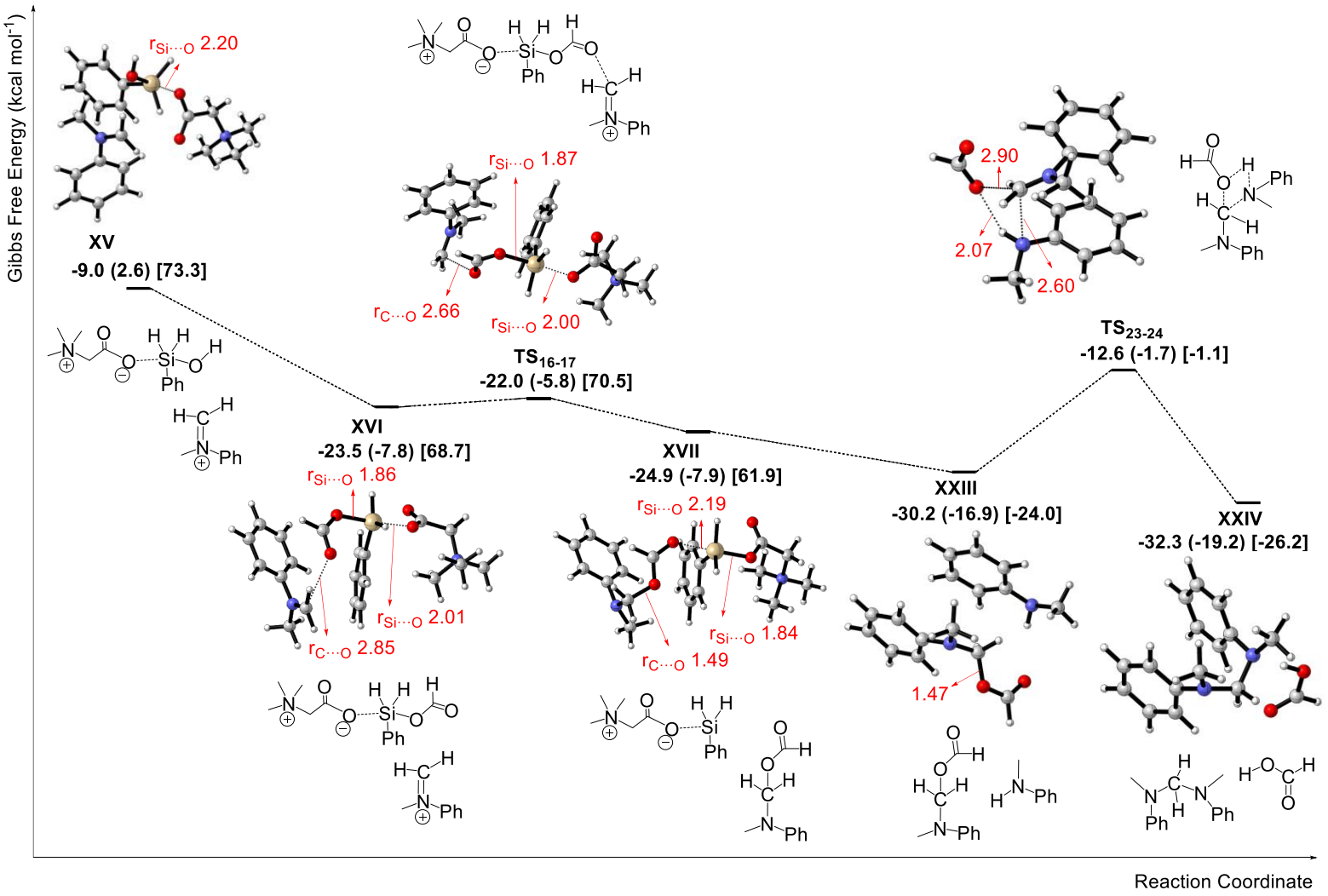

Figure 5.4.2.6. Computed free-energy profile for the reactions in pathway 1. *The relative free energies given in kcal mol^{-1} are calculated by using SMD(CH_3CN) M06-2X/6-311++G(d,p)//ωB97XD/6-31+G(d,p). The relative free energies given in kcal mol^{-1} in round brackets are calculated by using SMD(CH_3CN) ωB97XD/6-311++G(d,p)//ωB97XD/6-31+G(d,p). Free energies calculated in gas phase are quoted in square brackets. Bond distances are shown in Å in red. Molecular graphics were produced by CYLview.*

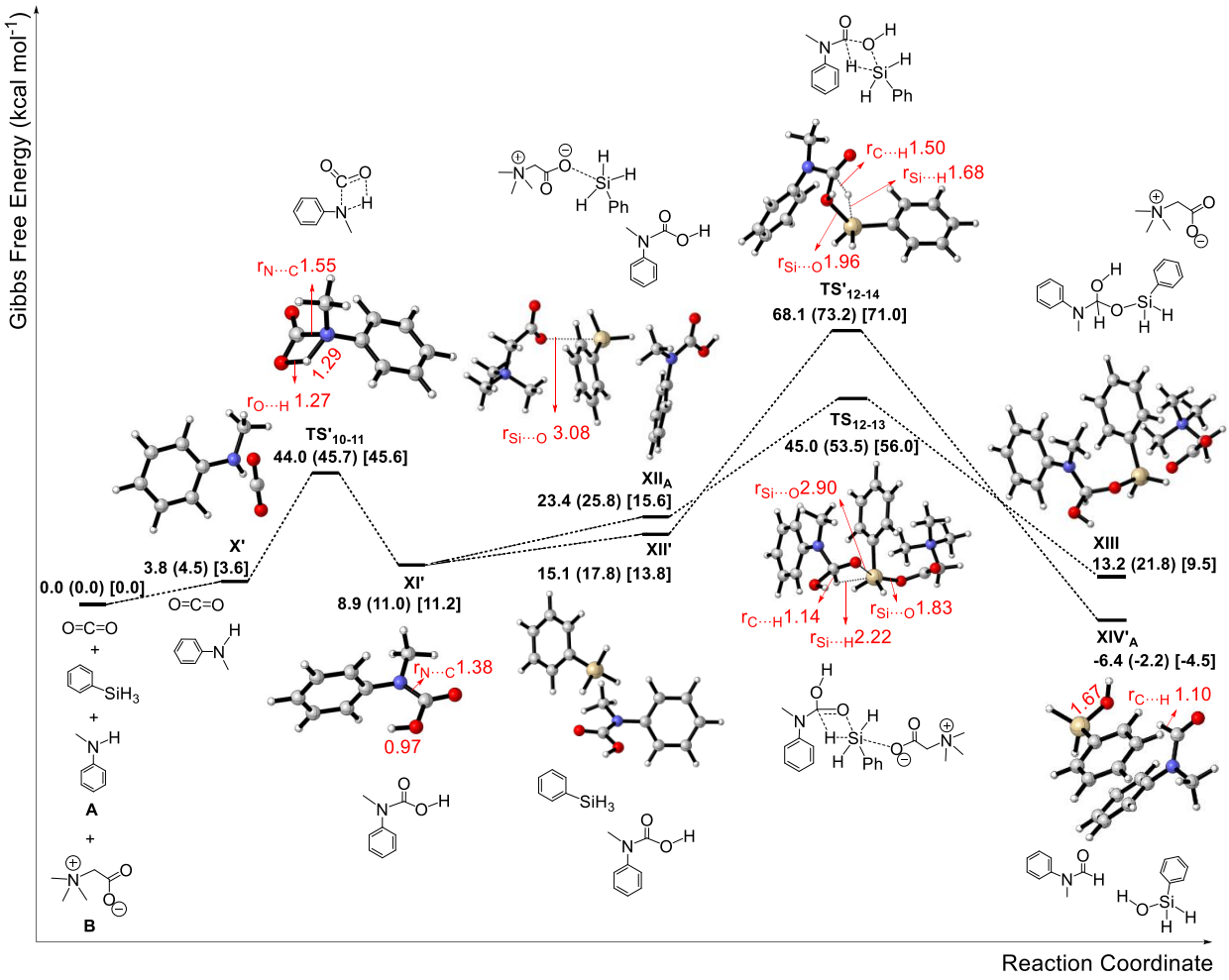

Figure 5.4.2.7. Computed free-energy profile for the reactions in pathway 2. *The relative free energies given in kcal mol^{-1} are calculated by using SMD(CH_3CN) M06-2X/6-311++G(d,p)//ωB97XD/6-31+G(d,p). The relative free energies given in kcal mol^{-1} in round brackets are calculated by using SMD(CH_3CN) ωB97XD/6-311++G(d,p)//ωB97XD/6-31+G(d,p). Free energies calculated in gas phase are quoted in square brackets. Bond distances are shown in Å in red. Molecular graphics were produced by CYLview.*

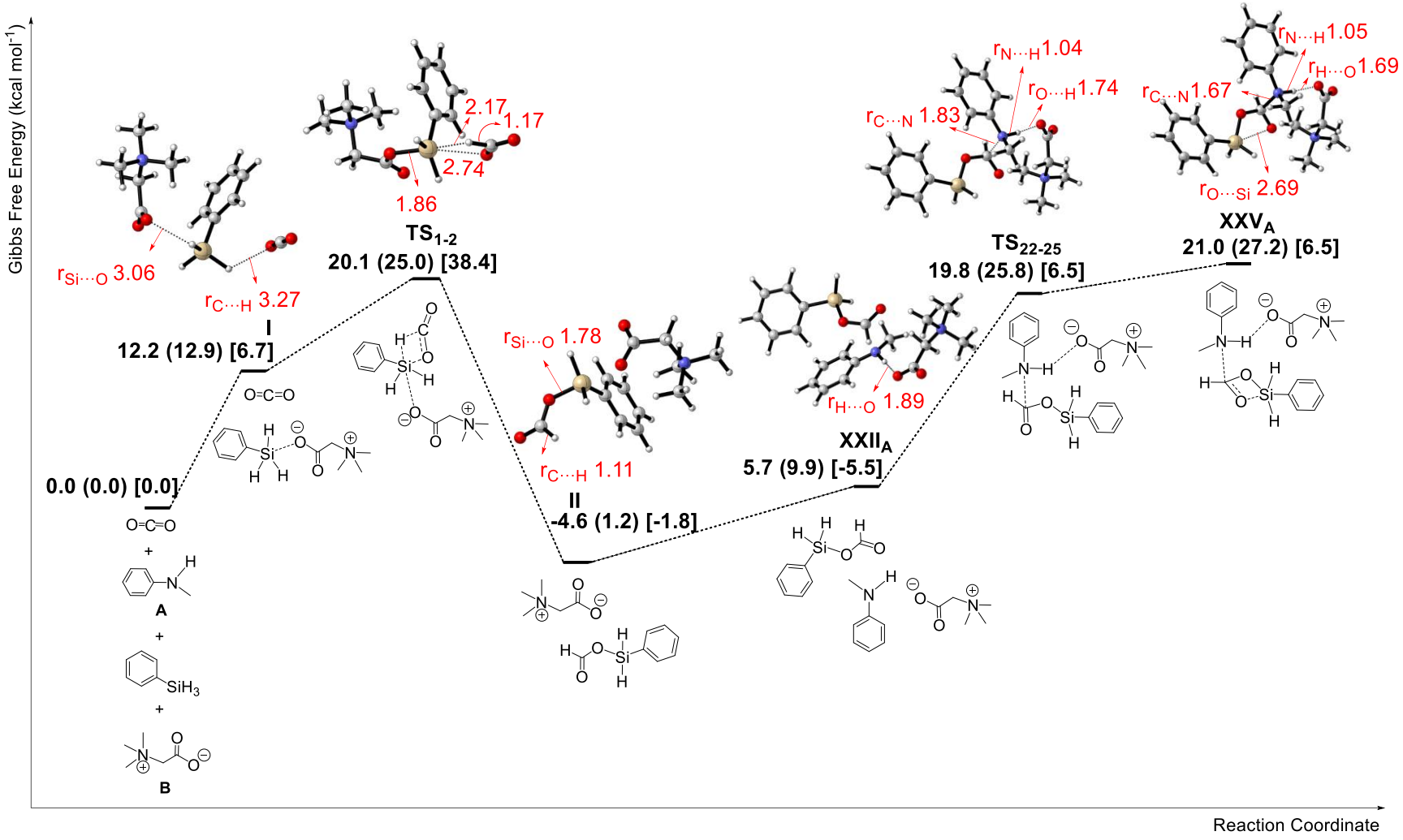

Figure 5.4.2.8. Computed free-energy profile for the reactions catalysed by glycine betaine in pathway 3. *The relative free energies given in kcal mol^{-1} are calculated by using SMD(CH_3CN) M06-2X/6-311++G(d,p)//ωB97XD/6-31+G(d,p). The relative free energies given in kcal mol^{-1} in round brackets are calculated by using SMD(CH_3CN) ωB97XD/6-311++G(d,p)//ωB97XD/6-31+G(d,p). Free energies calculated in gas phase are quoted in square brackets. Bond distances are shown in Å in red. Molecular graphics were produced by CYLview.*

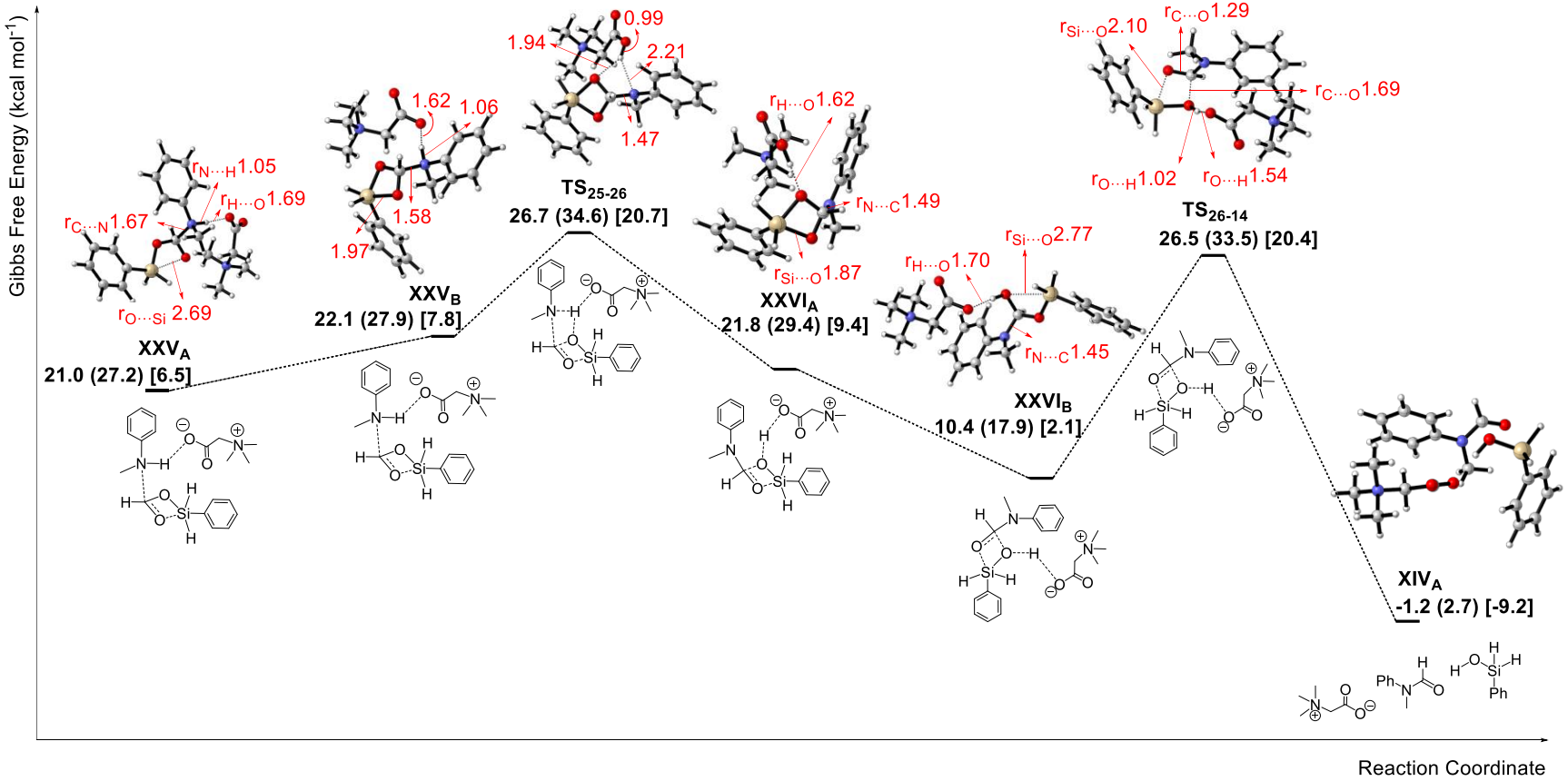

Figure 1 ***Figure 5.4.2.9. Computed free-energy profile for the reactions catalysed by glycine betaine in pathway 3.*** *The relative free energies given in kcal mol^{-1} are calculated by using SMD(CH_3CN) M06-2X/6-311++G(d,p)//ωB97XD/6-31+G(d,p). The relative free energies given in kcal mol^{-1} in round brackets are calculated by using SMD(CH_3CN) ωB97XD/6-311++G(d,p)//ωB97XD/6-31+G(d,p). Free energies calculated in gas phase are quoted in square brackets. Bond distances are shown in Å in red. Molecular graphics were produced by CYLview.*

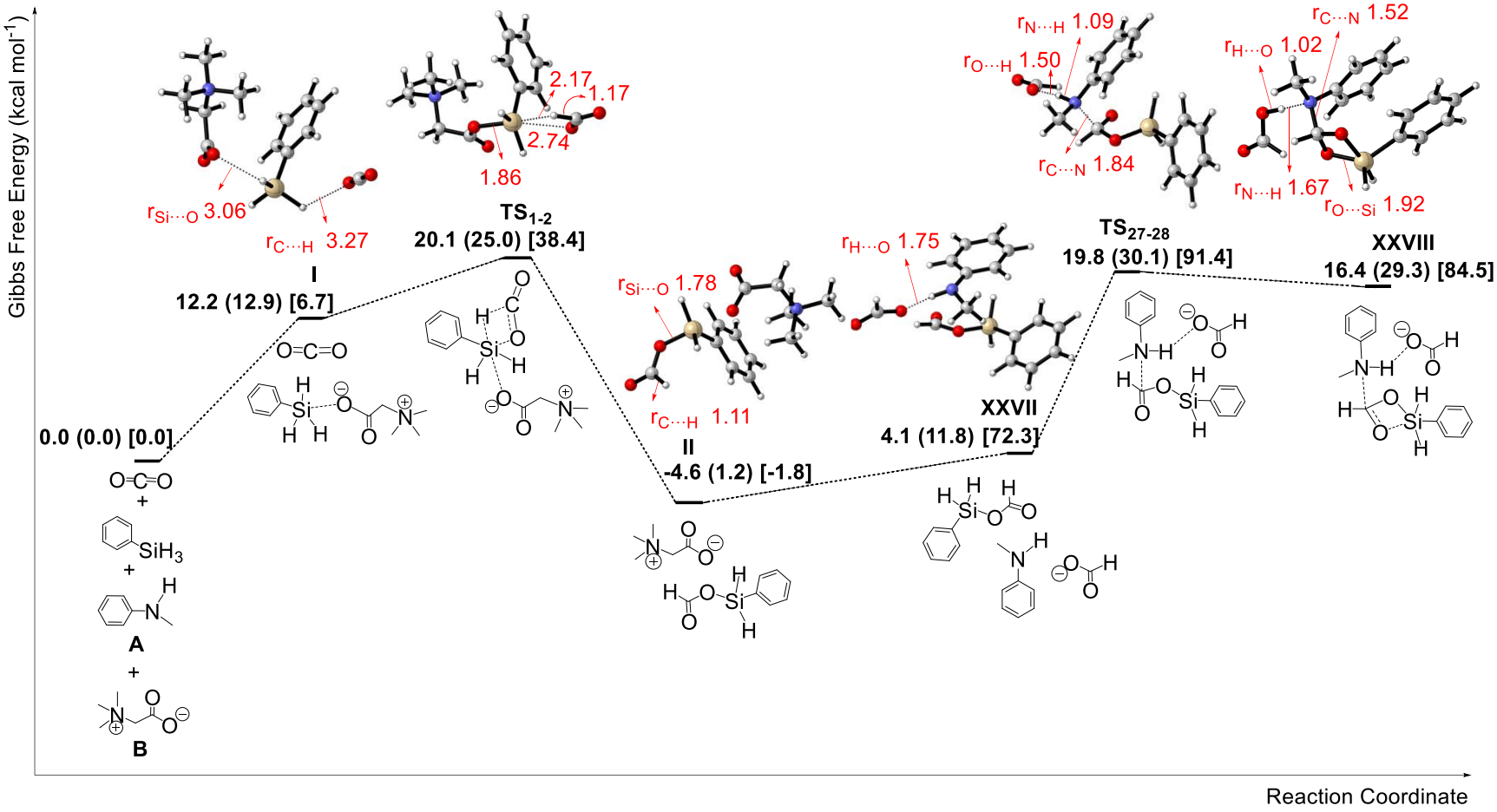

Figure 5.4.2.10. Computed free-energy profile for the reactions catalysed by glycine betaine and $HCOO^-$ in pathway 3. *The relative free energies given in kcal mol^{-1} are calculated by using SMD(CH_3CN) M06-2X/6-311++G(d,p)//ωB97XD/6-31+G(d,p). The relative free energies given in kcal mol^{-1} in round brackets are calculated by using SMD(CH_3CN) ωB97XD/6-311++G(d,p)//ωB97XD/6-31+G(d,p). Free energies calculated in gas phase are quoted in square brackets. Bond distances are shown in Å in red. Molecular graphics were produced by CYLview.*

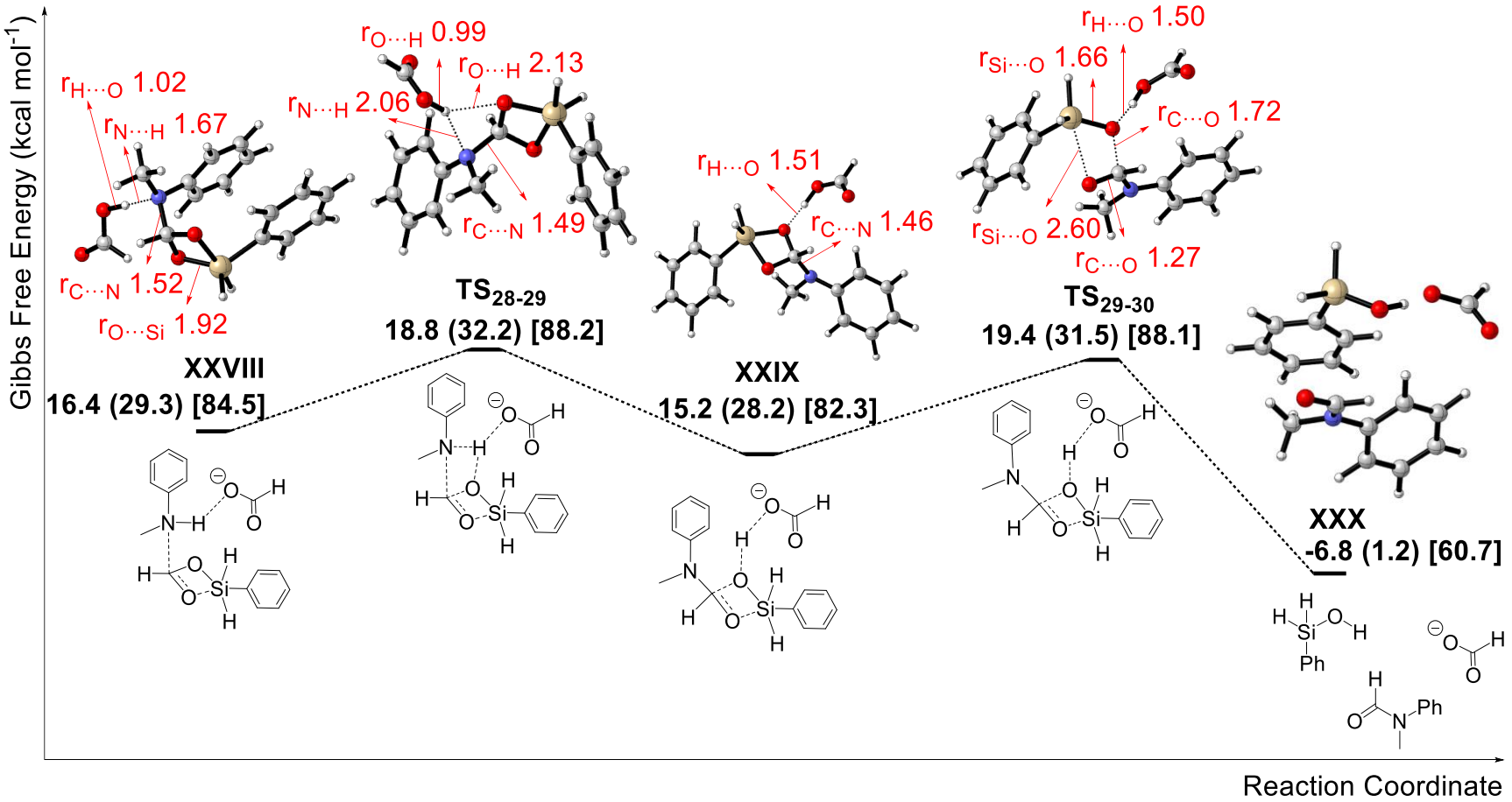

Figure 5.4.2.11. Computed free-energy profile for the reactions catalysed by glycine betaine and $HCOO^-$ in pathway 3. *The relative free energies given in kcal mol^{-1} are calculated by using SMD(CH_3CN) M06-2X/6-311++G(d,p)//ωB97XD/6-31+G(d,p). The relative free energies given in kcal mol^{-1} in round brackets are calculated by using SMD(CH_3CN) ωB97XD/6-311++G(d,p)//ωB97XD/6-31+G(d,p). Free energies calculated in gas phase are quoted in square brackets. Bond distances are shown in Å in red. Molecular graphics were produced by CYLview.*

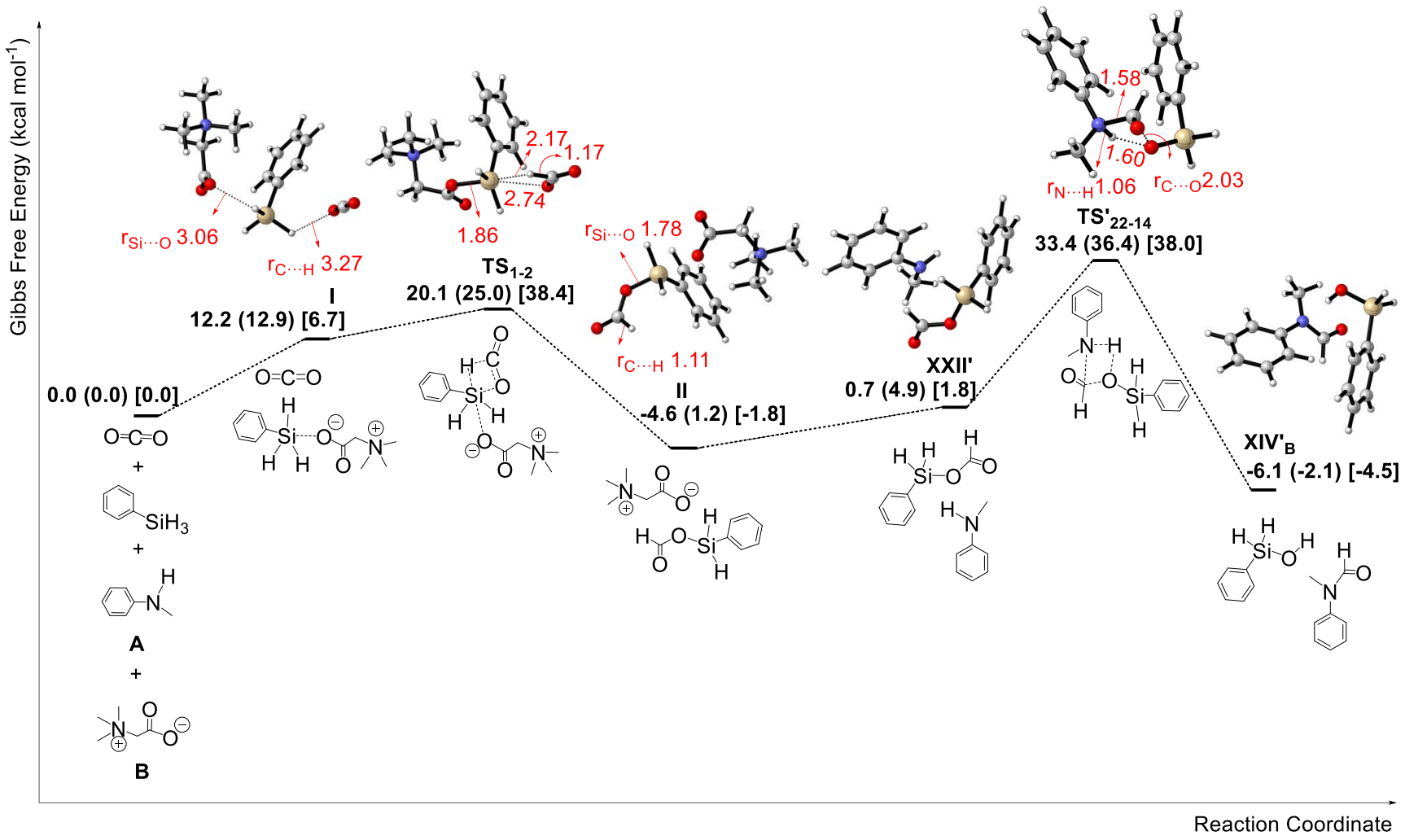

Figure 5.4.2.12. Computed free-energy profile for the reactions catalysed by glycine betaine in pathway 3. *The relative free energies given in kcal mol^{-1} are calculated by using SMD(CH_3CN) M06-2X/6-311++G(d,p)//ωB97XD/6-31+G(d,p). The relative free energies given in kcal mol^{-1} in round brackets are calculated by using SMD(CH_3CN) ωB97XD/6-311++G(d,p)//ωB97XD/6-31+G(d,p). Free energies calculated in gas phase are quoted in square brackets. Bond distances are shown in Å in red. Molecular graphics were produced by CYLview.*

5.4.3 The glycine betaine catalysed reactions after considering the energy correction method

In **chapter 5**, the reaction mechanism proposed in **figure 5.4.0.1** was optimised using SMD(CH_3CN)[73] ωB97XD[74]/6-311++G(d,p)//ωB97XD[74]/6-31+G(d,p). The ωB97XD/6-31+G(d,p) frequencies were used for thermal and entropic corrections at 298.15 K and 1 atm. Since the thermal corrections (G_{corr}) are calculated based on the ideal gas phase model, they overestimate the entropy contributions to the free energies for reaction in solvents, in particular for reactions involving multicomponent changes. The reason of the overestimation is that the Gaussian software ignores the suppressing effect of the solvent on the rotational and translational freedoms of substrates. The entropy overestimation of the approach was also demonstrated experimentally.[87, 88] Because no standard quantum mechanics-based method is available to accurately calculate the entropy in a solution, several approximate methods for energy correction have been put forward, for example, the MHP scheme proposed by Martin et al., the Yu scheme proposed by Yu and co-workers, and the energy correction method based on 'the theory of free volume'. According to the MHP method, a correction of (n-m)×4.3 kcal mol^{-1} applies to a process from m- to n-components at 298.15 K and 1 atm.[88] In terms of the Yu scheme, Yu and co-workers did experiments and found that the ideal gas model could overestimate the entropic contributions by 50-60% in their cyclization reactions. This experimental result indicates that a scaling factor of about 0.5 may be applied to the gas phase entropic contributions as a rough estimation.[87, 89] For the energy correction method based on 'the theory of free volume', a correction of -2.6 (or 2.6) kcal/mol is used for 2-to-1 (or 1-to-2) reactions.[90-93] In literature, there are many examples which uses the MHP scheme.[60, 62, 64] This section will use the MHP scheme with 4.3 kcal/mol as the energy correction factor. **Table 5.4.3.1**, **table 5.4.3.2** and **table 5.4.3.3** show how the activation free energy barrier ($\Delta G^{\ddagger}_{sol}$) changes

before and after applying the energy correction method in the three pathways proposed in **figure 5.4.0.1**. $\Delta G^{\ddagger}_{sol}$ and $\Delta G^{\ddagger}_{sol,c}$ represent the activation free energy barriers before and after using the energy correction method. The values of $\Delta G^{\ddagger}_{sol}$ are from **chapter 5.4.2** and they are calculated using SMD(CH_3CN) ωB97XD/6-311++G(d,p)//ωB97XD/6-31+G(d,p). **Table 5.4.3.1** shows the activation free energy barriers in pathway 1. It can be concluded form **table 5.4.3.1** that the rate-determining step (RDS) in pathway 1 after considering the energy correction is the reaction via TS_{3-4} with the $\Delta G^{\ddagger}_{sol}$ of 24.9 kcal/mol. **Table 5.4.3.2** shows the activation free energy barriers in pathway 2. After applying the energy correction method, the RDS in pathway 2 is the reaction via TS_{12-13} with the $\Delta G^{\ddagger}_{sol}$ of 40.6 kcal/mol. **Table 5.4.3.3** shows the activation free energy barriers in pathway 3. After applying the energy correction method, the RDS in pathway 3 is the reaction via TS_{1-2} with the $\Delta G^{\ddagger}_{sol}$ of 16.4 kcal/mol. To sum up, the rate-determining steps in the three pathways after considering the energy correction are unchanged. Since the reaction mechanism in **figure 5.4.0.1** is proved from both **section 5.4** and **section 5.4.2**, it is still true after considering the energy correction in **section 5.4.3**.

Table 5.4.3.1. *The activation free energy barriers of the reactions in pathway 1*

	species	$\Delta G^{\ddagger}_{sol}$ (kcal/mol)	n-m	$\Delta G^{\ddagger}_{sol,c}$ (kcal/mol)
pathway 1	**I**	12.9	-2	4.3
	TS_{1-2}	25.0		16.4
	II	1.2		-7.4
	III	8.9	-3	-4.0
	TS_{3-4}	37.8		24.9
	IV	24.4		11.5
	TS_{4-5}	26.0		13.1
	V_A	0.5		-12.4
	V'$_B$	-9.5	-2	-18.1
	TS'$_{5-6}$	18.7		10.1
	VI'	-10.7		-19.3
	VII'	-11.4		-20.0
	TS'$_{7-8}$	17.4		8.8

	VIII'	-14.3		-22.9

Table 5.4.3.1.(continued) *The activation free energy barriers of the reactions in pathway 1*

	species	$\Delta G^{\ddagger}_{sol}$ (kcal/mol)	n-m	$\Delta G^{\ddagger}_{sol,c}$ (kcal/mol)
pathway 1	**IM2**	2.1	-2	-6.5
	TS_{IM}	21.5		12.9
	IM3	15.5		6.9
	IX	-6.6	-4	-23.8
	$TS_{9\text{-}15}$	4.3		-12.9
	XV	2.6		-14.6
	XVIII	5.1		-12.1
	$TS_{18\text{-}19}$	6.3		-10.9
	XIX	-48.5		-65.7
	XX	-7.5		-24.7
	$TS_{20\text{-}21}$	3.3		-13.9
	XXI	-39.3		-56.5
	XVI	-7.8	-5	-29.3
	$TS_{16\text{-}17}$	-5.8		-27.3
	XVII	-7.9		-29.4
	XXIII	-16.9	-4	-34.1
	$TS_{23\text{-}24}$	-1.7		-18.9
	XXIV	-19.2		-36.4

Table 5.4.3.2. *The activation free energy barriers of the reactions in pathway 2*

	species	$\Delta G^{\ddagger}_{sol}$ (kcal/mol)	n-m	$\Delta G^{\ddagger}_{sol,c}$ (kcal/mol)
pathway 2	**X'**	4.5	-1	0.2
	$TS'_{10\text{-}11}$	45.7		41.4
	XI'	11.0		6.7
	XII_A	25.8	-3	12.9
	$TS_{12\text{-}13}$	53.5		40.6
	XIII	21.8		8.9
	XII'	17.8	-2	9.2
	$TS'_{12\text{-}14}$	73.2		64.6
	XIV'_A	-2.2		-10.8

Table 5.4.3.3. *The activation free energy barriers of the reactions in pathway 3*

	species	$\Delta G^{\ddagger}_{sol}$ (kcal/mol)	n-m	$\Delta G^{\ddagger}_{sol,c}$ (kcal/mol)
pathway 3	**I**	12.9	-2	4.3
	TS_{1-2}	25.0		16.4
	II	1.2		-7.4
	$XXII_A$	9.9	-3	-3.0
	TS_{22-25}	25.8		12.9
	XXV_A	27.2		14.3
	XXV_B	27.9		15.0
	TS_{25-26}	34.6		21.7
	$XXVI_A$	29.4		16.5
	$XXVI_B$	17.9		5.0
	TS_{26-14}	33.5		20.6
	XIV_A	2.7		-10.2
	I	12.9	-2	4.3
	TS_{1-2}	25.0		16.4
	II	1.2		-7.4
	XXVII	11.8	-4	-5.4
	TS_{27-28}	30.1		12.9
	XXVIII	29.3		12.1
	TS_{28-29}	32.2		15.0
	XXIX	28.2		11.0
	TS_{29-30}	31.5		14.3
	XXX	1.2		-16.0
	I	12.9	-2	4.3
	TS_{1-2}	25.0		16.4
	II	1.2		-7.4
	XXII'	4.9		-3.7
	TS'_{22-14}	36.4		27.8
	XIV'_B	-2.1		-10.7

5.4.4 Conclusion

To sum up, the formamide, the methylamine and the aminal are produced from the reactions between $PhSiH_3$, CO_2, the amine and glycine betaine. The detailed reaction mechanism is shown in **figure 5.4.0.1**. When SMD(CH_3CN) ωB97XD/6-311++G(d,p)//ωB97XD/6-31+G(d,p) is used, the activation free energy barriers of the rate-determining steps to produce the formamide, the

aminal and the methylamine are 32.2 kcal/mol, 37.8 kcal/mol and 37.8 kcal/mol. When SMD(CH_3CN) M06-2X/6-311++G(d,p)//ωB97XD/6-31+G(d,p) is used, the activation free energy barriers of the rate-determining steps to produce the formamide, the aminal and the methylamine are 20.1 kcal/mol, 28.9 kcal/mol and 28.9 kcal/mol. Since the experiments done by He and co-workers and Han and co-workers occur under mild conditions (≤100 °C, ≤0.5 MPa)[37, 58], the activation free energy barriers found from my DFT calculations are reasonable.

Chapter 6 Conclusion and future work

6.1 Conclusion

The main themes discussed in this thesis are background of my research and the reaction mechanism of glycine betaine catalysed CO_2 reduction. To facilitate these studies, we employ a range of computational chemistry tools, including quantum chemical methods and thermodynamics in computational chemistry. Some of the theoretical fundamental understanding of quantum chemical methods are elucidated using methods based on wave function methods and methods based on the density functional theory.

In Chapter 1, after giving a basic background of global warming, the rapidly evolving field of CO_2 reduction is critically reviewed, emphasizing on the applications in non-metal catalysed CO_2 reduction.

Chapter 2 describes methodologies in computational chemistry. Quantum chemical methods, including methods based on wave function methods and methods based on the density functional theory, are explained. Thermodynamics in computational chemistry is also introduced.

Chapter 3 introduces experimental findings of glycine betaine catalysed CO_2 reduction. The reaction mechanism of the reaction is next proposed. Computational methods applied in my research is discussed. Finally, interactions between reactants and glycine betaine are discussed.

Chapter 4 presents energy profiles of the reactions under no catalyst.

Chapter 5 shows the reaction mechanism of glycine betaine catalysed CO_2 reduction.

Finally, here in the last paragraph, give some concluding remarks on the work of the thesis and my thoughts on the field of research in general.

6.2 Major contributions

The major contribution of this thesis is that the reaction mechanism of glycine betaine catalysed CO_2 reduction was carried with meaningful insights discussed. Our calculated mechanism explains the experiment observations.

6.3 Recent update in literature published computational studies of glycine betaine catalysed CO_2 reduction

In 2020, Liu and co-workers investigated the mechanism of catalytic formylation and methylation of CO_2 with N-methylaniline and Ph_2SiH_2 using density functional theory (DFT) calculations.[94] They calculated the reaction mechanism at M06-2X/6-311++G(d,p) // IEFPCM(CH_3CN)-M06-2X/6-311G(d,p) level of theory.[94] From their calculations, they got the reaction mechanism to produce the formamide, the aminal and the methylamine. Their reaction mechanism is shown in **figure 6.3.1** and the three products (the formamide, the aminal and the methylamine) are highlighted in red. **Figure 6.3.1** shows that their reaction mechanism is different from my reaction mechanism. In their reaction mechanism, the production of the aminal involves reactions of water and the production of the methylamine involves the formation of CO_2.

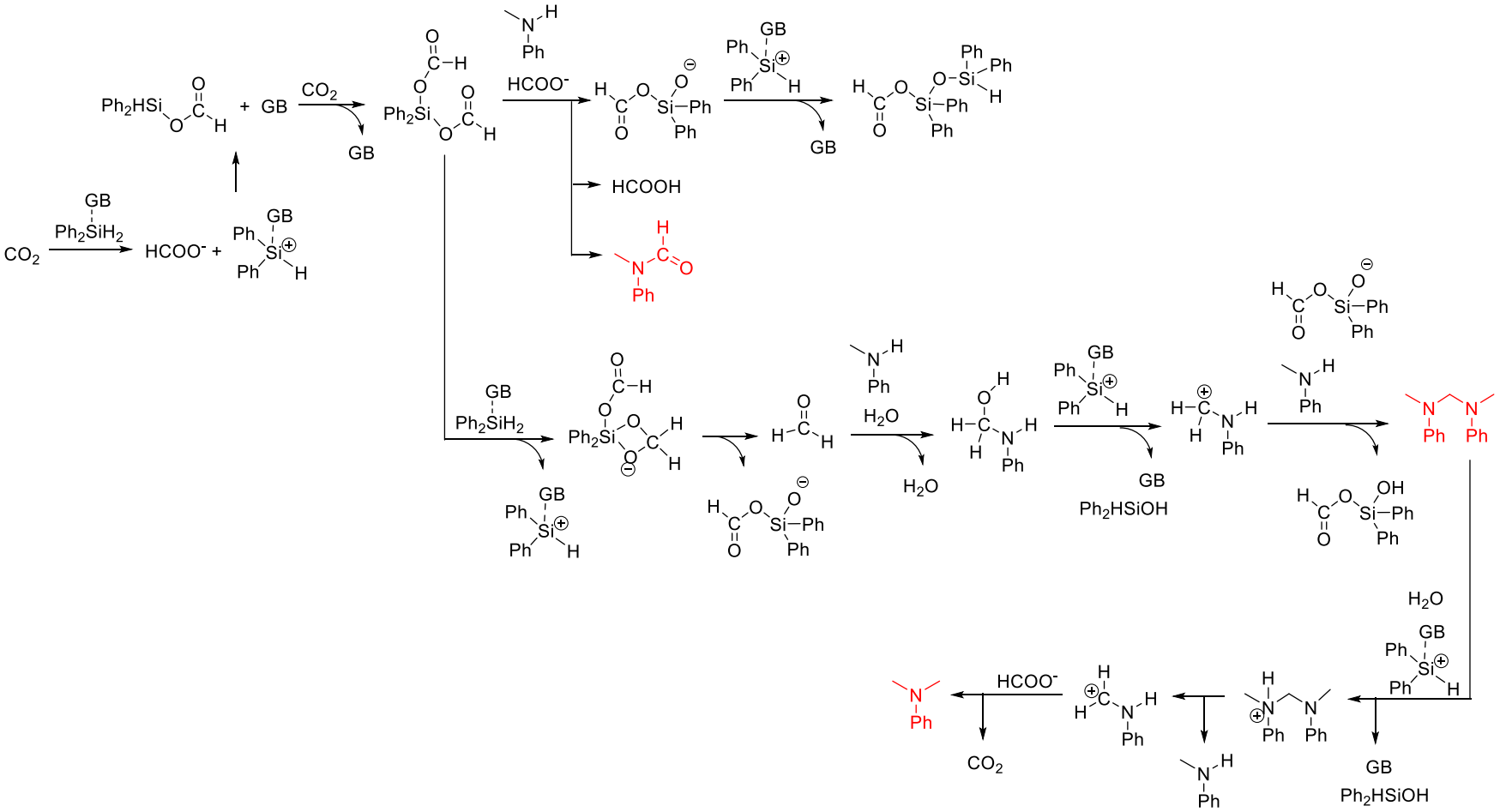

Figure 6.3.1. *The reaction mechanism calculated by Liu and co-workers*[94]

6.4 Future work

Global warming is a big issue worldwide. With the emphasis of carbon neutrality, we believe more and more fundamental research for CO_2 mitigation and conversion will be carried out. And I will continue my personal research interest in this area.

Bibliography

1. Drake, F., *Global Warming*. Routledge: Florence, UNITED KINGDOM, 2000.
2. Kielland, N.; Whiteoak, C. J.; Kleij, A. W., Stereoselective Synthesis with Carbon Dioxide. *Adv. Synth. Catal.* **2013,** *355*, 2115-2138.
3. Omae, I., Recent developments in carbon dioxide utilization for the production of organic chemicals. *Coord. Chem. Rev.* **2012,** *256*, 1384-1405.
4. Tsuji, Y.; Fujihara, T., Carbon dioxide as a carbon source in organic transformation: carbon–carbon bond forming reactions by transition-metal catalysts. *Chem. Commun.* **2012,** *48*, 9956-9964.
5. Yang, Z.-Z.; He, L.-N.; Gao, J.; Liu, A.-H.; Yu, B., Carbon dioxide utilization with C–N bond formation: carbon dioxide capture and subsequent conversion. *Energy Environ. Sci.* **2012,** *5*, 6602-6639.
6. Yaashikaa, P. R.; Senthil Kumar, P.; Varjani, S. J.; Saravanan, A., A review on photochemical, biochemical and electrochemical transformation of CO2 into value-added products. *J. CO2 Util.* **2019,** *33*, 131-147.
7. Ema, T.; Miyazaki, Y.; Koyama, S.; Yano, Y.; Sakai, T., A bifunctional catalyst for carbon dioxide fixation: cooperative double activation of epoxides for the synthesis of cyclic carbonates. *Chem. Commun.* **2012,** *48*, 4489-4491.
8. Nakano, K.; Hashimoto, S.; Nozaki, K., Bimetallic mechanism operating in the copolymerization of propylene oxide with carbon dioxide catalyzed by cobalt–salen complexes. *Chem. Sci.* **2010,** *1*, 369-373.
9. Watile, R. A.; Bagal, D. B.; Deshmukh, K. M.; Dhake, K. P.; Bhanage, B. M., Polymer supported diol functionalized ionic liquids: An efficient, heterogeneous and recyclable catalyst for 5-aryl-2-oxazolidinones synthesis from CO2 and aziridines under mild and solvent free condition. *J. Mol. Catal. A: Chem.* **2011,** *351*, 196-203.
10. Dai, Y.; Feng, X.; Wang, B.; He, R.; Bao, M., Preparation and application of air-stable P,N-bidentate ligands for the selective synthesis of δ-lactone via

the palladium-catalyzed telomerization of 1,3-butadiene with carbon dioxide. *J. Organomet. Chem.* **2012,** *696*, 4309-4314.

11. Gu, L.; Zhang, Y., Unexpected CO2 Splitting Reactions To Form CO with N-Heterocyclic Carbenes as Organocatalysts and Aromatic Aldehydes as Oxygen Acceptors. *J. Am. Chem. Soc.* **2010,** *132*, 914-915.

12. Tanaka, R.; Yamashita, M.; Nozaki, K., Catalytic Hydrogenation of Carbon Dioxide Using Ir(III)−Pincer Complexes. *J. Am. Chem. Soc.* **2009,** *131*, 14168-14169.

13. Maeda, C.; Miyazaki, Y.; Ema, T., Recent progress in catalytic conversions of carbon dioxide. *Catal. Sci. Technol.* **2014,** *4*, 1482-1497.

14. Peterson, S. L.; Stucka, S. M.; Dinsmore, C. J., Parallel Synthesis of Ureas and Carbamates from Amines and CO_2 under Mild Conditions. *Org. Lett.* **2010,** *12*, 1340-1343.

15. Hori, Y.; Murata, A.; Takahashi, R., Formation of hydrocarbons in the electrochemical reduction of carbon dioxide at a copper electrode in aqueous solution. *J. Chem. Soc., Faraday Trans. 1* **1989,** *85*, 2309-2326.

16. Lim, R. J.; Xie, M.; Sk, M. A.; Lee, J.-M.; Fisher, A.; Wang, X.; Lim, K. H., A review on the electrochemical reduction of CO2 in fuel cells, metal electrodes and molecular catalysts. *Catal. Today* **2014,** *233*, 169-180.

17. Wu, J.; Huang, Y.; Ye, W.; Li, Y., CO_2 Reduction: From the Electrochemical to Photochemical Approach. *Adv. Sci.* **2017,** *4*, 1700194.

18. Riduan, S. N.; Zhang, Y.; Ying, J. Y., Conversion of Carbon Dioxide into Methanol with Silanes over N-Heterocyclic Carbene Catalysts. *Angew. Chem. Int. Ed.* **2009,** *48*, 3322-3325.

19. Berkefeld, A.; Piers, W. E.; Parvez, M., Tandem Frustrated Lewis Pair/Tris(pentafluorophenyl)borane-Catalyzed Deoxygenative Hydrosilylation of Carbon Dioxide. *J. Am. Chem. Soc.* **2010,** *132*, 10660-10661.

20. Das Neves Gomes, C.; Jacquet, O.; Villiers, C.; Thuéry, P.; Ephritikhine, M.; Cantat, T., A Diagonal Approach to Chemical Recycling of Carbon Dioxide:

Organocatalytic Transformation for the Reductive Functionalization of CO2. *Angew. Chem. Int. Ed.* **2012,** *51*, 187-190.

21. Jacquet, O.; Frogneux, X.; Das Neves Gomes, C.; Cantat, T., CO_2 as a C1-building block for the catalytic methylation of amines. *Chem. Sci.* **2013,** *4*, 2127-2131.

22. Li, Y.; Fang, X.; Junge, K.; Beller, M., A General Catalytic Methylation of Amines Using Carbon Dioxide. *Angew. Chem. Int. Ed.* **2013,** *52*, 9568-9571.

23. Beydoun, K.; vom Stein, T.; Klankermayer, J.; Leitner, W., Ruthenium-Catalyzed Direct Methylation of Primary and Secondary Aromatic Amines Using Carbon Dioxide and Molecular Hydrogen. *Angew. Chem. Int. Ed.* **2013,** *52*, 9554-9557.

24. Li, Y.; Sorribes, I.; Yan, T.; Junge, K.; Beller, M., Selective Methylation of Amines with Carbon Dioxide and H2. *Angew. Chem. Int. Ed.* **2013,** *52*, 12156-12160.

25. Fontaine, F.-G.; Stephan, D. W., Metal-free reduction of CO2. *Curr. Opin. Green Sustain. Chem.* **2017,** *3*, 28-32.

26. Courtemanche, M.-A.; Légaré, M.-A.; Rochette, É.; Fontaine, F.-G., Phosphazenes: efficient organocatalysts for the catalytic hydrosilylation of carbon dioxide. *Chem. Commun.* **2015,** *51*, 6858-6861.

27. Khandelwal, M.; Wehmschulte, R. J., Deoxygenative Reduction of Carbon Dioxide to Methane, Toluene, and Diphenylmethane with [Et2Al]+ as Catalyst. *Angew. Chem. Int. Ed.* **2012,** *51*, 7323-7326.

28. Wehmschulte, R. J.; Saleh, M.; Powell, D. R., CO2 Activation with Bulky Neutral and Cationic Phenoxyalanes. *Organometallics* **2013,** *32*, 6812-6819.

29. Mukherjee, D.; Sauer, D. F.; Zanardi, A.; Okuda, J., Selective Metal-Free Hydrosilylation of CO2 Catalyzed by Triphenylborane in Highly Polar, Aprotic Solvents. *Chem. Eur. J.* **2016,** *22*, 7730-7733.

30. Courtemanche, M.-A.; Légaré, M.-A.; Maron, L.; Fontaine, F.-G., Reducing CO2 to Methanol Using Frustrated Lewis Pairs: On the Mechanism of

Phosphine–Borane-Mediated Hydroboration of CO2. *J. Am. Chem. Soc.* **2014,** *136*, 10708-10717.

31. Knopf, I.; Cummins, C. C., Revisiting CO2 Reduction with NaBH4 under Aprotic Conditions: Synthesis and Characterization of Sodium Triformatoborohydride. *Organometallics* **2015,** *34*, 1601-1603.

32. Lu, Z.; Hausmann, H.; Becker, S.; Wegner, H. A., Aromaticity as Stabilizing Element in the Bidentate Activation for the Catalytic Reduction of Carbon Dioxide. *J. Am. Chem. Soc.* **2015,** *137*, 5332-5335.

33. Courtemanche, M.-A.; Pulis, A. P.; Rochette, É.; Légaré, M.-A.; Stephan, D. W.; Fontaine, F.-G., Intramolecular B/N frustrated Lewis pairs and the hydrogenation of carbon dioxide. *Chem. Commun.* **2015,** *51*, 9797-9800.

34. Jun, K.-W.; Roh, H.-S.; Kim, K.-S.; Ryu, J.-S.; Lee, K.-W., Catalytic investigation for Fischer–Tropsch synthesis from bio-mass derived syngas. *Appl. Catal. A* **2004,** *259*, 221-226.

35. Ashley, A. E.; Thompson, A. L.; O'Hare, D., Non-Metal-Mediated Homogeneous Hydrogenation of CO2 to CH3OH. *Angew. Chem. Int. Ed.* **2009,** *48*, 9839-9843.

36. Saeidi, S.; Amin, N. A. S.; Rahimpour, M. R., Hydrogenation of CO2 to value-added products—A review and potential future developments. *J. CO2 Util.* **2014,** *5*, 66-81.

37. Liu, X.-F.; Li, X.-Y.; Qiao, C.; Fu, H.-C.; He, L.-N., Betaine Catalysis for Hierarchical Reduction of CO_2 with Amines and Hydrosilane To Form Formamides, Aminals, and Methylamines. *Angew. Chem. Int. Ed.* **2017,** *56*, 7425-7429.

38. Yuehui, L.; Xianjie, F.; Kathrin, J.; Matthias, B., A General Catalytic Methylation of Amines Using Carbon Dioxide. *Angew. Chem. Int. Ed.* **2013,** *52*, 9568-9571.

39. Yuehui, L.; Iván, S.; Tao, Y.; Kathrin, J.; Matthias, B., Selective Methylation of Amines with Carbon Dioxide and H2. *Angew. Chem. Int. Ed.* **2013,** *52*, 12156-12160.

40. Kassem, B.; Thorsten, v. S.; Jürgen, K.; Walter, L., Ruthenium-Catalyzed Direct Methylation of Primary and Secondary Aromatic Amines Using Carbon Dioxide and Molecular Hydrogen. *Angew. Chem. Int. Ed.* **2013,** *52*, 9554-9557.

41. Lei, Z.; Zhaobin, H.; Xiaoyu, Z.; Zheng, W.; Kuiling, D., Highly Efficient Ruthenium-Catalyzed N-Formylation of Amines with H2 and CO2. *Angew. Chem. Int. Ed.* **2015,** *54*, 6186-6189.

42. Q., N. T. V.; Woo-Jin, Y.; Shū, K., Effective Formylation of Amines with Carbon Dioxide and Diphenylsilane Catalyzed by Chelating bis(tzNHC) Rhodium Complexes. *Angew. Chem. Int. Ed.* **2015,** *54*, 9209-9212.

43. Frogneux, X.; Jacquet, O.; Cantat, T., Iron-catalyzed hydrosilylation of CO2: CO2 conversion to formamides and methylamines. *Catal. Sci. Technol.* **2014,** *4*, 1529-1533.

44. Motokura, K.; Takahashi, N.; Kashiwame, D.; Yamaguchi, S.; Miyaji, A.; Baba, T., Copper-diphosphine complex catalysts for N-formylation of amines under 1 atm of carbon dioxide with polymethylhydrosiloxane. *Catal. Sci. Technol.* **2013,** *3*, 2392-2396.

45. Liu, H.; Mei, Q.; Xu, Q.; Song, J.; Liu, H.; Han, B., Synthesis of formamides containing unsaturated groups by N-formylation of amines using CO2 with H2. *Green Chem.* **2017,** *19*, 196-201.

46. Santoro, O.; Lazreg, F.; Minenkov, Y.; Cavallo, L.; Cazin, C. S. J., N-heterocyclic carbene copper(i) catalysed N-methylation of amines using CO2. *Dalton Trans.* **2015,** *44*, 18138-18144.

47. Cui, X.; Dai, X.; Zhang, Y.; Deng, Y.; Shi, F., Methylation of amines, nitrobenzenes and aromatic nitriles with carbon dioxide and molecular hydrogen. *Chem. Sci.* **2014,** *5*, 649-655.

48. Rongchang, L.; Xiaowei, L.; Yaju, C.; Wuying, Z.; Xiantai, Z.; Hongbing, J., Cooperative Catalytic Activation of Si−H Bonds: CO2-Based Synthesis of Formamides from Amines and Hydrosilanes under Mild Conditions. *ChemSusChem* **2017,** *10*, 1224-1232.

49. González-Sebastián, L.; Flores-Alamo, M.; García, J. J., Selective N-Methylation of Aliphatic Amines with CO2 and Hydrosilanes Using Nickel-Phosphine Catalysts. *Organometallics* **2015,** *34*, 763-769.

50. Fang, C.; Lu, C.; Liu, M.; Zhu, Y.; Fu, Y.; Lin, B.-L., Selective Formylation and Methylation of Amines using Carbon Dioxide and Hydrosilane Catalyzed by Alkali-Metal Carbonates. *ACS Catal.* **2016,** *6*, 7876-7881.

51. Liu, X.-F.; Qiao, C.; Li, X.-Y.; He, L.-N., Carboxylate-promoted reductive functionalization of CO2 with amines and hydrosilanes under mild conditions. *Green Chem.* **2017,** *19*, 1726-1731.

52. Christophe, D. N. G.; Olivier, J.; Claude, V.; Pierre, T.; Michel, E.; Thibault, C., A Diagonal Approach to Chemical Recycling of Carbon Dioxide: Organocatalytic Transformation for the Reductive Functionalization of CO2. *Angew. Chem. Int. Ed.* **2012,** *51*, 187-190.

53. Jacquet, O.; Das Neves Gomes, C.; Ephritikhine, M.; Cantat, T., Recycling of Carbon and Silicon Wastes: Room Temperature Formylation of N–H Bonds Using Carbon Dioxide and Polymethylhydrosiloxane. *J. Am. Chem. Soc.* **2012,** *134*, 2934-2937.

54. Gao, X.; Yu, B.; Yang, Z.; Zhao, Y.; Zhang, H.; Hao, L.; Han, B.; Liu, Z., Ionic Liquid-Catalyzed C–S Bond Construction using CO2 as a C1 Building Block under Mild Conditions: A Metal-Free Route to Synthesis of Benzothiazoles. *ACS Catal.* **2015,** *5*, 6648-6652.

55. Enguerrand, B.; Jacky, P.; Thibault, C., Carbon Dioxide Reduction to Methylamines under Metal-Free Conditions. *Angew. Chem.* **2014,** *126*, 12382-12386.

56. Yang, Z.; Yu, B.; Zhang, H.; Zhao, Y.; Ji, G.; Ma, Z.; Gao, X.; Liu, Z., B(C6F5)3-catalyzed methylation of amines using CO_2 as a C1 building block. *Green Chem.* **2015,** *17*, 4189-4193.
57. Xiao-Fang, L.; Ran, M.; Chang, Q.; Han, C.; Liang-Nian, H., Fluoride-Catalyzed Methylation of Amines by Reductive Functionalization of CO_2 with Hydrosilanes. *Chem. Eur. J.* **2016,** *22*, 16489-16493.
58. Xie, C.; Song, J.; Wu, H.; Zhou, B.; Wu, C.; Han, B., Natural Product Glycine Betaine as an Efficient Catalyst for Transformation of CO_2 with Amines to Synthesize N-Substituted Compounds. *ACS Sustainable Chem. Eng.* **2017,** *5*, 7086-7092.
59. Zhang, S.; Mei, Q.; Liu, H.; Liu, H.; Zhang, Z.; Han, B., Copper-catalyzed N-formylation of amines with CO2 under ambient conditions. *RSC Adv.* **2016,** *6*, 32370-32373.
60. Li, W.; Kim, C. K., A Theoretical Study on the Mechanism of Methylation of N-methylaniline with CO2 and Silyl Hydrides. *Bull. Korean Chem. Soc.* **2017,** *38*, 12-18.
61. Li, X.-Y.; Zheng, S.-S.; Liu, X.-F.; Yang, Z.-W.; Tan, T.-Y.; Yu, A.; He, L.-N., Waste Recycling: Ionic Liquid-Catalyzed 4-Electron Reduction of CO_2 with Amines and Polymethylhydrosiloxane Combining Experimental and Theoretical Study. *ACS Sustainable Chem. Eng.* **2018,** *6*, 8130-8135.
62. Lu, Y.; Gao, Z.-H.; Chen, X.-Y.; Guo, J.; Liu, Z.; Dang, Y.; Ye, S.; Wang, Z.-X., Formylation or methylation: what determines the chemoselectivity of the reaction of amine, CO_2, and hydrosilane catalyzed by 1,3,2-diazaphospholene? *Chem. Sci.* **2017,** *8*, 7637-7650.
63. Wang, B.; Cao, Z., Sequential covalent bonding activation and general base catalysis: insight into N-heterocyclic carbene catalyzed formylation of N–H bonds using carbon dioxide and silane. *RSC Adv.* **2013,** *3*, 14007-14015.
64. Zhang, C.; Lu, Y.; Zhao, R.; Menberu, W.; Guo, J.; Wang, Z.-X., A comparative DFT study of TBD-catalyzed reactions of amines with CO_2 and

hydrosilane: the effect of solvent polarity on the mechanistic preference and the origins of chemoselectivities. *Chem. Commun.* **2018,** *54*, 10870-10873.

65. Zhou, Q.; Li, Y., The Real Role of N-Heterocyclic Carbene in Reductive Functionalization of CO_2: An Alternative Understanding from Density Functional Theory Study. *J. Am. Chem. Soc.* **2015,** *137*, 10182-10189.

66. Chong, C. C.; Kinjo, R., Hydrophosphination of CO_2 and Subsequent Formate Transfer in the 1,3,2-Diazaphospholene-Catalyzed N-Formylation of Amines. *Angew. Chem. Int. Ed.* **2015,** *54*, 12116-12120.

67. Huang, F.; Lu, G.; Zhao, L.; Li, H.; Wang, Z.-X., The Catalytic Role of N-Heterocyclic Carbene in a Metal-Free Conversion of Carbon Dioxide into Methanol: A Computational Mechanism Study. *J. Am. Chem. Soc.* **2010,** *132*, 12388-12396.

68. Riduan, S. N.; Ying, J. Y.; Zhang, Y., Mechanistic Insights into the Reduction of Carbon Dioxide with Silanes over N-Heterocyclic Carbene Catalysts. *ChemCatChem* **2013,** *5*, 1490-1496.

69. Frogneux, X.; Blondiaux, E.; Thuéry, P.; Cantat, T., Bridging Amines with CO2: Organocatalyzed Reduction of CO_2 to Aminals. *ACS Catal.* **2015,** *5*, 3983-3987.

70. Hulla, M.; Laurenczy, G.; Dyson, P. J., Mechanistic Study of the N-Formylation of Amines with Carbon Dioxide and Hydrosilanes. *ACS Catal.* **2018,** *8*, 10619-10630.

71. Nicholls, R. L.; McManus, J. A.; Rayner, C. M.; Morales-Serna, J. A.; White, A. J. P.; Nguyen, B. N., Guanidine-Catalyzed Reductive Amination of Carbon Dioxide with Silanes: Switching between Pathways and Suppressing Catalyst Deactivation. *ACS Catal.* **2018,** *8*, 3678-3687.

72. Liu, X.-F.; Ma, R.; Qiao, C.; Cao, H.; He, L.-N., Fluoride-Catalyzed Methylation of Amines by Reductive Functionalization of CO_2 with Hydrosilanes. *Chem. Eur. J.* **2016,** *22*, 16489-16493.

73. Marenich, A. V.; Cramer, C. J.; Truhlar, D. G., Universal Solvation Model Based on Solute Electron Density and on a Continuum Model of the Solvent Defined by the Bulk Dielectric Constant and Atomic Surface Tensions. *J. Phys. Chem. B* **2009,** *113*, 6378-6396.

74. Chai, J.-D.; Head-Gordon, M., Long-range corrected hybrid density functionals with damped atom–atom dispersion corrections. *Phys. Chem. Chem. Phys.* **2008,** *10*, 6615-6620.

75. Lee, C.; Yang, W.; Parr, R. G., Development of the Colle-Salvetti correlation-energy formula into a functional of the electron density. *Phys. Rev. B: Condens. Matter Mater. Phys.* **1988,** *37*, 785-789.

76. Becke, A. D., Density-functional thermochemistry. III. The role of exact exchange. *J. Chem. Phys.* **1993,** *98*, 5648-5652.

77. Zhao, Y.; Truhlar, D. G., Density Functionals with Broad Applicability in Chemistry. *Acc. Chem. Res.* **2008,** *41*, 157-167.

78. Zhao, Y.; Truhlar, D. G., The M06 suite of density functionals for main group thermochemistry, thermochemical kinetics, noncovalent interactions, excited states, and transition elements: two new functionals and systematic testing of four M06-class functionals and 12 other functionals. *Theor. Chem. Acc.* **2008,** *120*, 215-241.

79. Grimme, S.; Ehrlich, S.; Goerigk, L., Effect of the damping function in dispersion corrected density functional theory. *J. Comput. Chem.* **2011,** *32*, 1456-1465.

80. Glendening, E. D.; Badenhoop, J. K.; Reed, A. E.; Carpenter, J. E.; Bohmann, J. A.; Morales, C. M.; Landis, C. R.; Weinhold, F. *NBO 6.0*: Theoretical Chemistry Institute, University of Wisconsin, Madison, 2013.

81. Tian Lu, F. C., J. Comput. Chem., 33, 580-592 (2012).

82. Contreras-García, J.; Johnson, E. R.; Keinan, S.; Chaudret, R.; Piquemal, J.-P.; Beratan, D. N.; Yang, W., NCIPLOT: a program for plotting non-covalent interaction regions. *J. Chem. Theory Comput.* **2011,** *7*, 625-632.

83. Johnson, E. R.; Keinan, S.; Mori-Sánchez, P.; Contreras-García, J.; Cohen, A. J.; Yang, W., Revealing Noncovalent Interactions. *J. Am. Chem. Soc.* **2010,** *132*, 6498-6506.

84. Tian, L.; Feiwu, C., Multiwfn: A multifunctional wavefunction analyzer. *J. Comput. Chem.* **2012,** *33*, 580-592.

85. Legault, C. Y. *CYLview, 1.0b*: Université de Sherbrooke, http://www.cylview.org, 2009.

86. Humphrey, W.; Dalke, A.; Schulten, K., VMD: Visual molecular dynamics. *J. Mol. Graphics.* **1996,** *14*, 33-38.

87. Liang, Y.; Liu, S.; Xia, Y.; Li, Y.; Yu, Z.-X., Mechanism, Regioselectivity, and the Kinetics of Phosphine-Catalyzed [3+2] Cycloaddition Reactions of Allenoates and Electron-Deficient Alkenes. *Chem. Eur. J.* **2008,** *14*, 4361-4373.

88. Martin, R. L.; Hay, P. J.; Pratt, L. R., Hydrolysis of Ferric Ion in Water and Conformational Equilibrium. *J. Phys. Chem. A* **1998,** *102*, 3565-3573.

89. Yu, Z.-X.; Houk, K. N., Intramolecular 1,3-Dipolar Ene Reactions of Nitrile Oxides Occur by Stepwise 1,1-Cycloaddition/Retro-Ene Mechanisms. *J. Am. Chem. Soc.* **2003,** *125*, 13825-13830.

90. Ariafard, A.; Brookes, N. J.; Stranger, R.; Yates, B. F., DFT Study on the Mechanism of the Activation and Cleavage of CO2 by (NHC)CuEPh3 (E = Si, Ge, Sn). *Organometallics* **2011,** *30*, 1340-1349.

91. Liu, B.; Gao, M.; Dang, L.; Zhao, H.; Marder, T. B.; Lin, Z., DFT Studies on the Mechanisms of the Platinum-Catalyzed Diboration of Acyclic α,β-Unsaturated Carbonyl Compounds. *Organometallics* **2012,** *31*, 3410-3425.

92. Liu, Q.; Lan, Y.; Liu, J.; Li, G.; Wu, Y.-D.; Lei, A., Revealing a Second Transmetalation Step in the Negishi Coupling and Its Competition with Reductive Elimination: Improvement in the Interpretation of the Mechanism of Biaryl Syntheses. *J. Am. Chem. Soc.* **2009,** *131*, 10201-10210.

93. Schoenebeck, F.; Houk, K. N., Ligand-Controlled Regioselectivity in Palladium-Catalyzed Cross Coupling Reactions. *J. Am. Chem. Soc.* **2010,** *132*, 2496-2497.
94. Yue, Z.; Zhao, J.; Du, P.; Liu, G.-X., Insights into Naturally Occurring Compound Catalyzed Formylation and Methylation Reactions of Amines with CO2: The Origins of Chemoselectivity. *ACS Sustainable Chem. Eng.* **2020,** *8*, 11967-11976.